REVIEW ARTICLE

Nickel oxide thin films grown by chemical deposition techniques: Potential and challenges in next-generation rigid and flexible device applications

Mari Napari[1,2] 🔘　│　Tahmida N. Huq[1] 🔘　│　Robert L. Z. Hoye[1,3] 🔘　│
Judith L. MacManus-Driscoll[1] 🔘

[1]Department of Materials Science and Metallurgy, University of Cambridge, Cambridge, UK

[2]Centre for Electronics Frontiers, Zepler Institute for Photonics and Nanoelectronics, University of Southampton, Southampton, UK

[3]Department of Materials, Imperial College London, London, UK

Correspondence
Robert L. Z. Hoye and Judith L. MacManus-Driscoll, Department of Materials Science and Metallurgy, University of Cambridge, 27 Charles Babbage Road, Cambridge CB3 0FS, UK.
Email: r.hoye@imperial.ac.uk (R. L. Z. H.) and jld35@cam.ac.uk (J. L. M.-D.)

Abstract

Nickel oxide (NiO_x), a p-type oxide semiconductor, has gained significant attention due to its versatile and tunable properties. It has become one of the critical materials in wide range of electronics applications, including resistive switching random access memory devices and highly sensitive and selective sensor applications. In addition, the wide band gap and high work function, coupled with the low electron affinity, have made NiO_x widely used in emerging optoelectronics and p-n heterojunctions. The properties of NiO_x thin films depend strongly on the deposition method and conditions. Efficient implementation of NiO_x in next-generation devices will require controllable growth and processing methods that can tailor the morphological and electronic properties of the material, but which are also compatible with flexible substrates. In this review, we link together the fundamental properties of NiO_x with the chemical processing methods that have been developed to grow the material as thin films, and with its application in electronic devices. We focus solely on thin films, rather than NiO_x incorporated with one-dimensional or two-dimensional materials. This review starts by discussing how the p-type nature of NiO_x arises and how its stoichiometry affects its electronic and magnetic properties. We discuss the chemical deposition techniques for growing NiO_x thin films, including chemical vapor deposition, atomic layer deposition, and a selection of solution processing approaches, and present examples of recent progress made in the implementation of NiO_x thin films in devices, both on rigid and flexible substrates. Furthermore, we discuss the remaining challenges and limitations in the deposition of device-quality NiO_x thin films with chemical growth methods.

KEYWORDS
atomic layer deposition, chemical vapor deposition, electronics, nickel oxide, solution processing, thin films

1 | INTRODUCTION

Oxide semiconductors have made significant progress over the past decade, gaining widespread use across a range of electronic devices, including thin-film transistors, photovoltaics, light-emitting diodes, sensors, non-volatile memory devices, and catalysts, among many other applications.[1-6] In particular, the resilience of the electronic properties of the oxides against mechanical deformation or degradation during operation under ambient conditions, as well as the ability to fabricate device quality oxides at low temperature,[3,7,8] has made metal oxide semiconductors leading materials of choice for flexible electronics based on polymer, cellulose, fabric, and elastomeric substrates.[1,4,9]

These flexible devices are enabling a wide range of new applications, including intelligent packaging, wearable systems, epidermal devices, artificial skins for robots, biomimetic medical implants, and advanced surgical tools. More detailed reviews on oxides for flexible electronics are given in References 1 and 4.

Most works on oxide electronics for both flexible and rigid applications have focused on n-type semiconductors.[1,4] p-Type oxides are more challenging because the valence band maxima of most oxides are composed of O $2p$ orbitals, which are more localized than the metal cation s orbitals in the conduction band minimum. As a result, hole mobilities tend to be lower than electron mobilities, which impacts, for example, the performance of hole transport layers in optoelectronic devices. Despite these challenges, p-type oxides are critically important for a wide range of emerging applications, including transparent complementary metal-oxide semiconductors (CMOS) for integrated circuits, hole transport layers (HTL) for photovoltaics, flexible p-n junctions, and sensors.[10-13] Three of the most common p-type oxides are tin monoxide (SnO), cuprous oxide (Cu_2O), and nickel oxide (NiO_x). Both SnO and Cu_2O are metastable at room temperature, and can form the more stable n-type SnO_2 or lower band gap cupric oxide (CuO) as a phase impurity.[4,9,14] In contrast, NiO_x is stable under ambient conditions.

Nickel oxide is one of the most studied transition metal oxides and its attractiveness stems from its electronic properties, as well as its low-toxicity, and composition of low-cost and abundant elements. The optical band gap is wide (with reported values ranging from 3.4 to 4.3 eV[15]), making the material transparent over the visible wavelength range. The work function can also be tuned over a wide range, from 3.7 to 6.7 eV by changing the defect density, composition, or surface dipole.[16] The valence band maximum, located at 5.4 eV relative to the vacuum level,[17] is aligned with the highest occupied molecular orbitals (HOMOs) or valence band maxima of a wide range of thin-film active layers for photovoltaics and light-emitting diodes, including lead-halide perovskites, lead-free perovskite-inspired materials, and organic materials.[18-21] Coupled with the low electron affinity, enabling electrons to be blocked, NiO_x is widely used as a hole transport layer in next-generation solar cells or hole-injection layer in light-emitting diodes. It is also an electrochromic material with a high coloration efficiency.[22-24] NiO_x has a high-temperature coefficient of resistance, high theoretical specific capacity of 718 mA h g^{-1} (compared to 372 mA h g^{-1} for graphite[25]) and high catalytic activity, making the material actively explored for supercapacitors,[26] thermistors,[27] Li-ion batteries,[28] and catalysts for CO or H_2O oxidation.[29,30]

As a simple binary oxide, NiO_x thin films can be grown with a wide range of deposition techniques. These include physical vapor deposition (PVD), such as sputtering and pulsed laser deposition (PLD); chemical vapor deposition (CVD), including atomic layer deposition (ALD); and a family of chemical-based solution deposition techniques, such as spin-coating or inkjet printing. While PVD techniques provide exceptional control over the film composition and electronic properties, the scalability, and low cost of the chemical-based deposition techniques make them appealing alternatives. Recent developments with the chemical-based deposition methods have led to lower processing temperatures, and the ability to deposit at atmospheric pressure with higher throughput. These have made these chemical deposition methods compatible with the polymer and cellulose substrates used for flexible electronics. Different CVD and ALD approaches, including aerosol-assisted CVD and spatial ALD, as well as several different solution-based techniques, including spray pyrolysis and sol-gel spin- and dip-coating, have been demonstrated for NiO_x film growth. In particular, these techniques often result in non-stoichiometric NiO_x films and therefore a range of different film properties. Postprocessing by annealing or plasma treatment have been widely developed to tailor the properties of the films for their specific applications.

In this review, we discuss the different chemical-based techniques for depositing NiO_x thin films, and how the precursor chemistry and growth methods used affect the film composition and electrical properties (Figure 1). We also present the recent progress made in the fabrication of rigid and flexible devices with NiO_x thin films grown by chemical-based routes and how the versatile properties of these films can be tailored to match the target applications.
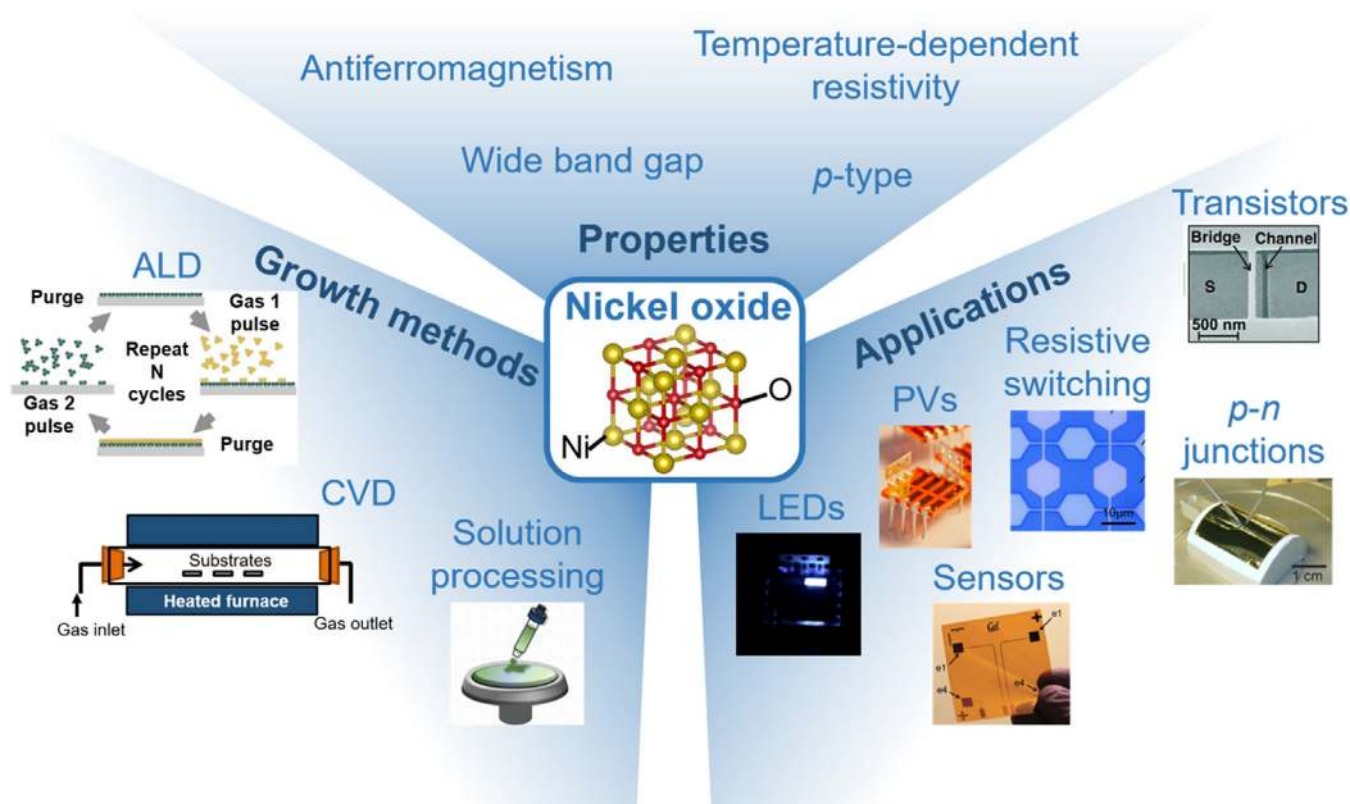
FIGURE 1 Schematic overview of the topics covered in this Review on NiO$_x$: material properties, growth methods, and applications in devices. Images have been reproduced with permission. ALD: Alam et al,[237] copyright 2018 by Elsevier; Solution processing: Park et al,[1] copyright 2019 by Wiley; LEDs: Hoye et al[217]; Sensors: Khan et al,[233] copyright 2016 by Wiley; Resistive switching: Yanagida et al[238]; *p-n* junctions Münzenrieder et al,[155] copyright 2013 by Elsevier; Transistors: Ante et al,[239] copyright 2011 by Wiley; PVs: Photo credit to Steve Penney

2 | EFFECT OF NON-STOICHIOMETRY ON THE ELECTRICAL AND MAGNETIC PROPERTIES OF NIO$_X$

In stoichiometric NiO, both ions are octahedrally coordinated. The Ni^{2+} cations have filled $3d^8$ orbitals with similar energy to the O $2p^6$ orbitals, and it is expected that these orbitals hybridize in the valence band maximum (as illustrated in Figure 2A).[16,17,31-33] There are also empty $3d^9$ orbitals which form the conduction band minimum and these orbitals are separated from the $3d^8$ orbitals by a large energy difference due to strong electron correlation (Figure 2A).[17] Originally, it was thought that the band gap of NiO was formed between the Ni $3d^8$ and $3d^9$ orbitals, making NiO a Mott-Hubbard insulator. However, later work showed NiO to be a charge transfer insulator, with the band gap formed between the O $2p^6$ and Ni $3d^9$ orbitals.[17,31-33] Owing to its wide band gap, NiO in its stoichiometric form is insulating with a room temperature resistivity of $>10^{13}$ Ω cm.[16] At room temperature, NiO is antiferromagnetic, and becomes
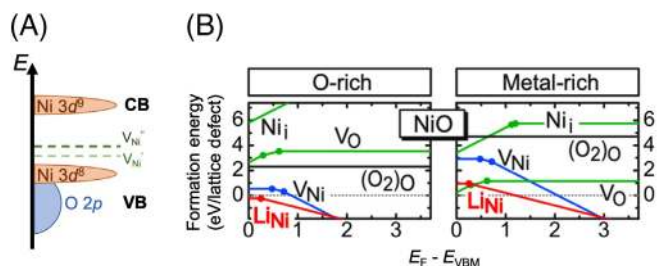

FIGURE 2 A, Band structure of nickel oxide about the band gap, based on the work in References 17 and 31–33. The transition levels for the 0/−1 and −1/−2 charge states of the nickel vacancy inside the band gap are indicated with dashed lines. B, Computed defect diagrams for NiO grown under O-rich and Ni-rich conditions. Reproduced with permission from Lany et al.[34] Copyright 2007 by the American Physical Society

paramagnetic above its Néel temperature of 523 K. In the paramagnetic state, NiO has a cubic unit cell with a NaCl crystal structure. Below the Néel temperature, all spins on each (111) plane are parallel, and spins on adjacent (111) planes are antiparallel. This results in a small

contraction along the [111] axis, and the distorted crystal structure is considered to be rhombohedral with an angle of 90.4°.[35] These antiferromagnetic domains have been characterized by neutron Laue diffraction.[36]

Acceptor levels can be introduced in nickel oxide through doping or through nickel vacancies. The defect equilibria for the formation of nickel vacancies are given by Equations (1) to (3).[37]

$$\frac{1}{2}O_2 \rightleftharpoons O_O^X + V_{Ni}^X \qquad (1)$$

$$V_{Ni}^X \rightleftharpoons V_{Ni}' + h^\bullet \qquad (2)$$

$$V_{Ni}' \rightleftharpoons V_{Ni}'' + h^\bullet \qquad (3)$$

In Equations (1)-(3), O_O refers to oxygen occupying a lattice site and V_{Ni} refers to a nickel vacancy. In Kröger-Vink notation, x refers to a neutral charge, ′ refers to a negative charge, ″ a double negative charge, and • refers to a positive charge. When nickel oxide reacts with oxygen gas, a lattice oxygen site is formed, which requires a lattice nickel site as well, but this is vacant. The nickel vacancy releases two holes to form a doubly negatively charged vacancy and makes the material p-type.[37]

Several experimental and theoretical papers have reported that nickel vacancies readily form. For example, Lany et al reported defect calculations showing that acceptor nickel vacancies have two transition levels in the band gap with low formation energies under oxygen-rich conditions (Figure 2B). The donor oxygen vacancy defect has much higher formation energies and are, thus, less likely to form. Non-stoichiometric NiO_x would therefore be expected to be nickel-deficient and p-type.[34] Experimental results have confirmed that nickel vacancies form under oxygen-rich conditions.[16] Choi et al have found that the conductivity of NiO_x increased with the partial pressure of oxygen (P_{O_2}), and was proportional to $P_{O_2}^{0.2}$ at temperatures between 1100°C and 1400°C, which suggested that the nickel vacancies were doubly ionized.[37] Each hole released by a nickel vacancy can be considered to be equivalent to the formation of two Ni^{3+} from each vacant Ni^{2+} because the release of a hole in the valence band is equivalent to an electron from the $3d^8$ orbital being excited to the acceptor level in the band gap. Thus, each doubly ionized nickel vacancy can be considered to be equivalent to the formation of two Ni^{3+}.[16] Under oxygen-poor conditions (metal-rich), calculations predict the formation energy of oxygen vacancies to be lower than that of nickel vacancies. However, the transition level of the oxygen vacancy is predicted to be closer to the valence band than the conduction band, and this deep

donor is then expected to not lead to significant charge-compensation.[34] Non-stoichiometric NiO_x is therefore expected to be p-type and this has been confirmed experimentally in several reports since the 1960s.

Another common way to increase the carrier concentration of holes in nickel oxide is to dope with lithium and obtain nickel lattice sites occupied by lithium. An example of lithium-doping nickel oxide with Li_2O is given in Equation (4), showing how lithium on a Ni^{2+} site (Li_{Ni}') releases holes.[16,17,38]

$$\frac{1}{2}O_2 + Li_2O \rightleftharpoons 2O_O^X + 2Li_{Ni}' + 2h^\bullet \qquad (4)$$
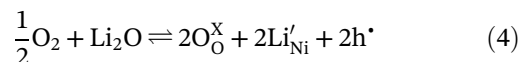
The hole effective mass for NiO_x measured at 670 to 1670 K has been reported to range from 0.8 to 1 m_0, and the hole mobilities measured at high temperatures have been reported to be <1 $cm^2 V^{-1} second^{-1}$, measured from nickel oxide single crystals through temperature-dependent conductivity and Seebeck coefficient measurements.[37] However, there is a disagreement in the literature on whether the conduction mechanism is due to band-like conduction or small polaron hopping. Polarons are heavy quasi-particles that occur due to strong interactions between holes and the surrounding lattice, and polaron-mediated conduction occurs through hopping between lattice sites.[17] Measurements of lithium-doped nickel oxide at high temperatures >1300 K suggest that the conduction mechanism is band-like transport.[37] However, measurements of the conductivity and Seebeck coefficient of NiO_x at 130 to 330 K suggest that carrier transport occurs by small polaron hopping, and that the room temperature mobility is 0.011 to 0.047 $cm^2 V^{-1} second^{-1}$.[17]

Apart from temperature-dependent conductivity and Seebeck coefficient measurements, the hole mobilities in NiO_x thin films are widely determined by Hall effect measurements. However, this would not be entirely valid if NiO_x films were antiferromagnetic. As discussed, the conductivity of NiO_x strongly varies with the stoichiometry. An important question is whether nickel oxide remains antiferromagnetic when it is nonstoichiometric. Bachmann et al measured the magnetic characteristic of non-stoichiometric ALD NiO_x films but their results remained inconclusive on whether the films exhibited antiferromagnetic or diamagnetic behavior.[39] Dubey et al investigated the effect of stoichiometry on the magnetization and Néel temperature of NiO_x.[40] The samples were prepared by thermal decomposition of nickel nitrate hexahydrate and measured to have ca. 40% excess oxygen. In these non-stoichiometric samples, the Néel temperature remained between 480 and 530 K, close to that of stoichiometric NiO, suggesting the non-stoichiometric

NiO_x to remain antiferromagnetic. Recently, we investigated the magnetic properties of NiO_x thin films deposited by plasma-enhanced ALD (PEALD), and sol-gel spin-coating. We measured the composition and bonding state of the Ni and O elements using X-ray photoemission spectroscopy (XPS). XPS is a surface-sensitive method, with an interaction depth of 1 to 10 nm, and can be used to measure the elemental composition with a resolution of 0.05 at%.[41] Elements with different bonding states can also be distinguished by their different binding energies (a Review of XPS analysis can be found in Reference 42). From our previous XPS measurements on the PEALD and spin-coated NiO_x films, we found that both deposition methods resulted in nickel deficient films with significant Ni^{3+} present (Figure 3A,B) and with the Ni/O ratio varying between 0.6 and 0.7 (Figure 3C). The PEALD films were polycrystalline with dominant (200) orientation, while the sol-gel films were too thin to give diffraction peaks. Despite non-stoichiometric composition and differences in microstructure, all the measured films showed antiferromagnetic behavior, measured as
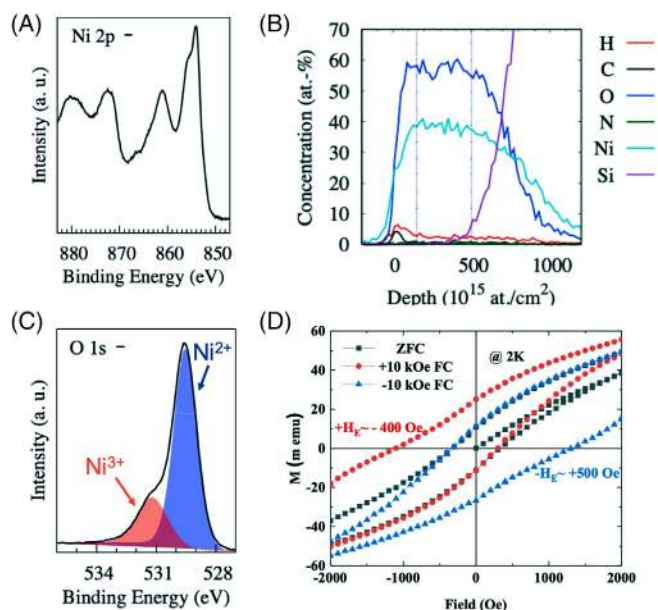
an exchange bias shift in in-plane magnetic hysteresis at 2 K temperature (Figure 3D).[44]

As the antiferromagnetism of the material adds uncertainty to the Hall effect measurements, alternatives are needed to reliably investigate the electronic properties of NiO_x films. One alternative to Hall measurements is electrochemical Mott-Schottky analysis, in which the capacitance (C) generated from a depletion region is measured at different applied DC biases (V). From a plot of C^{-2} against V, the carrier concentration can be obtained. By measuring the resistivity of the NiO_x film, the mobility can also be determined, with the appropriate circuit model.[45,46] Another method is to obtain the mobility through field-effect measurements from fabricated thin-film transistor structures, which will be discussed more in Section 6.2.

Although film stoichiometry, and therefore its electrical properties, can be precisely controlled in some PVD techniques (such as pulsed laser deposition) by tuning P_{O_2} and deposition temperature,[47] there is less control in chemical-based deposition techniques. This is because the film stoichiometry is governed by the reaction chemistry during the deposition. Hence, the precursors and deposition conditions used play a key role in defining the film characteristics and properties.

3 | CHEMICAL DEPOSITION OF NICKEL OXIDE THIN FILMS

3.1 | CVD of nickel oxide

CVD is an attractive technique for the fast growth of thin films with varying thicknesses and compositional uniformity over large areas, with high reliability and reproducibility. Key to CVD is the precursor chemistry. CVD of NiO_x relies mostly on metal-organic (MO) precursors, typically β-diketonate, (amino)alkoxide, and cyclopentadienyl complexes, and O_2 gas is used as an oxidizer. In most cases, an additional oxygen source is needed also with oxygen coordinated precursors, that is, precursors that contain O atoms in the molecule. Reported (MO)-CVD NiO_x processes are collected in Table S1, showing the wide variety of processes (including aerosol-assisted and atmospheric pressure CVD) and temperatures used, ranging from 105°C up to 750°C.

These result in amorphous, polycrystalline, or epitaxial films, depending on the deposition conditions and the substrate material. The reports in Table S1 also cover some demonstrations of the potential CVD NiO_x films in devices, including electrochromics,[22,48] and resistive switching.[49] In addition to thin films, CVD can also be utilized in growing NiO_x nanoparticles, for example, for

FIGURE 3 X-ray photoemission spectroscopy measurements of plasma-enhanced atomic layer deposited (PEALD) NiO_x films showing the (A) Ni $2p$ and (B) O $1s$ core level peaks. The O $1s$ core level spectrum has been fitted according to Reference 43 to show the components due to lattice oxygen (bonded to Ni^{2+}) and defect states (Ni^{3+}). C, Time-of-flight elastic recoil detection analysis (ToF-ERDA) elemental depth profile of plasma-enhanced atomic layer deposited (PEALD) NiO_x. D, In-plane magnetic hysteresis loops of 6 nm $Ni_{80}Fe_{20}$ / PEALD NiO_x bi-layer at 2 K. The field cooled (FC) hysteresis shows an exchange bias H_x of −400/+500 Oe. Reproduced with permission from Napari et al.[44] Copyright Wiley 2020

catalysis and gas sensing applications.[29,50] Across all device applications discussed in this review, polycrystalline (and in some cases amorphous) NiO_x is used. Indeed, in most cases, the same processing method can give either amorphous or polycrystalline films, often depending on the deposition temperature, giving wide tunability over a range of properties. For example, Battiato et al found that amorphous NiO_x, grown by CVD at below 450°C, was smoother than polycrystalline NiO_x and had higher transmittance below the band gap.[51] On the other hand, polycrystalline films have higher mobility, which is important in TFT applications. Epitaxial NiO_x films have mostly been grown for fundamental investigations into its properties, as well as efforts to demonstrate the capabilities of new CVD processes.[48,52,53] Epitaxial films are also preferred in applications where high resistivity is required. This is due to the lower defect density in the epitaxial films with a near-stoichiometric composition.[54,55] Achieving improved p-type conductivity in epitaxial films requires doping, such as with Li (refer to Section 2).[56]

The majority of reports focus on process development and material characterization, and only a few papers present and discuss electrical properties of the films. Wang et al deposited NiO_x films from methylcyclopentadienyl nickel ($Ni[MeCp]_2$) and O_2 on sapphire using photo-assisted CVD at 510°C to 600°C.[57] They observed that the film morphology changes from small (<10 nm) and anomalous grains to large (80 nm) cubic-shaped crystalline grains with strong (111) preferred orientation with increasing deposition temperature. The temperature also affected the optical and electrical properties: the band gap decreased from 3.93 to 3.55 eV, and the Hall effect measurements of the p-type films showed an increase in resistivity from ca. 460 to 1940 Ω cm as the deposition temperature increased. The mobility increased slightly from 0.28 to 0.54 cm^2 V^{-1} second^{-1} while the hole concentration dropped from 4.8·10^{16} cm^{-3} to 5.9·10^{15} cm^{-3}, respectively.[57] While the changes in the electrical properties could be attributed to the improvements in the film crystallinity leading to a decrease in Ni^{2+} vacancies, the possible changes in the film stoichiometry was not reported. $Ni(MeCp)_2$ was also used as a precursor by Zhao, Lee et al who used atmospheric pressure spatial atomic layer deposition (AP-SALD) in CVD mode at 350°C, with O_2 gas as the oxidant.[46] The resistivity of the films was ~10^3 Ω cm, and the carrier concentration, determined by Mott-Schottky analysis, was 1.6·10^{18} cm^{-3}, with the corresponding hole mobility 3·10^{-3} cm^2 V^{-1} second^{-1}.[46] NiO_x films grown with the same deposition system using a NiCpAllyl precursor and O_2 at 300°C were measured to be nonstoichiometric with Ni/O ratio of ~0.6.[44] The electrical properties of the films were determined with Hall effect measurements, and the carrier concentration was found to be ~10^{16} cm^{-3}, and mobility on the order of 0.1 cm^2 V^{-1} second^{-1}.[44] The orders of magnitude difference in both values in films grown with comparable chemistries and conditions is more likely due to the choice of the measurement technique rather than a real measure of the film properties (refer to Section 2).

Resistivity values between 10^2 and 10^4 Ω cm have also been obtained in polycrystalline NiO_x films deposited using nickel thenoyl-trifluoroacetone tetra-methylethylenediamine (Ni[tta]·tmeda) and O_2 at 350°C to 550°C by Battiato et al.[51] They measured a work function of 5.1 eV in the as-deposited films. However, the effect of the deposition temperature on the electrical properties was not reported, and the film stoichiometry was established through Raman measurements.[51]

The effect of film stress on the resistivity of NiO_x thin films was reported by Roffi et al who deposited epitaxial films on (001) Al_2O_3, and (100) and (111) MgO substrates at 300°C to 600°C at atmospheric pressure using NiCpAllyl and O_2.[58] They observed that the stress in the films results in cation vacancies to accommodate for the lattice mismatch. Hence, with compressive stress the improved crystallinity by the higher deposition temperature leads to more nickel vacancies, which creates more carriers and decreases the resistivity, while with tensile stress the improved crystallinity is achieved with fewer vacancies and carriers, and the resistivity increases.[58] They also investigated the effect of the flow ratios of O_2 and nickel precursor, and showed that the increase in O_2 flow decreases the resistivity by an order of magnitude from 2700 to 250 Ω cm, which they attribute to the improved crystallinity. However, the effect of the O_2 flow rates on the film stoichiometry cannot be excluded as the film composition was not measured.[58] The importance of the substrate and NiO_x film stress is highlighted also by Lo Nigro et al who used CVD grown epitaxial NiO_x thin films as dielectrics in wide band gap semiconductor AlGaN/GaN devices.[54,55] The dielectric properties of the films were determined from the $C - V$ measurements, with relative permittivity $\epsilon_r = 11.7$. The application of the 20 nm NiO_x dielectric reduced the leakage current of the devices by 2-3 orders of magnitude.[54,55]

Currently, there are no reports directly correlating the effect of stoichiometry with the electrical characteristics of CVD grown NiO_x, and extrapolation from different reports can be challenging. XPS has typically been used to determine the film stoichiometry, but quantification is difficult due to the complexity of the Ni 2p peak shapes resulting from multiplet splitting, shake-up, and plasmon loss structure.[43] However, it has been shown that the film composition is strongly dependent on the deposition

process and conditions. For example, it was shown that a process using cyclopentadienyl nickel and O_2 at 200°C to 500°C can result in a high content of metallic Ni^0 in the films, if the O_2 flow is insufficient.[59] But the Ni^0 component disappears with higher O_2 flow rates at similar temperatures.[60] However, neither of these report the film stoichiometry. Min et al presented XPS measured Ni/O ratio of 1.2 in their films deposited using $Ni(dmamb)_2$ and O_2. These Ni-rich films also showed resistive switching behavior, though the initial resistivity values were not reported. Kondrateva et al showed excess oxygen in their NiO_x films deposited using ethylcyclopentadienyl nickel ($Ni[EtCp]_2$) and $O_2 + O_3$, with Ni/O ratio of 0.85,[61] but no electrical properties were reported.

Doping NiO_x films with Li has also been recently demonstrated with CVD. Ikenoue et al deposited un-doped and doped NiO_x using a "mist"-CVD with nickel acetylacetonate ($Ni[acac]_2$) and Li(acac) or LiOH diluted in deionized water at growth temperatures of 500°C to 750°C. Both the un-doped and Li-doped films grew epitaxially on terraced α-Al_2O_3 substrates, shown in Figure 4. The un-doped films showed high resistivity values of $>10^6$ Ω cm, and the Li-doping with different concentrations resulted in reduced resistivity by 1 to 5 orders of magnitude, depending on the Li precursor and its concentration. The p-type conductivity was confirmed by Seebeck measurements, but the hole mobility and density in the films were not further investigated.[56]

CVD is a standard technique for depositing many high-quality materials for different device applications. Oxides, like NiO_x, typically require high temperatures that are not compatible with flexible substrates. However, as seen in Table S1, with a right choice of precursor chemistry it is possible to deposit NiO_x by CVD at temperatures as low as 200°C. This opportunity, together with the recent advances in atmospheric pressure deposition includes CVD as a potential deposition technique of p-type NiO_x films for flexible device applications.

3.2 | ALD of Nickel Oxide

Similar to CVD of NiO_x thin films, ALD also relies on the reactivity of the nickel precursors, and the chemistry of the precursors is similar to what is used in CVD processing. Unlike CVD, where the reactions take place in the gas phase, ALD growth is governed by self-limiting reactions of sequentially applied precursors. The reported ALD processes for NiO_x are presented in Table S2. To maintain surface-limited growth, the deposition temperatures in ALD are generally lower than in CVD, typically below 300°C to avoid the thermal decomposition of the
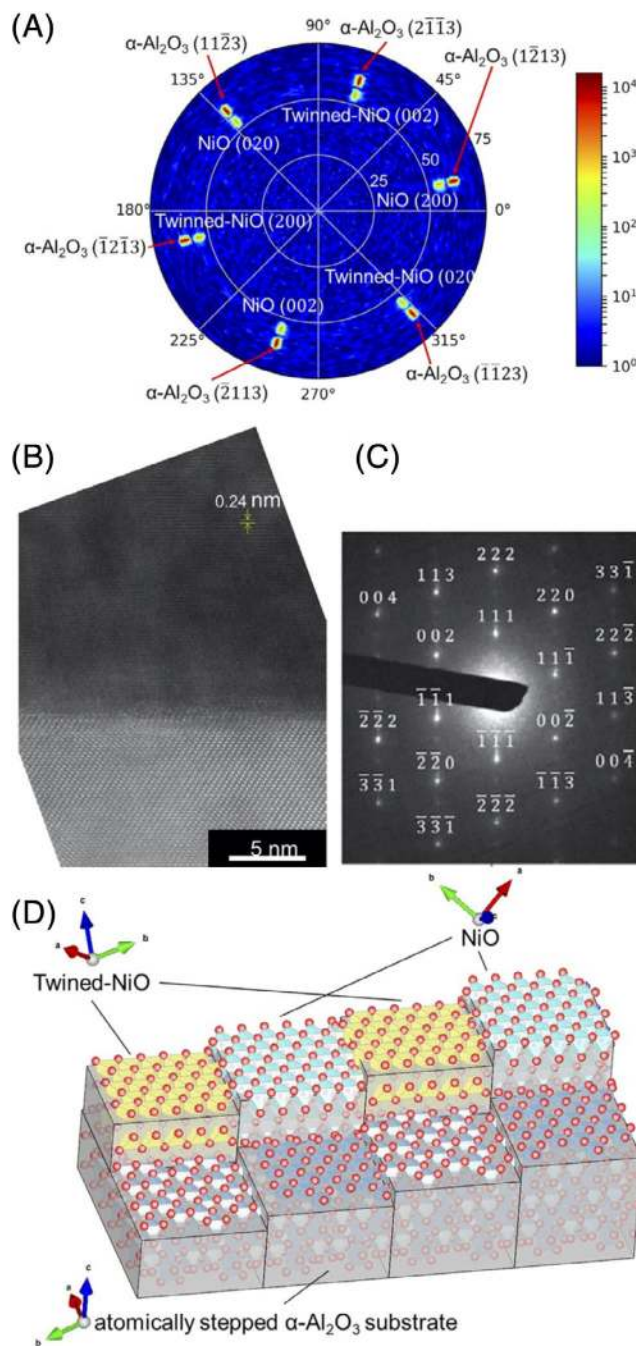

FIGURE 4 A, X-ray diffraction (XRD) pole figure of the {200} planes of mist-CVD grown un-doped NiO_x film on α-Al_2O_3 measured at $2\Theta = 43.383°$. B, High-resolution transmission electron microscopy (HRTEM) and C, a selected area electron diffraction (SAED) image of Li-doped NiO_x film. D, Schematic illustration of epitaxial NiO_x film growth on atomically stepped α-Al_2O_3 substrate. The periodic structure of the film is in accordance with the two types of terraces on the substrate. Reproduced with permission from Ikenoue et al.[56] Copyright Elsevier 2019

precursor molecules. However, the low temperature also limits the reactivity of the precursors and hence stronger oxidants, such as ozone or O_2 plasma, are often needed

for successful deposition. The reduced reactivity also leads to longer pulsing times being required to achieve saturated growth, and low growth per cycle values of less than 1 Å are typical for ALD NiO_x processing. The advantage of ALD, however, is the superior conformality of ultrathin pinhole-free films over complex three-dimensional nanostructures, as demonstrated, for example, with anodic aluminium oxide (AAO) templates[53,62,63] and carbon nanotubes.[64] Figure 5 shows an example of conformal ALD NiO_x coating over AAO nanopores with aspect ratio of 1:70. In addition to NiO_x thin films, ALD has also been applied to grow NiO_x and metallic Ni nanoparticles, where in the latter case the metallic material is typically formed by post-deposition reduction of

the NiO_x films[26,65-69] or by exposing the film to hydrogen plasma species during the deposition.[70]

Like CVD, most papers on ALD of NiO_x are focused on process development and the characterization of the material properties, and the reports on the electrical behavior of the films are sparse. More attention has been paid to the elemental characterization of the films. Due to the difficulties in the quantitative analysis of the composition, XPS has typically been used to confirm the absence of the impurities in the films instead of providing more detailed compositions. For example, when using cyclopentadienyl complexes as precursors, carbon contamination in the films can be significant, especially at lower deposition temperatures.[28,71] In one of the earliest reports on ALD of NiO_x by Kumagai et al highly nickel deficient films with Ni/O ratio of ca. 0.45 was measured by Rutherford Backscattering Spectrometry (RBS)[72] although the high deposition temperature of 400°C indicates that the cyclopentadienyl nickel precursor used may have decomposed at the substrate, leading to uncontrolled CVD-type growth with deviated composition. However, nickel deficiency (with Ni/O ratio on the order of 0.7-0.9) in the films grown using cyclopentadienyl complexes has been also reported at lower deposition temperatures.[39,73] Interestingly, later also Ni-rich films have been proposed by using cyclopentadienyl and ethylcyclopentadienyl nickel and oxygen plasma.[28,74] Ji et al presented XPS results of films grown with $Ni(EtCp)_2$ at temperatures of 100°C to 325°C with Ni/O ratio of 1.1 to 1.14.[74] Koshtyal et al measured similar results for their plasma process with $NiCp_2$ with, Ni/O ratio of 1.15.[28] However, these films, grown at 300°C, also contained a significant amount of carbon (12%). Similar to CVD, ALD using an aminoalkoxide precursor, $Ni(dmamb)_2$, has been found to give nickel rich films with a Ni/O ratio of 1.3, as measured by time-of-flight elastic recoil detection analysis (ToF-ERDA).[75] According to Ko et al the high nickel content stems from the presence of metallic nickel in the films.[76] These films were shown to have high resistivity of $1.7 \cdot 10^7$ Ω cm and a work function of 4.18 eV.[76] A work function of 4.3 eV has also been measured from films grown by a similar type of precursor, $Ni(dmamp)_2$ and water.[77] Recently, Holden et al reported an ALD process with Ni(DAD) and O_2, resulting in films with a Ni/O ratio of 1.1 to 1.2, as measured by XPS. However, the authors acknowledge that the surface sputtering by Ar ions prior to the XPS measurement may have distorted the composition.[78]

While p-type conductivity has sometimes been confirmed solely through p-n heterojunction diodes (refer to Section 6.3),[78] there are a few reports of direct measurements of ALD NiO_x carrier properties, mostly of the carrier concentration and work function of the films. The
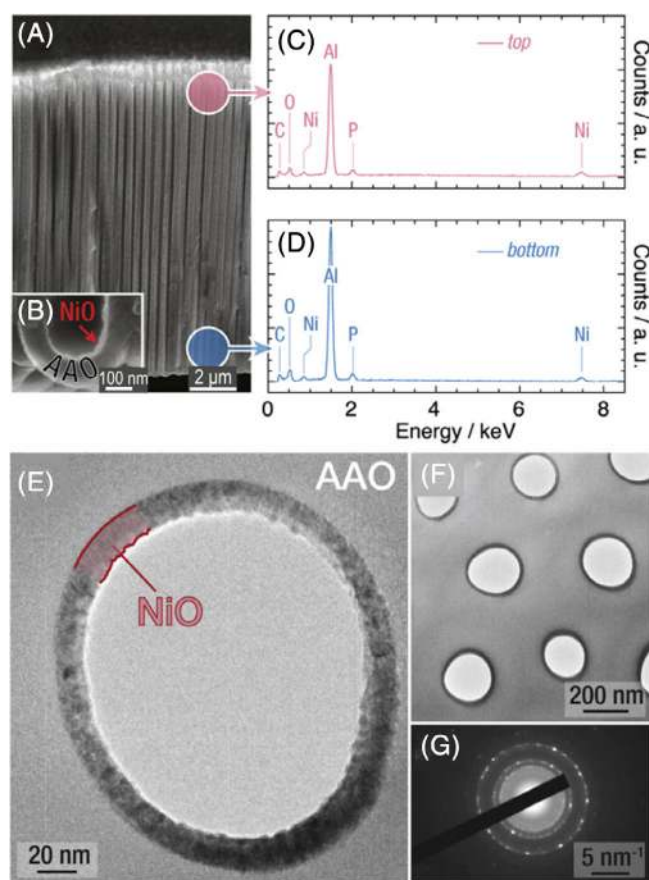

FIGURE 5 A, Scanning electron microscopy (SEM) cross-sectional image of an anodic aluminium oxide (AAO) membrane with 14 μm deep nanopores coated by ALD NiO_x thin film using bis (ethylcyclomentadienyl)nickel ($Ni(EtCp)_2$) and O_3 at 250°C. B, A high magnification SEM cross-section of the apex of a single pore. C-D, SEM-EDX spectra recorded from the top and bottom of the membrane, respectively. Similar peak intensities indicate conformal coating over the high aspect ratio nanopores. E-F, TEM top views of the NiO_x film on the ion milled AAO membrane. G, SAED pattern of the polycrystalline NiO_x film. Reproduced with permission from Barr et al.[62] Copyright Elsevier 2015

reported values vary, which may be due to the different deposition parameters. But, as discussed in Section 2, different measurement techniques may result in different values. For example, Hsu et al used the Hall effect method to measure hole concentration of NiO_x films grown with an amidinate precursor and water.[79] Their measured carrier concentration of 10^{14} cm^{-3} is orders of magnitude lower than what has been reported by using electrochemical measurements. For example, Thimsen et al did an extensive study of the energy levels and electronic properties of ALD NiO_x, grown using a similar amidinate precursor, by electrochemical Mott-Schottky spectroscopy.[80] According to their results, the carrier concentration of the films was in the order of 10^{17} to 10^{18} cm^{-3}, depending on the film thickness, and was further increased up to 10^{21} cm^{-3} by post-deposition annealing at O_2 at temperatures 300°C to 600°C. They also estimated a very low hole mobility (10^{-5}-10^{-3} cm^2 V^{-1} second^{-1}).[80] High carrier concentrations, 10^{19} to 10^{20} cm^{-3}, by Mott-Schottky analysis have also been reported for as-deposited films grown using aminoalkoxide and cyclopentadienyl precursors.[81] Mott-Schottky analysis was also used to estimate the work function by flat band potential and valence band position (E_{VB}) of the ALD NiO_x. Based on these measurements work functions of 5.0 to 5.1 eV[82] and 5.3 to 5.4 eV[80] were obtained.

The majority of the reported applications using ALD grown NiO_x films are related to its use as a hole transport layer in solar cells,[63,81] and other rigid devices. However, ALD in general has proven to be compatible technique for depositing films also on flexible substrates. Many oxide materials, including Al_2O_3,[83,84] ZnO,[85,86] and TiO_2[87,88] have been deposited using thermal or plasma-enhanced ALD near or at room temperature. ALD growth of oxides on many plastic materials has been reported,[86,89,90] and device applications, such as flexible thin-film transistors have been demonstrated.[91,92] The high throughput variants of ALD, such as spatial ALD and especially roll-to-roll ALD have been shown to have great potential in coatings for flexible electronics, and have already been used, for example, to deposit diffusion barrier films for device encapsulation, as well as conformal coatings on nanostructured substrates.[93-96] Further details on spatial ALD can be found in Reference 6 and 97. The lowest temperature that could be used in ALD growth of NiO_x films is typically limited by the low volatility of the nickel precursors, as well as their poor reactivity. The current literature also lacks examples of ALD NiO_x thin films on flexible substrates. However, processes compatible with such applications have already been demonstrated. For example, aminoalkoxide precursors Ni(dmamb)$_2$ and Ni(dmamp)$_2$ can be used to grow films

with H_2O at <150°C,[76,77,98-100] and a plasma-enhanced ALD process with $Ni(MeCp)_2$ at temperatures as low as 50°C was reported recently.[81]

3.3 | Solution deposition of nickel oxide

The family of chemical-based solution deposition methods include sol-gel processes, chelate processes, and decomposition of organometallic precursors. A wide range of techniques exist, including spray pyrolysis, spin- and dip coating, and inkjet printing. Compared to vapor deposition techniques, the advantage of solution deposition is a lack of need for expensive vacuum setups. This has made solution processing the most widely used approach for oxide thin film deposition for many applications. Like ALD and CVD, some solution processing techniques are suitable for large-area deposition, and can be used to grow high-quality thin films at low deposition temperatures.

3.3.1 | Spin-coating

The typical sol-gel route to preparing NiO_x thin films involves spin-coating a sol containing the nickel precursor over the substrate to form a film, which is then annealed in air. During annealing, the process steps are: (a) thermal decomposition (pyrolysis) of the nickel precursor, (b) hydrolysis to form metal hydroxides, (c) condensation to form metal-oxygen (M-O) bonds from the metal hydroxide precursors, and (d) densification through the cross-linking of the M-O-M frameworks and formation of a crystal lattice.[101] The nickel precursor is typically nickel acetate, nickel nitrate or nickel formate, which are often used in their hydrated forms and complexed with amines (eg, monoethanolamine or ethylenediamine).[102-109] The complexing agent used affects the thermal requirement for decomposition. For example, it has been reported that nickel nitrate hexahydrate complexed with monoethanolamine has a thermal decomposition temperature of 500°C,[103] which reduces to 300°C when complexed with ethylenediamine.[102,103,108,109] Thermogravimetric analysis measurements of nickel formate complexed with ethylenediamine dissolved in a mixture of water and ethylene glycol showed that the solvent was removed at 120°C, followed by 77% mass loss at 180 to 240°C. The latter was attributed to the decomposition of nickel formate-diamine complex to NiO_x, and the loss of residual solvent and ethylenediamine ligands.[103]

However, the annealing temperatures required for thermal decomposition are too high for most polymer substrates used in flexible electronics (refer to Section 5).

Groups have developed approaches to deposit NiO_x thin films without any post-annealing required. This can be achieved by pre-synthesizing NiO_x crystals as nanoparticles and dispersing them in a solvent. For example, Zhang et al synthesized NiO_x nanoparticles by mixing nickel nitrate in water and increasing the pH to 10 by adding NaOH.[110] Reacting the nickel nitrate with sodium hydroxide results in the formation of nickel hydroxide.

By calcining these precipitates at 270°C for 2 hours in air, these hydroxides can be decomposed to NiO_x.[111] It was found that the calcination temperature is critical for controlling the yield of NiO_x: lower calcination temperatures resulted in nickel hydroxide remaining, whereas higher calcination temperatures resulted in large particles that could not form uniform films.[111] The nanoparticles formed at 270°C were 4 nm diameter and dispersed in an aqueous solvent to create the ink, which is stable for at least 15 days in air.[111] These nanoparticles could be spin-coated on rigid ITO/glass or flexible ITO-coated polyethylene terephthalate (PET) substrates. Without any post-annealing, the NiO_x was shown to be suitable hole transport layers for lead-halide perovskite solar cells.[110] The thickness could be adjusted by controlling the concentration of NiO_x nanoparticles in solution. Using an ink containing 2 wt% NiO_x nanoparticles resulted in films with 20 nm thickness. X-ray photoemission spectroscopy measurements showed the NiO_x film obtained to have significant Ni^{3+} as well as hydroxyl groups on the surface.[110] These hydroxyl groups may have originated from nickel hydroxide that did not completely decompose. Studies by Jiang et al have shown that the hydroxyl group content could be reduced by post-annealing the NiO_x nanoparticles at above 200°C. However, the O $1s$ peak associated with Ni^{3+} also increased. Ultraviolet photoemission spectroscopy measurements showed that post-annealing at 200°C resulted in the work function reducing from 5.25 eV (no annealing) to 4.61 eV (200°C post-annealing).[111]

3.3.2 | Solution combustion synthesis and UV-assisted synthesis

The temperature for forming NiO_x by solution processing can also be reduced by using an exothermic solution combustion synthesis method, as opposed to endothermic pyrolysis (refer to Section 3.3.1).[112] In solution combustion synthesis, an oxidizer (often a nitrate) and fuel are used. Acetylacetone (130°C, 784.4 J g^{-1}) and urea (220°C, 10570 J g^{-1}) are commonly used as fuels because they have low ignition temperatures and high enthalpies of combustion.[101,113] The exothermic combustion reaction results in intense heat being generated inside the film, which helps to form the M-O-M frameworks and remove residual organic components. The temperature required only needs to be above the ignition temperature, which is sufficient to form crystalline NiO_x but is low enough to be compatible with polymer substrates.[101,114]

Another approach to forming solution-processed oxides at low temperature is to use deep ultraviolet (DUV) irradiation. This results in the photochemical cleavage of alkoxy groups, which helps in the formation of M-O-M frameworks at temperatures as low as 150°C after only 30 minutes illumination.[115] UV illumination can also result in the photolysis of O_2, which can react with metal dangling bonds and fill oxygen vacancies.[116] Work on indium gallium zinc oxide films formed through DUV illumination showed that the films have comparable density as films formed through thermal decomposition at higher temperatures.[115] Growth of lithium-doped NiO_x by DUV exposure has been performed by Yang et al, who combined this process with solution combustion synthesis. Acetylacetonate was used as the fuel and nickel nitrate as the oxidizer. The spin-coated film was exposed to DUV radiation (253.7 and 184.9 nm wavelengths) before annealing at 150°C to activate combustion synthesis. The resultant films were phase-pure NiO_x, but had Ni^{3+} as well as Ni^{2+} present. These films were deposited onto PET substrates for flexible thin-film transistors.[114]

3.3.3 | Inkjet printing

Inkjet printing has attracted significant attention because it is better suited to growing films over large areas than spin-coating, is less wasteful and can deposit patterned films without requiring photolithography.[1] An inkjet printer is comprised of a printer head with micrometer-sized nozzles. Two common approaches are used to eject droplets from the nozzles: (a) thermal inkjet and (b) piezoelectric inkjet (illustrated in Figure 6). Thermal inkjet uses evaporated ink that is forced out of the nozzle. In contrast, piezoelectric inkjet releases the ink as small droplets by using piezoelectric nozzles that change when a bias is applied. The typical linewidth of inkjet-printed films is 20 to 50 μm, depending on the nozzle diameter and the surface tension and viscosity of the ink (usually 1-50 mPa s).[1,117]

A limitation of inkjet printing is that the throughput is limited, but researchers have attempted to overcome this by using multi-head devices.[1] Another important limitation is that the printed films can be non-uniform due to the evaporation rate of the solvent from the edges being different from the evaporation rate of the solvent
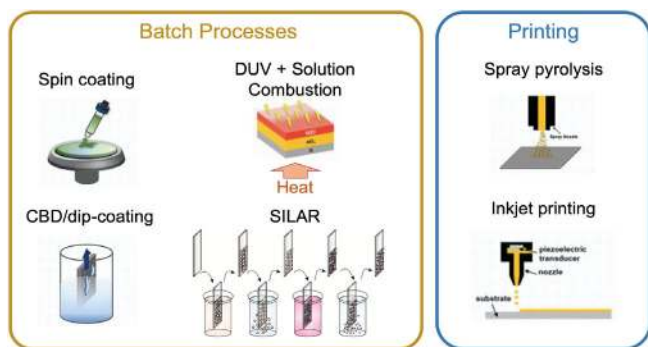
FIGURE 6 A schematic overview of solution chemical deposition processes discussed in Section 3.3 of this Review. DUV is Deep Ultra-Violet illumination. CBD is Chemical Bath Deposition. SILAR is Successive Ionic Layer Adsorption and Reaction. Adapted with permission from Park et al.[1] Copyright Wiley 2019

from the center.[1] This is known as the "coffee-effect". Efforts to overcome this include modifying the viscosity of the ink. For example, Hu et al added glycerol to their nickel precursor ink (comprised of nickel acetate dissolved in 2-methoxyethanol and complexed with mono-ethanolamine). By increasing the viscosity from 2.73 to 10.28 mPa s, droplets became uniform because the higher viscosity films had reduced capillary flow of particles from the center of the droplet to the faster-drying edges.[118]

Inkjet printing of nickel sol often requires high-temperature annealing after printing because the steps for forming the oxide are similar to spin-coating (Section 3.3.1). As with spin-coating, the deposition temperature can be lowered by pre-synthesizing the NiO_x as nanoparticles and dispersing them in a solvent (eg, water) to create an ink that can be deposited at room temperature without post-annealing, or with low-temperature post-annealing.[27,110] It is necessary to ensure that the nanoparticles are well suspended for the films to be uniform. Although this could be achieved using surfactants or capping agents, these would remain in the deposited film, which would reduce the temperature sensitivity of the NiO_x film or necessitate high-temperature post-annealing to remove the ligands. Huang et al found that an alternative to using surfactants was to maintain the pH between 2 and 8 to have a large zeta potential to prevent agglomeration, which was adjusted by adding strong acids and bases to the ink. Thermogravimetric analysis showed that an annealing temperature of at least 170°C was required to remove the water solvent and ethylene glycol additives. Annealing at ca. 200°C is compatible with a range of polymer substrates (Section 5).[27]

Ruscello et al reported another approach that required post-annealing at only 100°C. In this approach,

polyethylene oxide is added to the NiO_x nanoparticle ink as a sacrificial additive. Ethylene glycol was also added to increase the viscosity of the ethanol solvent in the ink to improve the morphology of the film deposited. The film was dried under vacuum before being annealed at 100°C for 10 minutes. Subsequently, the films were oxygen plasma treated for 1 minute. X-ray photoemission spectroscopy measurements showed that plasma treatment removed polyethylene oxide from the surface. From scanning electron microscopy measurements and device measurements, it was speculated that the role of the polyethylene oxide was to improve the dispersion of NiO_x nanoparticles in the film. However, too high polyethylene oxide resulted in pinholes that would lead to shunting when used as a hole transport layer in a solar cell.[119]

3.3.4 | Spray pyrolysis

Spray pyrolysis is another approach for depositing uniform NiO_x thin films over large area, with controllable thickness. In spray pyrolysis, liquid precursors are sprayed onto a heated surface, where they undergo pyrolytic reactions to form the oxide thin film. As such, spray pyrolysis requires a spray gun containing the precursor solution, atomizer for generating the spray, and a heated surface (eg, a hotplate), as well as a temperature controller. The atomizer is usually an ultrasonic nebulizer, electrostatic atomizer (forms droplets by exposing the liquid to short pulses of electric field), or air-blast atomizer (forms a spray by mixing the liquid with air).[120] The nickel precursors used are nickel chloride, nickel acetate, nickel acetylacetonate, nickel hydroxide, nickel sulfate, and nickel formate, which nickel chloride and nickel acetate being the most common.[120] The precursors are often in their hydrated form and deionized water is commonly used as the solvent because water takes part in the reaction.[120-126] Nickel chloride is popular because it can easily be dissolved in aqueous solvents and is readily available. The disadvantage is that HCl gas is evolved as a byproduct, which can corrode the spray pyrolysis equipment.[120] When droplets of hydrated nickel chloride solution are sprayed onto heated substrates, the solvent evaporates, solute deposits onto the substrate, and the hydrated nickel chloride then undergoes pyrolysis to form NiO_x.[121] However, the substrate temperature required to form crystalline NiO_x films was reported to be 300°C or larger,[120-122] with similar decomposition temperatures reported when using nickel acetate or nickel nitrate.[120,125,126] Spray pyrolysis is therefore not compatible with polymer substrates. However, across the different precursors, uniform, adherent, and crack-free NiO_x films have been achieved. The thickness of the films can

be controlled through the number of spray cycles used, but also with the precursor concentration, temperature, and volume of precursor sprayed.[120]

3.3.5 | Chemical bath deposition

Chemical bath deposition (CBD) is another low-cost method for growing NiO_x thin films. The substrates are suspended in a solution containing the Ni precursor and is held at room temperature or temperatures up to 100°C. The films formed are nickel oxyhydroxide (NiOOH) or nickel hydroxide (Ni[OH]$_2$), which need to be annealed at 300°C to 400°C in air to form NiO_x through decomposition of the hydroxide species.[23,127-130] CBD is therefore also not compatible with polymer substrates. However, the films grown by CBD are uniform and adherent to the substrate.

A common nickel precursor is nickel sulfate. Persulfate[23,127] and dichromate[128] additives need to be included in the mixed aqueous bath for the reaction to proceed, along with NH_3 to adjust the pH. Han et al reported that the persulfate played a direct role in reacting with nickel sulfate, such as no film formed without persulfate, although the exact reactions are not established.[23,127] Although the NiO_x phase appears at annealing temperatures above 300°C, XPS measurements have shown that OH^- species remain after annealing the films even at 500°C for 1 hour in air.[127] Another approach to forming NiO_x by CBD is to complex nickel sulfate with triethanolamine.[130] Nickel hydroxide films were formed at a temperature of 50°C after 1 hour, and post-annealing at 400°C in air was needed to form crystalline NiO_x.[130] Four-point measurements showed that after post-annealing at higher temperatures, the resistivity of the films reduced from 10^6 Ω cm to 10^3 Ω cm, along with an increase in the work function from 4.7 eV to 5.5 eV, showing the materials to become more p-type. XPS measurements showed the ratio of Ni^{2+} to Ni^{3+} peak to increase with increasing annealing temperature, suggesting fewer acceptor defects. But it is proposed that the increase in p-type conductivity is due to the filling of oxygen vacancies at higher annealing temperatures and a reduction in compensating defects.[130]

Apart from using nickel sulfate, nickel nitrate and urea can be used. During CBD growth, the bath needed to be held at 100°C for 1 hour. It is proposed that heating at 100°C decomposes urea to form CO_2 and NH_3, allowing the formation of Ni(OH)$_2$ from Ni^{2+}. The as-deposited films required post-annealing at 350°C to 400°C for 48 hours in air for NiO_x, which nevertheless retained surface hydroxyl groups.[129] However, temperature-dependent measurements showed that the activation energy for the resistivity was only 0.08 eV, which is significantly lower than the activation energy of NiO_x grown by spray pyrolysis.[121,129]

3.3.6 | Dip coating

Dip-coating is a variant of CBD that can produce homogeneous films at low-cost over large area. Dip-coating is advantageous because there is minimal waste of the precursors (unlike spin-coating) and the sol can be reused.[131] A substrate is dipped vertically into a solution containing the metal precursor, which is deposited onto both sides as the substrate is withdrawn. Just as with CBD and sol-gel, nickel nitrate, and nickel acetate can be used as the nickel precursors, dissolved in deionized water or ethylene glycol to form the sol.[132,133] Through dipping and withdrawing, a layer of sol adheres onto the substrate, the metal precursor undergoes hydrolysis, followed by condensation to form an extended framework as the film dries through evaporation.[131] To form NiO_x, the films from dipping required post-annealing at 400°C to 500°C for 2 hours in air, which is therefore not compatible with polymer substrates.[132,133] While the method reported by Wang et al resulted in phase-pure NiO_x (following annealing at 500°C), the method reported by Nazir Kayani et al, involving annealing at 400°C, which led to a large Ni_2O_3 diffraction peak. FTIR confirmed the presence of Ni_2O_3, as well as hydroxyl groups on the surface.[133]

In dip-coating, the thickness of the films depends on the viscosity, density and surface tension of the sol, concentration of the metal precursor, and the withdraw rate. The effect of the withdrawal rate can be understood by considering that there are two competing forces acting on the adsorbed sol: capillary forces and the weight of the sol that drains it. At lower withdrawal rates, capillary forces result in thicker films formed. Thus, increasing the withdrawal rate from very low results in thinner films. In contrast, at higher withdraw rates, the films become thicker with increasing rates because there is less time for the film to drain. Thus, withdrawal rates in between these regimes result in lowest thickness.[131]

3.3.7 | Successive ionic layer adsorption and reaction

Successive ionic layer adsorption and reaction (SILAR) is a form of layer-by-layer dip-coating. Instead of using one sol, multiple separate sols are used, with rinsing in between each step. In step 1, the substrate is immersed in a sol with a Ni^{2+} complexed with NH_3. The Ni^{2+} can be

TABLE 1 Comparison of the different growth techniques used for NiO$_x$ discussed in the review

Technique	Temperature range (°C)	Deposition time range[a]	Post-processing required?	Conformality	Large area compatibility	Flexible substrate compatibility	Precursor cost[b]	Equipment cost
Chemical vapor deposition	105-750	10 seconds to 20 minutes	No	High	High	Low	Medium	High
Atomic layer deposition	<100-800	10 to 160 minutes	No	Highest	High	Moderate	High	High
Sol-gel spin coating	60-350	<1 minute	Yes	Moderate	Moderate	High	Low	Low
Solution-combustion	200-300	Few minutes	Yes	Moderate	Moderate	High	Low	Low
Inkjet printing	RT-150	Few minutes	Yes	Moderate	Moderate	High	Low	Medium
Spray Pyrolysis	225-450	<1 minute	No	Moderate	High	Low	Low	Low
Chemical bath deposition	20-100	Few minutes	Yes	Moderate	Low	Low	Low	Low
SILAR	50-90	~10 minutes	Yes	Moderate	Low	Moderate	Low	Low

[a]Deposition time range for 10 nm thick film.
[b]Cost per 10 g of precursor, <£10 = low, £10-100 = medium, >£100 = high.

from $NiCl_2$ or $Ni(NO_3)_2.6H_2O$, and these are reacted with concentrated ammonia.[134-136] In the first step, the immersion time is 20 to 30 seconds.[134-136] In step 2, the substrate is withdrawn and immersed in hot deionized water. The temperature is usually 90°C and immersion time 7 to 20 seconds. After step 2, a layer of NiO$_x$ is formed. The film is then dried in air for 20-60 seconds at room temperature or 90°C. In step 4, the film is rinsed in deionized water to remove NiO$_x$ particles from the film.[134-136] X-ray diffraction measurements show that the films grown by SILAR have NiO diffraction peaks, which become stronger after post-annealing in air at 200°C to 400°C with strong {111} preferred orientation.[134] However, a challenge with SILAR is that the films formed can be cracked and still have adsorbed particles.[136] These particles could be removed through sonication or adjusting the pH of the sol in step 1 (eg, by adjusting the ratio of the nickel precursor and NH_3).[137]

To summarize and evaluate the advantages and disadvantages of the chemical growth methods discussed in this section, Table 1 provides a comparison of the key parameters. For example, it can be seen that whilst ALD offers the best conformality on the underlying structure, the growth rate is low and the precursor and equipment costs can be high in some cases.

4 | POST-DEPOSITION PROCESSING

To improve the properties of NiO$_x$ thin films, post-deposition treatments are often required. The most common processing is annealing, but other surface treatments, for example, with plasma or ultraviolet (UV) irradiation, are also commonly applied to modify the surface characteristics.

Annealing can be performed in oxidizing, inert, or reducing atmospheres, and is required especially if the films are prepared by solution deposition routes to ensure the complete removal of solvent residues from the films. Solution deposited films processed at low temperatures (<200°C) typically contain also significant fractions of nickel hydroxide species NiOOH and $Ni(OH)_2$ that can hinder (or sometimes help) the film performance in devices, and affect reproducibility. A post-deposition anneal is often added to the processing of solution deposited films, especially in the case of sol-gel spin- and dip-coating (Table S3). In addition to impurity removal and composition tuning, annealing can improve the thin film microstructure and enhance the crystallinity. However, the magnitude of changes in the different properties is strongly dependent on the film deposition and annealing conditions.[23,106,112,130,138-140]

Of the chemical vapor growth techniques, CVD is typically performed at the highest temperatures, at approximately 400°C (Table S1) and the film properties can be tuned by varying the deposition temperature and other growth conditions. Post-deposition annealing is generally not required even for epitaxial integration of the NiO$_x$ films. In ALD the typical deposition temperature is lower, ca. 200°C (Table S2). Post-deposition annealing in reducing atmospheres can be used as an alternative to H_2 plasma exposure to reduce the films to metallic Ni.[63,141,142] The effect of heat treatment on the NiO$_x$ film composition and properties has also been demonstrated. Bachmann et al showed that annealing at 700°C in air changed the Ni/O ratio in the films from 0.88 to 0.74, whereas annealing at the same temperature in Ar reduces the films to Ni metal.[39] On the other hand, rapid thermal annealing in N_2 at the same temperature has been shown to not have any effect on the optical properties of similar NiO$_x$ films.[143] In both examples, the films were grown by ALD using cyclopentadienyl

nickel and O_3. The effect of thermal treatment on the electrical properties of the ALD grown NiO_x films has also been investigated. For example, the annealing of 7.5 nm ALD NiO_x at 300°C in ambient conditions increased the work function of the film from 5.0 to 5.2 eV and the hole concentration from 4.9×10^{19} to 1.4×10^{20} cm^{-3}, which was associated with the decrease in hydroxide species on the film surface.[82] However, annealing has also been reported to lead to a decrease in the work function of the NiO_x films grown by solution processing, despite the observed decrease in the hydroxide species at the surface and in the bulk of the film.[139] Drastic changes in the carrier concentration upon annealing in oxidizing conditions, measured by electrochemical Mott-Schottky analysis have also been reported by others.[63,80] Thimsen et al reported the increase in hole concentration from 1.4×10^{17} to 7.3×10^{21} cm^{-3} in ALD NiO_x when annealed in an oxygen atmosphere at 600°C.[80] In these cases, the increase in carrier concentration can be directly linked to the increase in the amount of Ni vacancies in the films.

Post-deposition annealing has also been shown to be critical to device performance. For example, switching characteristics of thin-film transistors with solution deposited NiO_x active layers are significantly improved after annealing at 300°C to 350°C, while higher annealing temperature results in degradation in device characteristics (see Table 3 in Section 6.2). In addition, annealing of PEALD NiO_x hole transport layers at 300°C in air for 20 minutes was shown to improve the power conversion efficiency of the lead-halide perovskite solar cells from 13.89% to 17.07%.[81] However, the annealing conditions need to be tailored to each type of film and application to ensure optimized performance.

While being an effective way to tune the properties of thin films, heat treatments ≥300°C are not compatible with temperature-sensitive materials, such as plastic substrates used for flexible electronics. Therefore, alternatives have gained increasing attention. This is especially the case for photovoltaics, where tuning the work function is important for the optimization of the band alignment. Plasma treatments have proven to be beneficial. The additional advantage of the plasma treatment is the change in the surface wettability, which can enable the solution processing of additional layers on top of the NiO_x.[145,146] Oxygen plasma treatment is also commonly used to increase the work function of the films, and its effect, attributed to the increase in Ni vacancies as well as to the formation of NiOOH species has been well documented for films deposited by various techniques.[79,139,146-148] O_2 plasma treatments are less sensitive to the specific operating conditions than annealing. For example, Ullrich et al observed an increase in the work function of solution-processed NiO_x films from 4.4-4.9 eV to 5.5-5.6 eV with a 1-minute oxygen

plasma treatment with 900 W plasma power at 0.3 mbar pressure,[139] while a similar increase from 4.4 to 5.5 eV in APMOCVD NiO_x films was achieved also after a 3 minutes treatment with 100 W plasma power.[147]

Another post-processing technique to improve the quality of NiO_x films is UV-ozone treatment. Islam et al did a thorough investigation into the changes in the electrical properties of solution deposited NiO_x films after UV-ozone treatment.[149] They concluded that UV-ozone exposure, like oxygen plasma treatment, increases the number of hydrogen-containing nickel species on the film surface and induces the formation of Ni vacancies, which increases film conductivity. Similar UV-ozone treatments on ALD NiO_x in metal-insulator-semiconductor (MIS) structures showed a significant Schottky barrier height reduction.[149] UV-ozone treatment has proven to be especially effective in the fabrication of light-emitting-diodes (LEDs), where it improves the hole injection properties of the NiO_x films (refer to Section 6.5).[150,151] For example, Sun et al observed a significant improvement in the performance of quantum dot LEDs (QLEDs) when the NiO_x hole injection layer (HIL) was UV-ozone (UVO) treated for 20 minutes (Figure 7).[151] They attributed this improvement to the formation of nickel oxyhydroxide surface dipoles and Ni vacancies, as shown in the measured XPS spectra of the pristine and UVO-treated samples in Figure 7A-D, where the deconvoluted peaks associated with the oxyhydroxide and other Ni^{3+} defects increased significantly after UVO treatment. They demonstrated that this increased the work function of the NiO_x, and reduced the band bending at the interface of the NiO_x HIL and poly(9-vinylcarbazole) (PVK) hole transport layer, as shown in Figure 7E. This resulted in a smaller hole injection barrier and improved hole-injection, as evidenced by the higher hole current density in single-carrier devices and lower peak capacitance voltage (Figure 7F,G). As a result of the improved hole injection, the external quantum efficiencies increased from 8.3% (no UV-ozone treatment) to 10.9% (20 minutes UV-ozone treatment).[151]

UV-irradiation alone has also gained attention as a means to reduce the post-annealing temperature for sol–gel spin-coated oxide films. Illuminating a film immediately after spin coating with deep UV light (eg, 253.7 nm wavelength) can cleave alkoxyl groups, remove C and initiate condensation reactions for the formation of M-O-M bonds, resulting in densification.[115,152] As a result, the post-annealing temperature required can be significantly reduced from 300°C to 200°C. Kim et al showed with indium zinc oxide films that deep UV irradiation alone is sufficient to achieve operational TFTs, in which the irradiation process resulted in the film temperature reaching only 150°C.[115] Such an approach would be important for
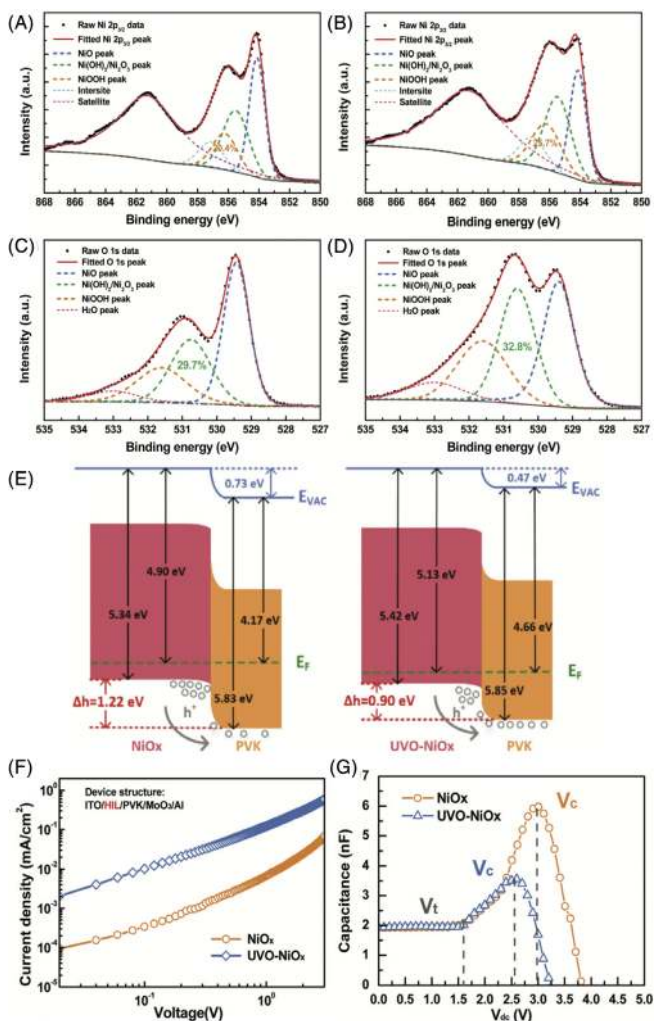
FIGURE 7 Deconvoluted Ni $2p_{3/2}$ and O $1s$ XPS spectra of, A and C, as-prepared and, B and D, UVO treated NiO$_x$. E, Influence of the UVO treatment on the band bending at the NiO$_x$/PVK (poly (9-vinylcarbazole)) interface. F, J-V characteristics of a hole-only quantum-dot-based light-emitting diode (QLED) device made to demonstrate the improved hole transport behavior of UVO treated NiO$_x$. G, C-V characteristics of QLEDs with NiO$_x$ and UVO-NiO$_x$. Reproduced with permission from Sun et al.[151] Copyright The Royal Society of Chemistry 2019

oxides grown by solution processing on polymeric substrates, since the required annealing temperature is significantly reduced. UV irradiation has been used to improve the properties of NiO$_x$ for tailored applications, such as electrochromics[153] and resistive switching random access memory devices.[152] Another approach to anneal solution-processed oxides at low temperature is flash lamp annealing. In this approach, a short (tens of ms), high brightness pulse of white light (introducing approx. 100 J cm^{-2}) is used to heat the spin-coated film and induce M-O-M bond formation. Researchers have also combined flash lamp annealing with a pre-exposure

to deep UV and near-infrared irradiation to hydrolyze the alkoxyl groups and initiate condensation prior to flash annealing. This was demonstrated with amorphous indium gallium zinc oxide films, with no post-annealing required,[154] and is an approach that could be adopted for solution-processed NiO$_x$.

5 | NICKEL OXIDE THIN FILMS FOR FLEXIBLE ELECTRONICS

5.1 | Growing importance of flexible electronics and their applications

Although the bulk of the work on NiO$_x$ and other oxides for electronics has focused on rigid substrates, there is an increasing demand for flexible, light-weight, stretchable, and soft devices.[1,4,155] This is to meet the requirements for a wide range of emerging applications, including smart labels, wearable electronics, flexible solar cells, epidermal devices, artificial skins, biomimetic medical implants, advanced surgical tools, curved displays, and foldable appliances.[4] But as well as fulfilling new consumer needs, electronics based on flexible substrates have the potential to be processed with higher throughput with a small footprint through roll-to-roll processing,[6] which can lead to lower production costs. The flexible substrates used are usually polymers, but cellulose and fabrics have also recently gained attention.[4,6,9] The key difference with traditional rigid electronics is that the processing temperature of the active layer material is limited to lower temperatures to avoid degrading the substrate used. Figure 8A presents the glass transition temperature of common polymer substrates. From this, it can be seen that most polymer substrates can only be processed at low temperature. Polyimide (PI) can be processed at 360°C to 400°C, but PI tends to be expensive. The lower cost and more common polymers, such as polyethylene terephthalate (PET) and polycarbonate (PC), have lower glass transition temperatures of 80°C and 147°C, respectively.[1]

5.2 | Current trends and challenges in nickel oxide growth on flexible substrates

Metal oxides have gained wide attention as the active layer material for flexible electronics.[1,9] This is because metal oxides have high transmittance, excellent mechanical properties, can be processed at low cost with low process complexity, can be grown at scale, and have electronic properties that are widely tunable.[4] Although most work has focused on n-type metal oxides, p-type oxides are
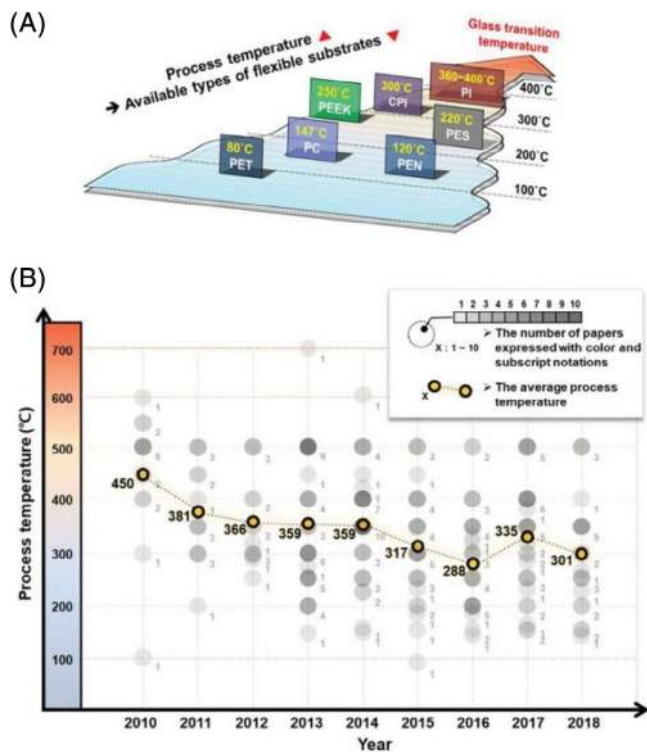
FIGURE 8 A, Flexible polymer substrates and their glass transition temperatures and B, trend in the average processing temperature of oxides made by solution processing. Reproduced with permission from Park et al.[1] Copyright Wiley 2019

essential for flexible CMOS (which is required for low power transistors), hole transport layers in flexible solar cells, and hole injection layers in flexible displays, flexible p-n diodes for AC-to-DC conversion, among other applications.[1,4,9,155] NiO_x has important advantages over the other p-type oxides investigated in flexible electronics (SnO and Cu_2O) due to its higher phase stability.[1,4,118] While the average processing temperature for metal oxides have been decreasing (Figure 8B), making them more suited to flexible substrates, the processing and post-processing of NiO_x (Sections 3 and 4) has tended to occur at >300°C. There has therefore been substantial work to develop routes for growing NiO_x with suitable electronic properties at lower temperatures compatible with most polymer substrates (eg, refer to Section 3.3).

Physical vapor deposition has traditionally been a common route to grow NiO_x thin films at low temperature, even close to or at room temperature. For example, Münzenrieder et al reported room temperature deposition of NiO_x by DC magnetron sputtering from a metallic Ni target, and 50% Ar-50% O_2 process gas. The temperature of the PI substrate used did not exceed 35°C, and the NiO_x films were confirmed to be p-type by Hall effect measurements.[155] Room-temperature growth by sputtering was also demonstrated by Wang et al, who

reported amorphous NiO_x films. Their XPS measurements also revealed the presence of a significant fraction of defective sites associated with Ni vacancies.[156] Solution-based approaches are also commonly used for depositing NiO_x onto flexible substrates and have the advantages of being processable in ambient air, without the risk of plasma damage to the polymer substrates. An important challenge related to solution processing, however, is that post-deposition annealing is often required to crystallize the films and remove the organic residues, often at above 350°C (refer to Section 3.3.1).[1] Reduced annealing temperatures to 190°C have been reported, but required longer annealing times of 10 hours to fully remove the solvent.[157] Spin-coating also results in high wastage of the precursor solution and the films are not uniform over large areas.[1] Making the processing of oxides compatible with the low glass transition temperatures of polymer substrates has been a challenge. Three of the methods that have currently been the most investigated for NiO_x on flexible substrates are inkjet printing, printing of pre-made NiO_x nanoparticles, and solution combustion synthesis, and these are discussed in Sections 3.3.1–3.3.3. However, as discussed in Sections 3 and 4, chemical vapor deposition routes, especially ALD have significant potential in low-temperature growth of metal oxide films.

It is critical that flexible electronics are reliable under distortion. Flexible electronics can be broadly categorized as those that are stretchable vs those that are non-stretchable. Stretchable electronics typically are based on an elastomeric substrate, such as polydimethylsiloxane, and need to be tested under stretching as well as bending. Flexible electronics based on polymer substrates (such as PI and PET) are bendable but not stretchable. In this case, the main test is static bending, in which the devices are bent to a certain radius of curvature. This can be achieved by taping the substrate to a curved surface that is either concave (device in compression) or convex (device in tension). The devices also need to be tested after repeated bend cycles. Techniques for doing this include push-to-flex, roller-flex, and one-belt-bending testing. In push-to-flex, the device is connected to two parts and the distance between these is decreased and increased repeatedly to change the device from bent to flattened. The advantage of this test is that it is simple, but the disadvantage is that the bending radius is not controlled and the location in the device that is bent is not controlled. In roller-flex, the device is wrapped around a tube with a well-defined radius. The device is pulled onto the roller and released to curve it to a well-defined radius repeatedly. However, concave bending could damage the device. On-belt-flex attaches the device onto a flexible belt, which is moved over a roller so that the device is curved when moving over the roller and flattened otherwise. This protects the

TABLE 2 Comparison of the state-of-the-art performance of devices using NiO_x covered in this review

Device	Role of NiO_x	NiO_x growth method	Key performance parameters	Performance values	References
Resistive switching	Active layer	Spin-coating	ON/OFF ratio	10^5	160
			Endurance	10^5 cycles	
			Retention	10^4 seconds	
Thin-film transistors	Active layer	Spin-coating	I_{on}/I_{off}	$\sim 10^5$	105
			μ_{FE}	25 cm^2 V^{-1} second^{-1}	
p-nheterojunctions	p-type layer	ALD	Leakage current	10^{-8} A cm^{-2}	80
			Rectification ratio	$\sim 10^4$ (1.2 V vs leakage current)	
Photovoltaics	Hole transport layer	Solution processing (nanoporous films)	Absorber layer	Lead-halide perovskite	161
			PCE	19.1%	
LEDs	Hole injection layer	Spin-coating	Emitter	FIrpic in TCTA:26DczPPy host	162
			EQE	16.2%	
			CIE coordinates	(0.14,0.30), blue-green	
Thermistors	Active layer	Inkjet printing of nanoparticles	Material constant for thermistor	4300 K	27
			Temperature coefficient of resistance	−5.84% K^{-1}	

device more during the test.[158] Static bend testing of electronics in which NiO_x is used as an active layer (ie, p-n diodes, thin film transistors, and thermistors) involved bending to a radius of curvature that is typically 10 mm.[155] It has been reported that cracks did not form in 120 nm thick NiO_x thin films prepared by reactive sputtering until the bend radius was below 10 mm.[27,155] Duan et al compared the efficiency of lead halide perovskite solar cells based on spin-coated NiO_x nanoparticles and found the performance to be similar when the device had a radius of curvature of 20 and 10 mm to when the device was flat. But when the radius of curvature was below 5 mm, the efficiency decreased.[159] It is also important to have metal electrodes with sufficient adhesion to the flexible substrate or active layers, and that the metal is sufficiently ductile to avoid cracking during the bend test. Metals that have been used with NiO_x include Ti,[155,156] Au,[155] Ni,[114] and Ag.[114]

6 │ NICKEL OXIDE THIN FILMS IN DEVICES

NiO_x plays a wide range of roles across multiple devices. In this section, we cover its application in resistive switching and thin-film transistors, where NiO_x is the active layer. We next cover p-n junctions, as well as photovoltaics and light-emitting diodes (LEDs), which make use of heterojunctions. We finish with a section on sensors, which includes thermistors. Table 2 gives a comparison of the state-of-the-art performance across these different device types, along with a selection of some of the important performance parameters. More detailed tables are given for thin-film transistors (Table 3) and photovoltaics (Table 4). We emphasize that many of these applications are not evaluated solely based on one parameter, and the device considered to have the "best" performance would depend on the application and the relative importance of different properties. Thus, the entries in Table 2 should be considered as examples of some of the highest performances achieved in different applications. Detailed discussions can be found in the respective sections for each device application.

6.1 │ Resistive switching

6.1.1 │ Properties and processing of NiO_x for resistive switching

Resistive switching random access memory (RRAM, ReRAM) is an emerging non-volatile information storage technology relying on electrically induced changes in the resistance of thin films. Resistive switching has been demonstrated in many different metal oxides, and the

TABLE 3 p-type thin-film transistors with NiO_x active layers deposited by chemical deposition methods, device structure, and performance

NiO_x deposition	TFT conf.	Dielectric	Electrodes (G, S, and D)	Annealing temperature (°C)	I_{on}/I_{off}	V_{th} (V)	SS (V dec^{-1})	μ_{FE} (cm^2 V^{-1} second^{-1})	Note	References
Spin-coating	bg	100 nm SiO_2	Si, Ni	200	$\sim10^3$	1.8	5.0	0.004	—	106
				250	4×10^4	12.8	2.3	0.07	—	
				300	40	18.1	5.2	0.078	—	
				350	3.8×10^4	12.2	6.1	0.003	—	
		50 nm Al_2O_3	Si, Ni	250	$\sim10^3$	−1.3	0.25	4.4	—	
Spin-coating	bg	100 nm SiO_2	Si, Ni	200	$\sim10^4$	10	4.1	~0.001	—	105
				300	10^5-10^6	15	2.2	0.73	—	
				400	10^4-10^5	17	3.6	0.24	—	
				500	$\sim10^4$	13	3.8	0.01-0.1	—	
		30 nm Al_2O_3		300	$\sim10^5$	−0.5	0.7	25	—	
Spin-coating	bg	ZrO_2 (unspecified thickness)	Si, Ni	150	10	—	—	—	5% Cu:NiO_x	101
				250	10^3	−0.25	0.18	0.03	5% Cu:NiO_x	
				350	$\sim10^4$	0.33	0.14	1.05	5% Cu:NiO_x	
Spin-coating	bg	100 nm Al_2O_3	Mo, Au	280	2.27×10^4	−1.04	0.5	0.36	—	144
				330	1.23×10^4	−1.24	0.44	0.17	—	
				280	9.8×10^5	−1.44	0.24	0.97	5% Sn:NiO_x	
				330	1.1×10^5	−1.32	0.24	0.33	5% Sn:NiO_x	
Solution combustion	bg	100 nm SiO_2	Si, Ni/Au	250	—	—	—	3.8×10^{-5}	—	112
				300	—	—	—	0.011	—	
				350	—	—	—	0.015	—	
				300	—	—	—	3.6×10^{-6}	—	
Solution combustion	bg	100 nm ZrO_2	ITO, Ni	150	10	−2.07	—	—	5% Li:NiO_x	114
				250	$\sim5 \times 10^4$	0.18	0.98	1.38	5% Li:NiO_x	
				150 + UV	10	−4.33	0.94	10^{-5}	—	
					$\sim10^4$	−1.05	0.62	0.02	1% Li:NiO_x	
					8×10^6	0.16	0.21	1.69	5% Li:NiO_x	
					$\sim10^3$	5.47	0.71	3.15	10% Li:NiO_x	
			(PET substrate)	150 + UV	10^5	—	0.54	1.41	5% Li:NiO_x	
Solution combustion	bg	ZrO_2 (unspecified thickness)	Si, Ni	150 + UV	30	—	—	—	—	101
					10^2	−0.6	0.48	10^{-4}-10^{-3}	2% Cu:NiO_x	
					10^4	0.45	0.13	1.5	5% Cu:NiO_x	
					5×10^2	1.2	0.54	1.87	10% Cu:NiO_x	
Solution combustion	bg	10 nm ZrO_2	ITO, Ni	150 + UV	9×10^2	0.6	0.27	0.7	5% Cu:NiO_x	101
		15 nm ZrO_2			8×10^3	0.3	0.22	1.3	5% Cu:NiO_x	
		24 nm ZrO_2			8×10^3	0.1	0.21	1.1	5% Cu:NiO_x	
		37 nm ZrO_2			10^3	−0.2	0.35	0.3	5% Cu:NiO_x	
Inkjet printing	bg	100 nm SiO_2	Si, Au	280	4.30×10^2	5.2	5.64	0.01	—	118
		50 nm Al_2O_3			5.30×10^4	−0.6	1.37	0.78	—	
		100 nm Al_2O_3			1.56×10^4	−3.5	1.68	0.41	—	

Abbreviation: bg, bottom gate.

switching properties of nickel oxide have been known since the 1960s.[180]

For resistive switching memory devices, there a number of device requirements. These include achieving high on-off ratios with low operating voltages, high endurance (defined as the number of SET/RESET cycles the device can undergo above certain on-off resistance ratio), and retention, which is the length of time for which the device resistance states remain stable after the SET/RESET operation. In addition, device scaling and uniformity are important parameters for practical applications. One mechanism for switching involves conductive filament (CF) formation of Ni vacancies or oxygen vacancies. This process is random and hence gives wide variation in high resistance states (HRS, OFF-state) and low resistance states (LRS, ON-state). The CF bridges the contacts and is formed by the collection of vacancies at structural defects when voltage is applied (LRS), and joule heating leads to the rupturing of the CF in the high resistance state (HRS).[98,181] For uniform LRS and HRS,

TABLE 4 PVs with nickel oxide hole transport layers

Device structure	NiO$_x$ deposition method	Post-deposition treatment	Band gap (eV)	Work function (eV)	PCE (%)	Notes	References
ITO/NiO$_x$/CH$_3$NH$_3$PbI$_3$/ PCBM/BCP/Al	Sol-gel spin-coating	Anneal at 300°C + UV-ozone treatment	—	5.4	7.8	LHP	104
ITO/NiO$_x$/BiOI/ZnO/Al	Sol-gel spin-coating	Anneal at 300°C	3.6	4.8	1.8	—	108
ITO/NiO$_x$/Perovskite/ PCBM/Al	AP-SALD (CVD mode)	20 seconds oxygen plasma treatment	3.76	5.4	17.1	LHP	46
ITO-PEN/NiO$_x$/ CH$_3$NH$_3$PbI$_3$/PCBM/Ag	Chemical precipitation	Anneal at 130°C	3.7	—	13.43	Flexible	163
ITO/NiO$_x$/P3HT:PCBM/ Ca/Al	Chemical precipitation	No treatment	3.64	5.25	3.83	OPV	111
ITO/NiO$_x$/CH$_3$NH$_3$PbI$_3$/ PCBM/Ag	ALD	Anneal at 300°C	—	5.02	16.43	LHP	82
FTO/NiO$_x$/ CH$_3$NH$_3$PbI$_3$/PCBM/Ag	Spin-coating	Anneal at 275°C	—	4.89	14.91	LHP	164
ITO/NiO$_x$/CH$_3$NH$_3$PbI$_3$/ PCBM/BCP/Ag	Nanoparticle spin-coating	Anneal at 150°C + UV-ozone treatment	—	5.24	15.9	LHP	165
ITO-PEN/NiO$_x$/ CH$_3$NH$_3$PbI$_3$/PCBM/Au	Nanoparticle spin-coating	Anneal at 150°C + UV-ozone treatment	—	5.24	11.8	LHP	165
FTO/TiO$_2$/ CH$_3$NH$_3$PbI$_3$/NiO$_x$/Ag	Nanoparticle spin-coating	No treatment	—	5.24	9.11	LHP	165
ITO/NiO$_x$/P3HT:PCBM/ Ca/Al	Spin-coating	Anneal at 250°C + oxygen plasma treatment	—	4.33	3.6	OPV	102
Glass/Mo/CIGSe/ZnO/ NiO$_x$/PTAA/Perovskite/ C$_{60}$/SnO$_2$/IZO/LiF	ALD	No treatment	—	—	21.6	Tandem	166
ITO/NiO$_x$/P3HT:PCBM/ Al	PLD	No treatment	3.6	5.4	5.16	OPV	15
ITO/NiO$_x$/P3HT:PCBM/ BCP/LiF/Al	O$_2$ plasma treating evaporated Ni	No treatment	3.3	5.0	3.54	OPV	167
ITO/NiO$_x$/P3HT:PCBM/ Al	RF sputtering	No treatment	3.65	—	3.26	OPV	168
AZO/NiO$_x$/P3HT: PCBM/Al	RF sputtering	No treatment	—	—	3.15	OPV	169
ITO/NiO$_x$/P3HT:PCBM/ LiF/Al	RF sputtering	No treatment	—	—	2.8	OPV	170
ITO/NiO$_x$/MoO$_3$/ZnTPP (or H$_2$TPP)/C$_{60}$/BCP/Al	Thermal oxidation of sputtered Ni	No treatment	3.5	5.0	—	OPV	171
ITO/NiO$_x$/PCDTBT: PCBM/Ca/Al	Spin-coating	Anneal at 300°C + oxygen plasma treatment	3.6	5.3	6.7	OPV	172
ITO/nc-TiO$_2$/P3HT: PCBM/NiO$_x$/Ag	Thermal evaporation	No treatment	3.3	—	1.45	OPV	173
ITO/NiO$_x$/P3HT:PCBM/ Al	Spin-coating	Anneal at 500°C	3.71	—	1.97	OPV	174

T A B L E 4 (Continued)

Device structure	NiO$_x$ deposition method	Post-deposition treatment	Band gap (eV)	Work function (eV)	PCE (%)	Notes	References
ITO/NiO$_x$/P3HT:PCBM/ LiF/Al	Inkjet printed	Anneal at 400°C + UV-ozone treatment	—	5.14	2.59	OPV	175
ITO/SnO$_2$/triple-cation perovskite/NiO$_x$/Au	Nanocrystal spin-coating	No treatment	—	4.19	12.7	LHP	176
ITO/NiO$_x$/P3HT/PCBM/ Ca/Al	ALD	Oxygen plasma treatment	3.56	5.32	3.4	OPV	79
ITO/SiO$_x$/NiO$_x$/P3HT: IC$_{60}$BA/Ca/Al	ALD	Oxygen plasma treatment	3.7	5.4	4.1	OPV	148
ITO/NiO$_x$/(FAPbI$_3$)$_{1-x}$(MAPbBr$_3$)$_x$/PCBM/ ZnO/Ag	Solution deposition	Drying at 100°C (12 hours) + anneal at 300°C	—	—	19.10	LHP	161
ITO/NiO$_x$/CH$_3$NH$_3$PbI$_3$/ ZnO/Al	Sol–gel spin-coating	Anneal at 300°C	—	5.05	16.1	LHP	177
ITO/NiO$_x$/pDTG-TPD: PCBM/LiF/Al	Solution deposition	Anneal at 275°C	—	5.19	7.8	OPV	107
ITO/NiO$_x$/PCDTBT: PCBM/Ca/Al	Spin-coating	Anneal at 400°C + oxygen plasma treatment	—	5.0	5.2	OPV	178
ITO/NiO$_x$/TQ1:PCBM/ LiF/Al	Nanocrystal spin-coating	Anneal at 175°C + UV-ozone treatment	—	5.6	6.08	OPV	179

as well as other properties, control over the vacancy density, and therefore the conductivity of the oxide, is critical. Other mechanisms involve tuning the Schottky barrier height, as well as charge-trapping processes which are highly dependent on defect concentration. All switching processes relate to control of defect concentration, but this is difficult to achieve in oxides by standard deposition methods.[182] To achieve greater performance in oxides, elimination of conductive filaments is necessary, as well as very careful control of oxygen vacancy concentrations, other intrinsic defect concentrations, and background electronic concentrations. A summary of some of the different performances achieved using chemical and physical deposition methods is given below.

CVD grown films were demonstrated by Min et al, who used dimethylamino methylbutanolate nickel (Ni (dmamb)$_2$) to grow NiO$_x$ for Pt/NiO$_x$/Pt capacitor structures.[49] Their example device had SET, RESET, and forming voltages of 1.3, 0.6, and 2.45 V, respectively, with a current compliance of 10 mA, and order of >10^2 difference between the LRS and

HRS. Ni(dmamb)$_2$ precursor has also been used in ALD processing with ozone to grow NiO$_x$ films for similar Pt/NiO$_x$/Pt stacks by You et al, who demonstrated 10^4 difference between the HRS and LRS, with SET, RESET, and forming voltages of 1.7, 1.0, and 8.1 V, respectively.[98]

The resistive switching properties of ALD grown NiO$_x$ with different metal electrode materials have also been evaluated. Song et al studied the growth of NiO$_x$ from bis (ethylcyclopentadienyl) nickel (Ni(EtCp)$_2$) and O$_2$ plasma.[73] Lamperti et al compared the ALD films grown using Ni(Cp)$_2$ precursor and O$_3$ on different electrode materials (Si, Ni, Pt, W, and TiN) and compared the film properties to the films deposited by e-beam evaporation.[183] They observed that the electronic density of the films grown by ALD was closer to the bulk values, and that the films grew on substrates with sharp and well-defined interfaces, making the technique attractive for future CMOS integration.[183] The devices with corresponding 25 to 30 nm ALD NiO$_x$ films had HRS of 10^6 to 10^8 Ω cm and LRS of 10^2 to 10^4 Ω cm after forming at 5 to 8 V.[184]

The switching of NiO_x is typically considered to be unipolar, that is, the same voltage polarity is used for both SET and RESET,[98,181] with the switching characteristics being independent of the electrode size in submicron devices,[185] but bipolar switching has also been demonstrated.[73,152] The type of switching has been shown to be dependent on the electrode materials used. For example, NiO_x films grown by PEALD exhibited unipolar switching when grown on Pt substrates, while bipolar behavior was observed on films with W bottom and Pt top electrodes over a wide temperature range of 25°C to 100°C.[73]

Wang et al demonstrated the viability of spin-coated NiO_x in write-once-read-many-times (WORM) memory devices, that base on irreversible switching from HRS to LRS, and investigated the effect of the film thickness to the WORM characteristics. The films were deposited using nickel acetate tetrahydrate and annealed at 550°C, and were measured to be oxygen-rich by SEM-EDX. They observed, that stable switching was only obtained with thicker (>80 nm) films with endurance better than 10^4. The current conduction mechanism in their WORM device is hopping and ohmic conduction, before and after writing, respectively, and it was concluded that the CF is formed by both Ni vacancies and Ag ion migration from the Ag top electrode in the $Ag/NiO_x/ITO$ devices.[186]

Besides digital on-off switching between the LRS and HRS, the potential of NiO_x in so-called memristor devices has also been acknowledged.[187] There the analog switching with multiple resistive states is attributed to Schottky barrier change at the oxide-electrode interface and migration of oxygen ions when an electric field is applied or to the changes in the local size of the CF.[152,160,187] The analog switching has been demonstrated in NiO_x films grown by solution deposition routes. Kannan et al prepared NiO_x films by sol-gel spin coating and demonstrated a performance of the $ITO/NiO_x/Al$ memory devices with four programmable resistive states, as well as stable device operation within retention times up to 10^4 seconds.[160] Similar behavior was observed also by Chu et al who prepared device stacks with spin-coated NiO_x and Pt and Ag bottom and top electrode, respectively.[152] Analog resistive switching was also observed in solution combustion processed films by Li et al, however, after the complete electroforming the performance of the device was changed to digital.[187]

Generally, the performance of chemically deposited NiO_x films in resistive switching devices does not significantly differ from films grown by PVD techniques.[184,188,189] The devices show adequate retention and endurance properties, but exhibit a wide variation in the resistive switching parameters. As resistive switching of PVD grown NiO_x has already been demonstrated on flexible substrates, such as PET[190] and Cu foils,[156] it might be assumed that chemical deposition routes could be adapted to memory devices for flexible electronics.

6.1.2 | NiO_x for flexible resistive switching

The high on-off ratio in NiO_x has been shown to be robust to bending in the films. Wang et al fabricated resistive switching devices on flexible copper foil, which acted as both the substrate and bottom electrode (with evaporated Ti as the top electrode). The NiO_x was deposited by reactive sputtering. The forming voltages reported were low, with the SET voltage required to reach the LRS only 0.75 V, and the RESET voltage to switch to the HRS only −0.95 V. After curving to compression and tension, the current-voltage sweeps were identical to the flat state. The performance remained stable after 200 bending cycles, with 85% of all devices showing similar resistive switching behavior. The SET voltage ranged from 0.6 to 0.95 V, and RESET voltage −0.7 to −1.15 V. Cui et al also reported NiO_x to be mechanically robust. In their case, they used a p-n junction of spin-coated NiO_x and TiO_2 nanoparticles. This p-n junction was deposited onto ITO-coated PET flexible substrate and had a solution-processed GaIn electrode on top. Fifty endurance cycles were applied, with a strain of 0.79% applied to the substrate. It was found that the LRS remained stable, while the HRS had some fluctuation. Overall, the ON/OFF ratio remained between 10^2 and 10^3, with a SET voltage of 1.0 V and RESET voltage of −0.8 V. The extrapolated ON/OFF ratio after 10 years is expected to be only 11.1% lower than the initial value. Finite element analysis modeling suggested that the main failure mechanism would be due to the formation of cracks initiating at grain boundaries that prevent the migration of conductive filaments (eg, oxygen vacancies).[191]

6.2 | Thin-film transistors

6.2.1 | Properties and processing of NiO_x for thin-film transistors

Metal oxide semiconductors have received attention for applications in thin-film transistors (TFTs), pushed forward by the successful realization of TFTs with n-type oxides, such as indium gallium zinc oxide (IGZO). However, the development of next-generation transparent electronics, especially low power complementary metal-oxide-semiconductor circuits (CMOS) for display applications, is being held back by the lack of high-performance

p-type oxide materials. In many p-type materials, the hole concentration is limited by the high formation energy of the acceptors for hole formation, for example, cation vacancies. As discussed in Section 2, this is not a major issue with NiO_x where the Ni vacancies readily form in oxygen-rich conditions, however, the large hole effective mass and low mobility limit the conductivity.[13] There is a great need to get p-type materials with sufficient carrier concentrations and mobilities in excess of a few cm^2 V^{-1} $second^{-1}$ to make p-type TFTs. Together with SnO and Cu_2O, NiO_x has been listed to be a potential candidate for p-type oxide TFTs and CMOS-devices, due to its tunable hole conductivity by controlling the nickel vacancy formation. However, there are only a few reports demonstrating transistor operation. Among these reports, most of the NiO_x films have been deposited with solution processing methods. The reported TFT performance with solution-processed NiO_x active layers are presented in Table 3.

Li et al used chemical combustion synthesis to fabricate NiO_x films for backgate TFTs with thermal SiO_2 as a gate dielectric. The TFTs with films annealed at 250°C to 400°C showed switching, but the switching ratios were modest (I_{on}/I_{off} < 10) and the maximum field-effect mobility achieved was μ_{FE} = 0.015 cm^2 V^{-1} $second^{-1}$.[112] The poor performance was attributed to the bad ohmic contact between the p-channel and the top electrodes, as well as the defects in the p-channel. Carbon impurities also remained in the films even after annealing, potentially degrading the device performance even further.[112] Liu et al attempted UV-ozone treatment with spin-coated NiO_x TFTs, but the switching properties were poor. However, the derived hole mobility of the devices was 0.141 cm^2 V^{-1} $second^{-1}$. They also investigated the effect of UV-Ozone treatment of the NiO_x on the device performance. While a significant improvement in hole injection properties in organic LEDs with similar films was observed, the hole mobility in TFTs was not affected by the UV-ozone treatment.[150] Spin-coating of NiO_x for TFTs was more successfully applied by Liu et al.[106] After annealing at 250°C their devices had a switching ratio of I_{on}/I_{off} ≈ 4 × 10^4 and a field-effect mobility of μ_{FE} = 0.07 cm^2 V^{-1} $second^{-1}$. The mobility was increased significantly to μ_{FE} = 4.4 cm^2 V^{-1} $second^{-1}$ when solution deposited Al_2O_3 was used as a gate oxide.[106] Using similar solution deposited amorphous NiO_x p-channel and Al_2O_3 dielectric layer even higher field-effect mobility, 25 cm^2 V^{-1} $second^{-1}$ was demonstrated by Shan et al.[105] The result is surprising, as the devices with the similar NiO_x layers spun on thermal SiO_2 have a mobility of <1 cm^2 V^{-1} $second^{-1}$. However, this is currently the highest reported value for field-effect mobility of a NiO_x TFTs, including devices with films made by physical vapor deposition methods.[192,193] The significant increase in the mobility when the SiO_2 dielectric is replaced by a high-k material has been explained by the reduced Fermi level pinning and trap state density in the dielectric-NiO_x interface. Doping is known to improve the p-type conductivity by valence band dispersion,[101] and successful attempts to improve the TFT performance by doping with Li,[114,194] Cu,[101] and Sn[144] have been demonstrated, but the mobilities have still been fairly modest, in the order of 1 cm^2 V^{-1} $second^{-1}$.

Recently, Hu et al demonstrated switching TFTs using inkjet-printed NiO_x films deposited from nickel acetate-based ink. Annealing studies showed that the best device performance was achieved through 280°C post-annealing in air (Figure 9), which resulted in the removal of excess NiOOH-species and optimal vacancy concentration in the amorphous films.[118] They also investigated the effect of the gate dielectric, and the best TFT characteristics (−0.6 V threshold voltage and field-effect mobility of 0.78 cm^2 V^{-1} $second^{-1}$) were achieved using 50 nm thick ALD Al_2O_3.[118]

The large discrepancies in the reported results demonstrate the challenges of manufacturing high performance p-type TFTs, and such large variations in the transfer properties is common for all p-type oxide TFTs.[13] As discussed earlier, the hole mobility in NiO_x is low, and defects in the films significantly suppress the mobility further. The density of such defects, including metal interstitials, higher valence state impurities, and grain boundaries, is strongly dependent on the processing and post-processing method and conditions. While high-mobility devices have been demonstrated by solution deposition, the limited uniformity of the film properties and reproducibility of the device performance hinders the use of solution processing in TFT manufacturing. Interestingly, there are as yet no reports on the use of CVD and ALD for depositing NiO_x p-channels for TFTs, though ALD grown films of other p-type oxide materials have been shown to perform in these devices.[91] Additionally, the device performance is dependent on the quality of the dielectric layer and the semiconductor/dielectric interfaces, and reducing the concentration of interface traps is critical for improving the mobility. In all the chemical deposition processes, the control of interfaces can add complexity as the effect of the additional chemistries (eg, solvents in solution processing and ligands in CVD and ALD precursors), need to be considered. Until the reproducible fabrication of high-mobility NiO_x device stacks are established, the low hole mobility of NiO_x films limits their effective implementation in CMOS. However, this could, to some extent, be compensated by device component scaling. More work is also required to investigate the stability of NiO_x-based devices under different
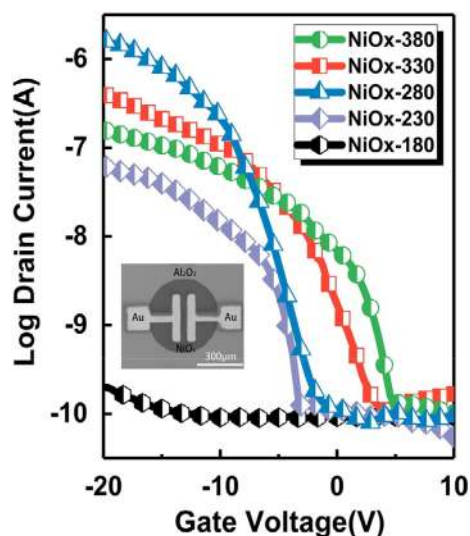
FIGURE 9 Transfer characteristics of p-type thin-film transistors (TFTs) with inkjet-printed NiO_x semiconducting channel, annealed at different temperatures in air. Inset shows an SEM image of a device. Reprinted with permission from Hu et al.[118] Copyright Elsevier 2018

conditions, although the first results on the negative bias stress measurements appear to be promising.[105]

6.2.2 | NiO_x for flexible thin-film transistors

Solution-processed TFTs have been reported to have similar performance on flexible substrates as on rigid substrates. For example, Yang et al used solution combustion synthesis, combined with deep UV irradiation to deposit NiO_x thin films that were annealed at only 100°C, which was compatible with flexible PET substrates. The NiO_x was doped with 5% Li to improve the mobility. The field-effect mobility, on/off ratio and subthreshold swing (SS) voltage for the flexible TFTs were $\mu_{FE} = 1.41$ cm^2 V^{-1} second^{-1}, $I_{on}/I_{off} = 10^5$, and SS = 0.54 V dec^{-1}, respectively. These were similar to the TFTs on rigid substrates, which were $\mu_{FE} = 1.69$ cm^2 V^{-1} s^{-1}, $I_{on}/I_{off} = 8 \times 10^6$, and SS = 0.21 V dec^{-1}. The threshold voltage was low (0.16 V). This was achieved by controlling the Li content to balance the higher on current and higher carrier concentration obtained with increasing Li. Higher carrier concentrations result in larger threshold voltages because a larger electric field is then required to deplete the active layer. For example, increasing the Li content to 10% resulted in the threshold voltage increasing to 5.47 V, along with a reduction in the switching ratio due to a higher off-state current.[114]

6.3 | p-n Heterojunctions

p-n heterojunctions are made from a p-type semiconductor in intimate electrical contact with an n-type semiconductor. This can be achieved by depositing a compact thin film of one of these semiconductors over a thin film of the other. At the heterojunction, the majority carriers are depleted, resulting in band bending and the formation of a built-in electric field. This built-in field leads to rectification, in which significant current will only flow when the p-n heterojunction is under forward bias (ie, a positive voltage is applied with the positive terminal connected to the p-type layer and negative terminal to the n-type layer). The current as a function of voltage is described by the diode equation, and the physics of p-n junctions are detailed in many textbooks, such as Reference 195. The p-n heterojunction is used in diodes, which can convert AC voltage (eg, from the mains or a triboelectric generator) to DC voltage through a rectifier circuit.[196] The key advantage of using wide band gap oxides, such as NiO_x, is that the devices have high transmittance, enabling transparent electronics, which are important for wearable devices and displays.[196] Beyond rectifiers, the p-n heterojunction forms the basis of a wide range of electronic devices, including photovoltaics (Section 6.4), in which the built-in electric field is essential for separating photogenerated carriers. p-n heterojunctions are also used for photodetectors, LEDs (Section 6.5) and sensors.[4,13]

The quality of a diode made from a p-n heterojunction is described by the ideality factor (η), the rectification ratio (ratio of current under forward and reverse bias), the reverse-bias current density (leakage current), and maximum reverse-bias before the device undergoes breakdown (breakdown voltage).[196] A perfect diode would have an ideality factor of 1, high rectification ratio, low leakage current, and significantly negative breakdown voltage. A diode ideality factor between 1 and 2 can occur when more than one carrier is involved in recombination (eg, radiative or Auger recombination). But often ideality factors exceed 2, which can be due to tunneling of carriers through the p-n heterojunction, multi-level recombination or shunting.[197,198] These effects can also result in the reverse-bias current density having a high saturation value, or not saturated at all. As such, p-n heterojunctions are useful for evaluating the quality of NiO_x grown by new chemical processing methods. For example, Thimsen et al[80] and Holden et al[78] grew NiO_x by ALD using novel precursors. These films resulted in leakage currents of 10^{-8} A cm^{-2} and 10^{-2} A cm^{-2}, respectively.[78,80] TiO$_2$ and n-Si were used as the n-type layers, respectively, in these heterojunctions. Although the diode ideality factors were well above 2

(ranging from 3.5 to 4.5),[78,80] the leakage currents and ideality factors were comparable to heterojunctions based on NiO_x grown by sputtering.[78,199] These high diode ideality factors were attributed to structural imperfections and interface defects states at the heterojunction.[155]

While the literature is lacking in reports of chemical-deposited NiO_x in flexible p-n heterojunctions, there are demonstrations with physical-vapor deposited NiO_x. Münzenrieder et al paired sputtered NiO_x with sputtered n-type indium gallium zinc oxide (IGZO), which is a high-mobility amorphous oxide[155] that can be deposited at room temperature.[3] This at least shows the potential of using NiO_x in flexible p-n heterojunctions. Ti top and bottom electrodes were used. A threshold voltage of approximately 1 V was obtained, with an on/off ratio of 10^3 to 10^4 and ideality factor of ca 3.2.[155] These values are comparable to Cu_2O/IGZO p-n diodes prepared on flexible polyethylene naphthalate (PEN) substrates by sputtering.[200] The NiO_x/IGZO diodes were strained in tension and compression by 0.25% by bending to a radius

of 10 mm (Figure 10). Under strain, the resistances at voltages >1 V were reduced, more so under compression than under tension. But between voltages of 0.1 and 0.4 V, when the current was controlled by the diode, the resistance decreased under tension, but increased under compression. IGZO is known to decrease its resistance under tension but increase under compression.[155] This is because the mobility has been found to increase under tension and decrease under compression.[201] Indeed, IGZO has been found to behave in a similar way to silicon and have a linear dependence of mobility with strain, and it is believed that the increase in mobility under tensile strain is due to the conduction band tail reducing.[202] In contrast, the resistance of metals increases under tension but decreases under compression. The contrasting changes in resistance may account for the different changes in resistance under tension/compression for the diodes at 0.1 to 0.4 V vs at >1 V. It is suggested that NiO_x changes its resistance in a similar way to IGZO.[155]

This is possible since amorphous and polycrystalline NiO_x also have band tails. But measurements would still need to be made to establish how the mobility varies with strain. We note, however, that these diodes based on sputtered heterojunctions had high leakage current (Figure 10). In contrast, the ALD NiO_x/TiO_2 reported by Thimsen et al had a significantly lower leakage current and higher rectification ratio. Both the TiO_2 and NiO_x were deposited at 250°C or lower, and are therefore compatible with flexible substrates. This motivates the future development of p-n heterojunctions based on chemical-deposited NiO_x.
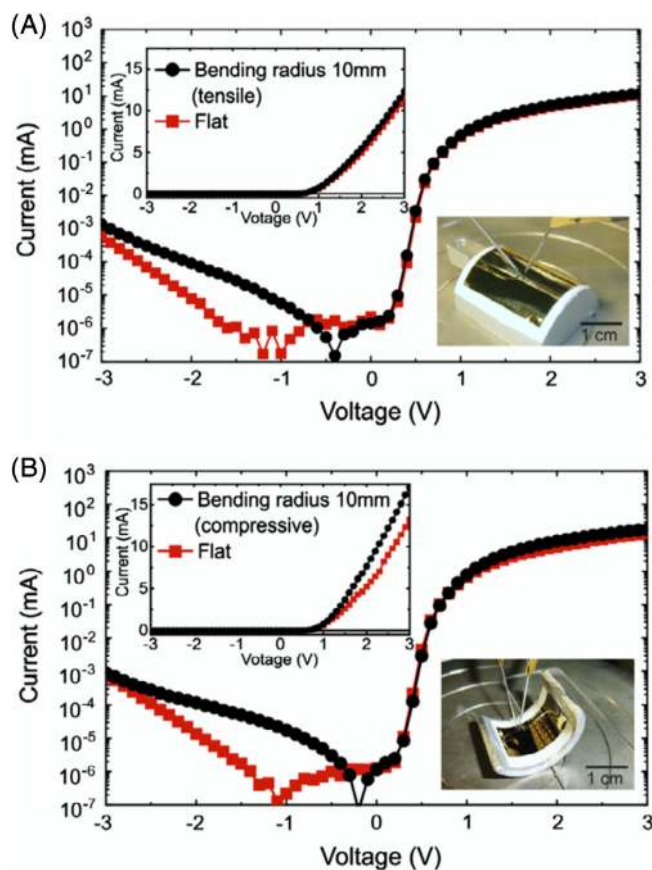

FIGURE 10 Performance of NiO_x/IGZO p-n junctions in the unstrained state vs (A) under tensile strain and (B) compressive strain. Inset photographs illustrate how the diodes are tested under static bending by taping the samples to a curved substrate with a fixed bending radius. Reprinted with permission from Münzenrieder et al.[155] Copyright Elsevier 2013

6.4 | Photovoltaics

6.4.1 | Properties and processing of NiO_x for photovoltaics

Nickel oxide is one of the most prominent p-type metal oxide materials investigated as a hole transport layer in solar cells due to its high stability in air, high transmittance to visible light and high work function that is easily tunable.[203] NiO_x was investigated in p-type dye-sensitized solar cells in the early 2000s.[204] Since then, NiO_x has been commonly investigated for organic photovoltaics (OPV) and more recently, in lead-halide perovskite (LHP) based devices. Initial work on NiO_x interlayers for OPVs was based on physical vapor deposition techniques (sputtering and pulsed laser deposition), but has since shifted to solution-based processing routes due to the simplicity, low-cost and reproducibility of these methods.[15,168,205-207]

For the photovoltaic (PV) community, the important parameters for hole transport layers include the band gap (transparency to visible light), electron affinity (which needs to be low to block electrons), and work function, which affects the band alignment between NiO_x and the absorber, and therefore how easily holes can be extracted. Hole transport layers also need to be conformal and pinhole-free to prevent shunting in devices. NiO_x has a band gap of ~3.6 eV and a tunable work function between 4.8 and 5.4 eV (shown in Table 4) which is ideal for many solar absorbers (Figures 11 and 12). The mobility of solution-processed NiO_x films are, however, typically low, and the values have not been widely reported in PV-based papers. The focus for most PV-based papers has been on optimizing the band alignment with the absorber, which is achieved by tuning the work function through optimizing the processing conditions and/or post-deposition processing. Some of the film properties of NiO_x films and the performance of the films in devices (mostly OPV and LHP) are collected in Table 4. There is a limited number of reports on chemical vapor deposition techniques because these methods require high growth temperatures which are often incompatible with the transparent conductive oxide. CVD deposition systems can also be expensive.[209,210]

Usually, NiO_x would be deposited beneath the absorber in a p-i-n device structure. This affords the widest range of fabrication techniques for the hole transport layer since there is no risk of damaging the absorber. The transparent conducting oxide-coated glass substrate is also more stable against different processing conditions.

There have been extensive studies on solution-processed NiO_x for organic solar cells, with differing polymer blends for the photoactive layer, different solvents for the NiO_x precursor, annealing temperature, and post-deposition treatments. Work function tuning results in values >5.0 eV and power conversion efficiencies (PCEs) between 3.6% and 7.8%.[102,107,172,178,179] The band alignment for common organic materials with charge transport layers are shown in Figure 11. In addition to solution processing, Shim et al reported the first use of ALD deposited NiO_x for polymer solar cells using Ni-AMD (Nickel Alkyl Amidinate) and H_2O precursor, with a deposition temperature of 150°C. Then, 25 nm films, with a band gap of 3.7 eV, were oxygen plasma treated for 3 minutes following deposition, which increased the work function from 4.7 eV to 5.4 eV with the formation of nickel oxyhydroxide species or nickel vacancies on the surface. In this device, a P3HT:IC_{60}BA blend was used as the photoactive layer and a PCE of 4.1% was achieved.[148] Another study deposited NiO_x using a nickel bis(N,N′-di-tert-butylacetamidinate) precursor (heated to 125°C) and unheated deionized water as the oxidant, with a reaction temperature of 200°C and pressure of $1·10^{-1}$ Torr.[79] Prior to spin-coating the photoactive layer, the NiO_x film was oxygen plasma treated for 7 seconds. Analysis of the XPS core spectra revealed the presence of Ni^{2+} vacancies, which should increase the p-type conductivity (Section 2).
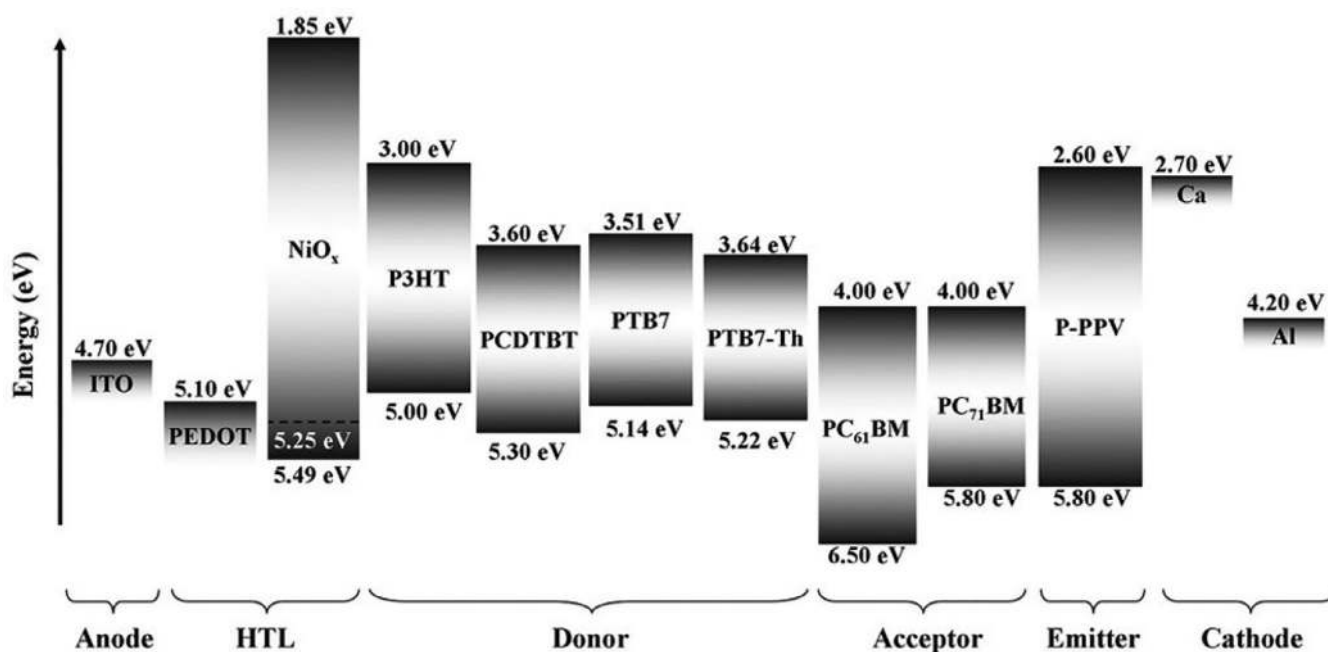

FIGURE 11 Detailed energy levels of different materials used in OPVs and OLEDs. Reprinted with permission from Jiang et al.[111] Copyright Wiley 2015
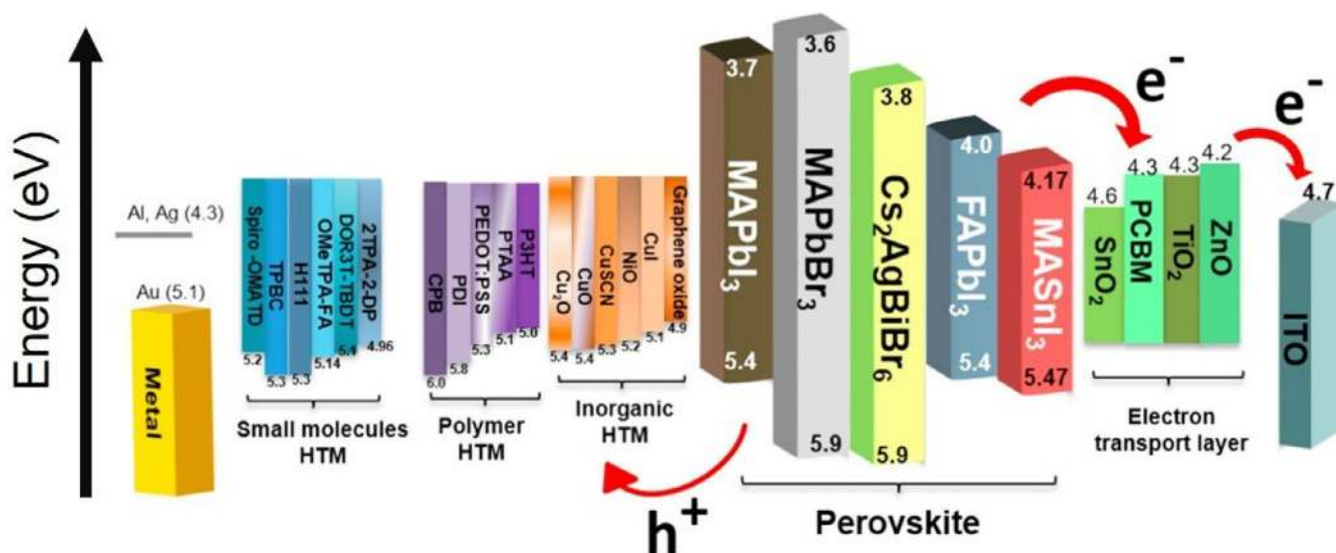
FIGURE 12 Energy levels of charge transport layers used in perovskite solar cells. Reprinted with permission from Bakr et al.[208] Copyright Elsevier 2017

However, the conductivity was low. The hole concentration of NiO_x films was $\sim10^{14}$ cm^{-3} from Hall measurements (which, of course, is a limited approach—refer to Section 2). But it was evident that the amount of Ni^{2+} vacancies was insufficient. Nevertheless, the 4 nm films had high transmittance reaching 95% over 400 to 600 nm wavelength. The band gap was found to be 3.56 eV and the work function increased from 5.12 eV to 5.32 eV with oxygen plasma treatment. The formation of Ni cation vacancies, as well as the formation of NiOOH (nickel oxyhydroxide) species, are usually the cause of increased work function with oxygen plasma treatment. The increased work function matched well with the highest occupied molecular orbital (HOMO) of P3HT in P3HT: PCBM bulk heterojunctions. The PCE (3.4%) was comparable to that of devices using poly(3,4-ethylenedioxythiophene):polystyrene sulfonate (PEDOT:PSS), which had an efficiency of 3.5%. PEDOT:PSS is a commonly used solution-processed hole transport layer in organic and LHP solar cells. But the high optical transmittance of NiO_x compared to PEDOT:PSS resulted in higher short-circuit current density, but the fill factor (FF) was lower, likely due to the low conductivity of the NiO_x.[79]

You et al reported a high-efficiency p-i-n LHP device (16.1%) using sol-gel spin-coated NiO_x which resulted in stable performance over 60 days, compared to just 5 days for PEDOT:PSS.[177] The improved V_{OC} leading to higher PCE was attributed to the favorable band alignment between the valence band maximum of NiO_x and the perovskite photoactive layer. Mali et al demonstrated the use of solution-processed nanoporous NiO_x films, which

exhibited excellent device air stability over 160 days (compared to 5-6 days for PEDOT:PSS) and a higher efficiency of 19.10% with $(FAPbI_3)_{0.85}(MAPbBr_3)_{0.15}$ as the photoactive layer.[161] The NiO_x films were dried at 100°C for 12 hours and annealed further at 300°C for 90 minutes before depositing the perovskite, which was crucial to optimize the morphology and electrical properties of the NiO_x film.

There are also a number of reports of ALD NiO_x in p-i-n LHP devices. The advantage of ALD is the ability to deposit pinhole-free ultrathin films. For example, Seo et al deposited 7.5 nm thick NiO_x in a p-i-n LHP stack with a high efficiency of 16.4%.[82] Annealing the films at 300°C increased the work function from 5.0 to 5.2 eV due to a reduction in the hydroxide groups on the surface. This resulted in improved band alignment between the HTL and the perovskite. Zhao, Lee et al demonstrated the use of an atmospheric pressure spatial ALD reactor operated in CVD mode to grow 30 nm NiO_x films for LHP solar cells.[46] The RMS roughness of the films was only ~0.6 nm, whereas other deposition techniques would yield surface roughnesses between 5-20 nm. Analysis of the Ni 2p and O 1 second XPS core level spectra revealed that the composition was $NiO_{1.13}$ and therefore non-stoichiometric. Through electrochemical impedance spectroscopy, the mobility of the films was determined to be $\sim3 \times 10^{-3}$ cm^2 V^{-1} second^{-1}. The band gap was 3.76 eV and work function 5.7 eV. LHP devices using NiO_x were more efficient than devices with PEDOT:PSS. This was attributed to the reduced surface roughness of the NiO_x (helping to reduce trap-assisted recombination) and the favorable energy alignment with the perovskite compared

to PEDOT:PSS. However, the contribution of surface roughness is unclear. Park et al reported surface roughness values of 2 to 5 nm for electrochemically deposited NiO_x, which was shown to enhance the fill factor and power conversion efficiency of devices.[211] A rougher surface has been believed to increase the contact area between the perovskite and hole extraction layer, and the exact role of surface roughness is in debate.

The most efficient LHP solar cells (currently certified at 25.2%) are based on a n-i-p structure with solution-processed mesoporous or planar TiO_2 as the electron transport layer (ETL), and organic hole transport layers (HTLs) on top.[212] HTLs are usually spiro-OMeTAD and PTAA. But Liu et al attempted to use spin-coated NiO_x nanoparticles instead, and this gave devices with ∼15% efficiency.[165] In contrast, p-i-n devices with doped NiO_x HTL below the perovskite have maximum reported PCEs of ∼20.5%.[213] Metal oxide HTLs are more cost-effective than their organic counterparts, which motivates the replacement of the organic HTL in n-i-p perovskite devices with inorganic HTLs. An option is to spin-coat oxide nanoparticles over the perovskite, but a solvent needs to be selected that does not degrade the perovskite layer (ruling out polar solvents). Chlorobenzene and other nonpolar solvents can be used.[165] Tirado et al investigated chemically precipitated NiO_x nanoparticles functionalized with oleic acid, oleylamine, and dispersed in chlorobenzene to form hydrophobic nanoparticles. No post-deposition treatment was required and the formation of the hydrophobic nanoparticles was believed to have led to the improved device stability that was found. The devices retained 90% of the initial PCE (12.7%) after 1008 hours in ambient air.

Beyond LHPs, NiO_x is being investigated for use in lead-free perovskite-inspired materials. We have reported the use of sol-gel spin-coated NiO_x for use in BiOI-based devices.[108] In this p-i-n device architecture, NiO_x was spin-coated and annealed at 300°C for 1 hour on ITO-coated glass before growing BiOI on top. However, the NiO_x has a work function of 4.8 eV, which is sub-optimal for BiOI, which has a deep work function of 5.1 eV. The resulting downwards band bending of BiOI at the NiO_x interface was found to be detrimental to charge extraction in the devices. In other systems, ultrathin (3-4 nm) polycrystalline NiO_x was grown by ALD onto CdTe based solar cells at 200°C.[214] The CdTe cells were annealed at 150°C for 30 minutes before testing. For materials characterization, a 30 nm thick layer of NiO_x was used. The RMS roughness of the 30 nm film was found to be 1.7 nm. The films had high transmittance, greater than 80% for wavelengths longer than 500 nm and a band gap of 3.55 eV. The addition of NiO_x to the CdTe device stack improved the efficiency from 7.57% to 8.69% which arose from an improvement in the V_{OC} and fill factor.

Section 4 on post-deposition processing outlines some of the most prominent techniques that the community uses to improve the NiO_x thin film properties, and are especially relevant when NiO_x is used as hole transport layers. Annealing, oxygen plasma treatment, and UV-ozone treatment (examples of which are in Table 4) are all used to tune the work function of NiO_x for improved band alignment with the photoactive layer.

Whilst there has been significant emphasis on tuning the work function of NiO_x, it has been reported that another parameter that may be more important is the effect of the NiO_x layer on the formation of the photoactive layer on top. For example, despite the low work function, solution-processed NiO_x played a key role in allowing sufficiently compact BiOI to form on top by chemical vapor deposition to achieve rectifying devices. In particular, the NiO_x enabled a slanted (012) preferred orientation of the BiOI, which allowed the high mobility direction of the BiOI platelets to connect the top and bottom electrodes.[108] Similar reports of the effect of NiO_x on the quality of the interface formed with polymer photoactive layers have been made.[107]

An important area of future work in NiO_x is in addressing the low conductivity. This is important for achieving higher efficiency devices. Discussions around this are beyond the scope of this Review but research groups are exploring routes to doping NiO_x with Li, Mg, Cu, or Cs to circumvent the high resistivity and low mobility. The review by Xiu et al contains summaries of the significant studies conducted into doping NiO_x.[215]

6.4.2 | NiO_x for flexible photovoltaics

Nickel oxide has been investigated as a hole transport layer in flexible LHP and organic solar cells. While spin-coating requires high-temperature annealing to avoid forming a contact barrier in the PV device, barrier-less extraction has been reported when using low-temperature processing with the spin-coating of NiO_x nanoparticles. Zhang et al deposited NiO_x nanoparticles by spin-coating at room temperature with no post-annealing. p-i-n structured methylammonium lead iodide devices on flexible PET/ITO substrates had an efficiency of 14.5%, which was close to the performance of similar devices on rigid substrates (17.6%). The lower performance was due to a lower fill factor (70.5% for flexible and 78.4% for rigid) and short-circuit current density (20.7 mA cm^{-2} for flexible and 21.8 mA cm^{-2} for rigid). This was attributed to the higher series resistance and lower transmittance of the ITO on the PET substrate. The

flexible devices retained 80% of the initial efficiency after 140 bending cycles.[110]

The same process for depositing NiO_x nanoparticles was used by Jiang et al for organic solar cells, including P3HT:PCBM bulk heterojunction devices. It was found that as-deposited NiO_x nanoparticles gave the highest performance (3.8%) compared to spin-coated NiO_x that was then post-annealed at 50°C to 300°C. This can be attributed to the reduction in work function, especially when post-annealing at above 200°C (Section 3.3.1), resulting in reduced open-circuit voltages in the solar cells.[111]

After a repeated bending, NiO_x forms cracks that ultimately result in a decrease in device performance. Duan et al used polydopamine to cross-link NiO_x nanoparticles in thin films. This was prepared by adding dopamine hydrochloride to an aqueous solution of NiO_x nanoparticles, which was spin-coated onto ITO-coated PET substrates and annealed at 120°C for 30 minutes. The cross-linked NiO_x films exhibited greater resilience for cracking. The films without cross-linking cracked after only 50 bending cycles, whereas perovskite devices with cross-linked NiO_x retained 70% of the original efficiency after 1000 cycles. Notably, this was achieved with a bending radius of 5 mm.[159] In contrast, sputtered NiO_x was reported to crack for bending radii less than 10 mm.[155] The device performance achieved with the cross-linked NiO_x was also higher (18.3% with cross-linking compared to 15.9% without cross-linking). The improvements were mainly in the open-circuit voltage, which was attributed to the higher quality perovskite film deposited on the cross-linked nickel oxide.[159]

6.5 | Light-emitting diodes

6.5.1 | Properties and processing of NiO_x for light-emitting diodes

Nickel oxide has been widely used as hole injection layers (HILs) in organic and quantum dot light-emitting diodes (OLEDs and QLEDs, respectively). This is due to the high work function of nickel oxide, enabling it to inject holes into a wide range of emitters. By far the most common method used to grow NiO_x for OLED and QLED applications is solution processing. The important metrics for LEDs include the luminance (L, cd m^{-2}), maximum current efficiency (CE$_{max}$, cd A^{-1}) power efficiency (PE, lm W^{-1}), and external quantum efficiency (EQE, %). The EQE depends on the hole injection efficiency, the balance between electron and hole current density in the emissive layer, and on the photoluminescence quantum yield of the emissive layer, which are all affected by the hole

injection level and the degree of non-radiative recombination at the interface between the HIL and emitter.[216] PEDOT:PSS is one of the most common HILs in OLEDs and QLEDs, but many groups have recently been exploring NiO_x as an alternative, owing to its greater stability, wide band gap and higher work function.[217,218]

Liu et al used solution-processed NiO_x HILs, and they reported that this gave one of the most efficient OLEDs with a tris(8-hydroxyquinolinato)aluminum emitter.[150] Improved performance was achieved by increasing the annealing temperature of the spin-coated NiO_x HIL from 275°C to 500°C. This resulted in an increase in the grain size from 10 nm to 30 nm, which improved hole injection and transport. UV-ozone treatment (for 5-10 minutes) on the NiO_x surface was shown to further improve the hole injection efficiency to 80%, which was higher than the hole injection efficiency of PEDOT:PSS. The OLEDs with NiO_x also had a higher power efficiency (75.5 ± 1.8 lm W^{-1}) than devices based on PEDOT:PSS (43.2 ± 1.0 lm W^{-1}), and also improved device stability (>6 weeks for NiO_x, compared to 2 weeks for PEDOT:PSS).[150]

Liu et al also reported that the NiO_x HILs annealed at the lowest temperature of 275°C had the lowest performance, and this was partly due to the presence of remnant hydroxyl groups on the surface, which reduces the work function and the hole injection efficiency.[150] The detrimental role of oxyhydroxide surface defects found on sol-gel spin-coated NiO_x films has also been reported by Chen et al, in which it was proposed that this accentuated exciton quenching at the emitter/HIL interface.[162] This was overcome by using a bilayer HIL based on NiO_x/PEDOT:PSS. NiO_x/PEDOT:PSS HILs used in a blue phosphorescent device exhibited a maximum current efficiency of 30.5 cd A^{-1} and maximum EQE of 16.2%, which are higher than the values reported for OLEDs with just NiO_x HILs or PEDOT:PSS HILs.[162]

Hyrbid QLEDs based on organic and inorganic charge-injection layers exhibit EQEs of approximately 20%, whereas all-inorganic QLEDs have typical EQEs of ~1% even though they demonstrate higher stability.[219-222] The limited EQE of QLEDs based on NiO_x was attributed to the low hole mobility, which reduces charge balance. However, Vasan et al fabricated a high-efficiency all-inorganic stack using alloyed CdSe/ZnS quantum dot emitters, with ZnO nanoparticles as the electron injection layer and solution-processed NiO_x as the HIL.[223] The mobility of the synthesized NiO_x thin film is reported to be $2.5 \cdot 10^{-4}$ cm^2 V^{-1} second^{-1} for films annealed at 500°C for 30 minutes in air. Even with a 1.8 eV hole injection barrier between the NiO_x and QD interface, a luminance of 120 000 cd m^{-2} at 10 V applied bias was achieved. This value is significantly higher than

previously reported all-inorganic QLEDs.[219] The EQE reached a maximum of 11.4% and a current efficiency of 144 cd A^{-1} was achieved.[223]

To improve the band alignment between NiO$_x$ and CdSe/ZnS core-shell QDs, Cao et al doped NiO$_x$ films with Cu.[224] Cu doping of nickel oxide at a level of 3 mol% increased the work function of NiO$_x$ from 5.4 to 5.6 eV. This resulted in more efficient hole injection, and a smaller charge imbalance, resulting in improved performance. Further increases in Cu content beyond 3 mol% resulted in reduced mobilities and decreased performance. The Cu-doped NiO$_x$ films were prepared through the sol-gel process, and mixing nickel nitrate hexahydrate and copper acetate tetrahydrate precursors together to form the sol. The films were annealed at 275°C to 475°C for 1 hour. Cu:NiO$_x$ films annealed at 275°C showed the best performance with a turn-on voltage of 3.0 V, maximum luminance of 61 030 cd m^{-2}, maximum EQE of 10.5%, CE$_{max}$ of 45.7 cd A^{-1} and a maximum power efficiency of 18.0 lm W^{-1}. These were improved over devices based on undoped NiO$_x$ annealed at 475°C.[224]

Beyond OLEDs and QLEDs, there has been an explosion of interest in lead-halide perovskite LEDs (PeLEDs). Like organic and QD materials, LHPs can be facilely grown through solution processing. The band gap (and therefore the emission wavelength) can be tuned from 1.55 eV to 3.2 eV by changing the halide composition (from iodide to bromide to chloride) or through quantum confinement (as QDs or nanoplatelets).[217] LHPs are advantageous over Cd-based QDs and organic emitters because they have been demonstrated to achieve significantly narrower, color-pure emission peaks, making them competitive for applications in ultra-high definition displays.[216,217] Through passivation, many perovskite compositions are now achieving photoluminescence quantum yields approaching unity.[217] The device structures investigated for PeLEDs are based on the structures used in OLEDs and QLEDs. As such, PEDOT:PSS has been a common HIL deposited under the perovskite. But it has been shown that the PEDOT:PSS surface is defective, and there is usually significant quenching of the emission in the perovskite layer.[217] NiO$_x$ has been widely explored as an alternative. Recently, Lee et al found that green-emitting formamidinium lead bromide (FAPbBr$_3$) crystallized with a lower trap density on NiO$_x$ than on PEDOT:PSS, resulting in reduced nonradiative recombination and improved charge balance. Both factors enabled higher EQEs of 14.6%, compared to only 4.2% for PeLEDs based on PEDOT:PSS.[218] However, other groups have found it necessary to add passivating interlayers between the NiO$_x$ and perovskite emitter to avoid quenching. This is especially important for blue-emitters, which have a wide band gap and a large hole-injection barrier if NiO$_x$ alone is used as the HIL. Gangishetty et al found that solution-processed NiO$_x$ quenched the emission of blue-emitting (469 nm wavelength) CsPbBr$_x$Cl$_{3-x}$ QDs, and it was speculated that this may be due to interface defects or charge transfer.[225] Although Gangishetty et al switched to an interface-modified organic HIL,[225] Liu et al were able to achieve efficient sky-blue PeLEDs (emitting at 483 nm wavelength) using 7 nm NiO$_x$ covered with the polymer TFB, as well as PVK. The TFB/PVK layer was 18 nm thick, and using this full-stack for hole injection and transport, an EQE of 9.5% was achieved, which, at the end of 2019, was the highest for sky-blue PeLEDs.[226]

6.5.2 | NiO$_x$ for flexible light-emitting diodes

Nickel oxide has also been used to fabricate foldable OLED displays.[227] Kim et al deposited NiO$_x$ by solution processing (using a sol-gel method) onto indium zinc oxide-coated PI substrates and annealed at 250°C. Tris(2-phenylpyridine) iridium (III) in a host of tris-[1-phenyl-1Hbenzimidazole] was used as the emissive layer, sandwiched between organic hole and electron transport layers. The organic LED was folded with a bend radius of 0.3 mm. After 1000 bending cycles, the luminance loss was only 7.8%. After 10 000 cycles, the luminance loss was 25.7%. The current density, luminous efficiency, and power efficiency remained very similar after 10 000 bend cycles compared to the initial performance.[227]

Sun et al reported the use of nickel oxide as an HIL in flexible quantum dot LEDs. These LEDs used green-emitting Cd$_x$Zn$_{1-x}$Se$_y$S$_{1-y}$ quantum dots on flexible PEN substrates. The strategy used to lower the deposition temperature of the solution-processed nickel oxide so that it was compatible with PEN was to use solution combustion synthesis (Section 3.3.2). Nickel nitrate hexahydrate was used as the oxidizer and acetylacetone as the fuel, and an ignition temperature of only 150°C was required. Whilst devices using nickel oxide outperformed those based on PEDOT:PSS as the control, the flexible LEDs were less efficient than LEDs based on rigid substrates (4.8% vs 10.9% EQE for LEDs on flexible vs rigid substrates respectively).[151] Future efforts to understand the factors limiting the performance of flexible devices (eg, distortion of the substrate during spin-coating) compared to their rigid counterparts are needed. Nevertheless, Sun et al demonstrated a low-temperature process for improving the performance of the nickel oxide HIL. This was achieved through room-temperature UV-ozone treatment, which resulted in an increase in the content of surface nickel hydroxide and Ni^{3+}, along with an

increase in the work function of the nickel oxide. This resulted in a reduction in the hole injection barrier, which increased the hole current density and improved the LED performance.[151]

6.6 | Sensors

6.6.1 | Properties and processing of NiO$_x$ for sensors

Oxide semiconductors have been utilized in a wide range of sensing applications, including the measurement of gas, temperature, biological substances, and so on. Gas sensors are the most common sensing application for p-type oxides, where they benefit from a more stable baseline and low humidity sensitivity compared to their n-type counterparts despite having generally a slightly lower sensitivity. Controlling the carrier concentration of the p-type oxide enables the fabrication of gas sensors with high sensitivity and selectivity. Potential additional advantages of p-type oxides include an improvement in recovery speed by oxygen absorption,[12] enhanced stability of the NiO$_x$ toward temperature and humidity, as well as ease of fabrication of NiO$_x$ films and nanostructures. These have made NiO$_x$ perhaps the most intriguing p-type oxide for gas sensors.[228] The gas sensing properties of NiO$_x$ have been demonstrated for several different gases, including ethanol, formaldehyde, NO$_2$, and H$_2$S.[50,228,229] Typically the NiO$_x$ is applied in gas sensors in the form of nanoparticles or nanostructures, to maximize the surface area to volume ratio. But thin films can also be used, utilized especially as coatings on porous templates or supports, for example, for p-n junctions, where a p-type NiO$_x$ thin film is grown on a n-type supporting material.[50] In sensor applications, chemical deposition methods are commonly used, for the aforementioned reasons.

For example, Navarrete et al used aerosol-assisted CVD to coat WO$_3$ nanowire sensors with NiO$_x$ nanoparticles, which resulted in a 5-fold increase in the response of the sensor towards H$_2$S in the ppm range, and more importantly, gave a solid response even in the presence of humidity, showing the suitability of the sensor to monitor in real application conditions.[50] Dirksen et al used a simple dip-coating approach to fabricate un-doped and Li-doped NiO$_x$ films for formaldehyde gas sensors. But the sensitivity, in the range of tens of ppm, was still lower than required for formaldehyde monitoring.[229] This was significantly improved by Lahem et al, who compared sol-gel and precipitation methods to synthesize NiO$_x$ nanostructured films and were able to detect formaldehyde concentrations <1 ppm at working temperatures around 200°C.[230] Sol-gel techniques were also used by Soleimanpur et al,[231,232] who tested the NiO$_x$ films for the sensing of hydrogen, ammonia, and methane gases. The porous polycrystalline films were confirmed to be non-stoichiometric with high Ni^{3+} concentration measured by XPS, and showed the highest sensitivity towards all the investigated gases at 175°C. For NH$_3$, the sensitivity with 25 ppm concentration, the defined threshold limit value, was acceptable with response percentage of 31%, showing the potential of NiO$_x$ films in practical applications. Slightly lower sensitivity was achieved for CH$_4$ within the lower explosive limit of few 1000 ppm.[231] The best sensitivity of the fabricated devices was achieved for H$_2$, where the corresponding response was 68% at 3000 ppm H$_2$, and was observed to decrease only by 5% when the humidity was introduced.[231,232] Besides gas sensing, NiO$_x$ can be applied to detect also other substances, such as glucose (detailed more in the next Section). Raza et al fabricated nanocomposites by coating stacked-cup carbon nanotubes (SCCNTs) with ALD NiO$_x$, utilizing the conformality of ALD, and varied the film thicknesses between 0.8 and 22 nm.[64] While their film consisted of nanoparticles, it was conformal and covered the CNT network uniformly. The best performing glucose sensors, achieved with 4 nm NiO$_x$ films, responded over a wide concentration range (LOD 0.1 μM) with enhanced sensitivity of 1250 μA cm^{-2} mM^{-1} and a response time of <2 seconds.

6.6.2 | NiO$_x$ for flexible sensors

Flexible NiO$_x$ films have been used for thermistors, in which the resistivity decreases with increasing temperature. NiO$_x$ is particularly advantageous because it has high-temperature sensitivity. This is quantified by the material constant for the thermistor (β). β is related to the resistance of the thermistor and temperature by Equation (5).[233]

$$R_t = R_0 e^{\beta\left(\frac{1}{T} - \frac{1}{T_0}\right)} \tag{5}$$

In Equation (5), R_t is the thermistor resistance at temperature T, and R_0 the resistance at the reference temperature T_0. Commercial thermistors require a material constant of 3500 K. NiO$_x$ films deposited from nanoparticle inks have been reported to have material constants of approximately 4300 K.[27,233] In contrast, graphene films only have a material constant of 1860 K.[27]

Another important parameter is the temperature coefficient of resistance (α), which is related to the material constant by Equation (6).[233]

$$\alpha = \frac{1}{R_t}\frac{dR_t}{dT} = -\frac{\beta}{T^2} \tag{6}$$

The temperature coefficient of resistance of NiO_x has been reported to be -5.84% K^{-1}. In contrast, inkjet-printed silver nanoparticles have been reported to have a temperature coefficient of resistance of only 0.11% K^{-1}. Commercial thermistors require a temperature coefficient of resistance of -4% K^{-1} at $20°C$, and this demonstrates the appeal of NiO_x.[27]

Flexible NiO_x thermistors have a key advantage over rigid thermistors in wearable electronics. Khan et al
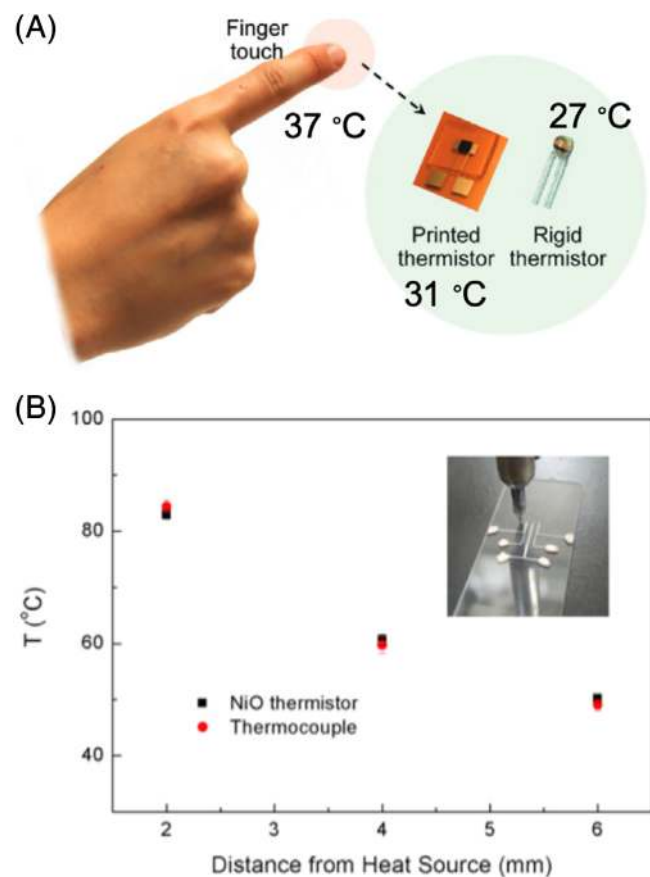
FIGURE 13 A, Comparison of stencil-printed thermistor on flexible substrate vs rigid thermistor for measuring the temperature of a finger. Reprinted with permission from Khan et al.[233] Copyright Wiley 2016. B, Use of an inkjet-printed NiO_x flexible thermistor array for measuring the temperature distribution from a heat source compared to a thermocouple. Note that the error bars are small, showing the uncertainty in the temperature measurement by both the NiO_x thermistor and thermocouple to be small. Reprinted with permission from Huang et al.[27] Copyright American Chemical Society 2013

demonstrated that NiO_x deposited onto a flexible PI substrate was able to more accurately measure the temperature of a finger because it could wrap around the finger more closely than a rigid thermistor (Figure 13A).[233] These flexible thermistors have been used in wearable health monitoring devices attached to the human body and have been demonstrated to be accurate and durable during exercise.[233]

NiO_x for flexible thermistors has been deposited from nanoparticle inks through inkjet printing and stencil printing. Huang et al prepared a NiO_x nanoparticle suspension in water and ethylene glycol without adding surfactants by controlling the pH, as detailed in Section 3.3.3. The thermistor was obtained by depositing the NiO_x nanoparticles on inkjet-printed silver electrodes and annealed at $200°C$, which is compatible with the PI substrates used. The NiO_x nanoparticles deposited were more compact when the substrate was held at room temperature during the printing process instead of heating at $70°C$ because the solvent evaporated more slowly, giving the NiO_x nanoparticles more time to settle. This resulted in thermistors with a higher material coefficient but lower resistivity. The printed thermistors had negligible hysteresis and there was very little difference in the electrical resistance in the flat state or bent state for bending radii between 10 and 70 mm. The advantage of inkjet printing is that numerous small thermistors can be printed on the same substrate, allowing a thermistor array to be made. This enables the spatial variation in temperature to be measured, and it was shown that the accuracy of an inkjet-printed thermistor array was similar to that of K-type thermocouple probes, with a response time that was almost as fast (Figure 13B).[27]

Kahn et al also used an ink of NiO_x nanoparticles in water. However, they used polystyrenebutadiene rubber (PSBR) to bind the nanoparticles together. Owing to the viscid nature of the mix, stencil printing was used to
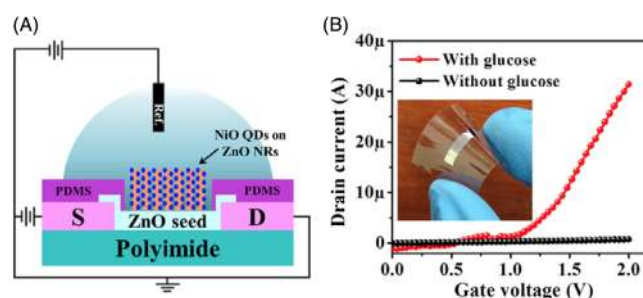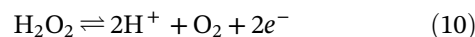
FIGURE 14 A, Diagram illustrating the structure of the flexible field-effect transistor for glucose sensing. B, Comparison of the drain current against gate voltage with or without glucose serum added. Reproduced with permission from Jung et al.[236] Copyright Elsevier 2018

deposit the nanoparticles instead of inkjet printing. The deposited film was annealed at 140°C for 2 hours before being encapsulated with a drop-cast Cytop fluoropolymer. Similar to the thermistors made by Huang et al, the films made by Kahn et al were deposited on PI, but inkjet-printed gold electrodes were used instead. Tape-testing showed that the deposited NiO_x films had high adhesion. The response time of the thermistors to a temperature change from 31°C to 22°C was 10 seconds, compared to 11 seconds for a rigid thermistor. The thermistors were bent with radii down to 25 mm, and the resistance of the NiO_x at room temperature changed by only 4%.[233]

Nickel oxide has also been used in the fabrication of metal oxide pH sensors. These are advantageous over standard glass electrode sensors, which are brittle,[234] need to be stored under wet conditions, and have large sizes.[235] Flexible pH sensors can be integrated into wearable electronics, electronic skin, and miniaturized electronic devices for the medical, food, and agricultural industries, as well as for environmental monitoring.[235] NiO_x is suitable for pH sensors because it is stable over a wide pH range, is biocompatible and has a high oxygen ion conductivity due to its high defect density. Chou et al deposited NiO_x by reactive sputtering on PET substrates with screen-printed silver electrodes. The voltage of the NiO_x sensor had an approximately linear dependence on pH over the measured range of 1 to 13. The sensitivity was 63 mV pH^{-1} at room temperature.[235] This is comparable to IrO_2 based pH sensors.[234] But NiO_x has the important advantage of being composed of less expensive elements than in IrO_2. It is proposed that the electrochemical potential in NiO_x pH sensors arises from the potential difference between NiO_x and the hydrated metal oxide. The drift rate exhibited by the NiO_x pH sensors was between −4 and 3 mV h^{-1}, which is comparable to the drift rate reported for ZrO_2 and a-Si:H/SiO_2 pH sensors.[235]

Nickel oxide has also been used as a catalytic layer in nonenzymatic flexible field-effect transistors for glucose sensors. Jung et al fabricated ZnO-based field-effect transistors. A sputtered ZnO layer was used between the Ag source and drain electrodes, which were deposited onto flexible PI substrates. The ZnO layer was used as a seed layer to grow ZnO nanorods by hydrothermal synthesis. These nanorods were 1.2 ± 0.2 μm long and 70 ± 10 nm wide. The ZnO nanorods were covered with NiO_x quantum dots deposited by RF sputtering from a NiO_x target (Figure 14A). Having NiO_x quantum dots mounted on the ZnO nanorods increased the surface area between the electrocatalytic NiO_x and the serum. The proposed reaction scheme is given by Equations (7)-(10)[236]:

$$NiO + OH^- \rightleftharpoons NiOOH + e^- \tag{7}$$

$$NiOOH + glucose \rightleftharpoons Ni(OH)_2 + gluconolactone \tag{8}$$

$$2Ni(OH)_2 + O_2 \rightleftharpoons 2NiOOH + H_2O_2 \tag{9}$$

$$H_2O_2 \rightleftharpoons 2H^+ + O_2 + 2e^- \tag{10}$$

It is proposed that OH^- adsorbs to the surface of the NiO_x quantum dots, leading to the formation of NiOOH (Equation (7)). This reacts with glucose to form $Ni(OH)_2$ and gluconolactone (Equation (8)). The $Ni(OH)_2$ further reacts with O_2 to form NiOOH and H_2O_2 (Equation (9)). The H_2O_2 reacts to release electrons (Equation (10)). Thus, the drain current in the field-effect transistor is higher when glucose is present (Figure 14B), and the drain current increases with the concentration of glucose, with a sensitivity of 13.1 μA cm^{-2} mM^{-1} for 0.001 to 10 mM concentrations, and 7.3 μA cm^{-2} mM^{-1} for 10 to 50 mM. These flexible glucose sensors can be used as low-cost, light-weight sensors in a clinical or industrial environment. However, the sensitivity displayed is lower than that of Fe_2O_3-ZnO nanorod non-enzymatic sensors, as well as other enzymatic sensors.[236]

[Correction added on 14 August 2020, after first online publication: The citations of Figures 13 and 14 have been reversed.]

7 | CONCLUSIONS AND OUTLOOK

Nickel oxide is a very well-known simple binary oxide with p-type behavior, for which the defect chemistry has been researched over several decades. The importance of this seemingly simple compound has come to the fore in a prominent way across a wide range of applications in electronics and energy devices only in very recent years. The p-type semiconducting properties of NiO_x are a key attribute for many applications from thin-film transistors to solar cells. While there are other competing p-type systems, either their compositions are too complex to be made by simple methods, or their stabilities against oxidation/reduction are poor and, hence, carrier properties are difficult to control. The different applications all have varying and specific property requirements from NiO_x thin films. There is certainly room for improvement of the different properties, for example, for thin-film transistor and in complementary metal-oxide semiconductor (CMOS). These include achieving higher mobilities, increased and reproducible control over the carrier concentration by controlling Ni vacancy concentration, reduction of defect traps both at the bulk of the films as well at the interfaces to prevent Fermi level pinning with contacts. Additionally, control of average Ni

valence is important (Ni, Ni^{2+} and even Ni^{3+} are possible), since variable cation valence leads to additional variation in the carrier concentration. For high-performance PVs and LEDs, more precise control over the work function and band gap of NiO_x, whilst not sacrificing in the hole mobility, are essential for the charge transport/injection layer.

As shown in this review, many of the properties of NiO_x, such as conductivity and work function, are sensitive to the deposition technique, choice of chemistry, and the growth conditions. These properties can be further modified through a wide selection of post-deposition treatments. More fundamental work is required to understand how to control the aforementioned properties. Optimization of chemically grown film properties would also strongly benefit from basic understanding studies (experiment and modeling) of epitaxial single-crystal-like films of different orientation, as well as much more perfect films grown at higher temperatures using physical vapor deposition methods. Translation of the information of perfect systems to low-temperature grown chemical ones is not necessarily straightforward but it is a key starting point to know what is possible.

The above near-equilibrium information needs also to be translatable and relevant to non-equilibrium conditions which are pertinent when using low-temperature chemical methods. Without such information, challenges will remain with the reproducibility of device performance. In addition, when the growth and processing temperatures are further reduced, there is the problem not just of limited crystallinity, but also of remnant impurities (organics and/or aqueous species) which lead to compromised and poorly controlled performance. On the other hand, such methods are absolutely necessary for many applications where reactions with other materials in the devices must be prevented and where film conformality is essential. New approaches, such as machine learning may well be the key to obtaining the necessary correlations to understanding the influences of non-equilibrium and other chemical effects.

CONFLICT OF INTEREST
The authors declare no conflicts of interest.

AUTHOR CONTRIBUTIONS
Mari Napari led in writing the abstract and Sections 1, 2, 3.1, 3.2, 4, 6.1, 6.2.1, 6.3, 6.6.1, and contributed to Section 3.3 and Tables 3, A2, A1, A3. Tahmida N. Huq led in writing Sections 6.4.1 and 6.5.1, as well as Table 4, Figures 1, 11, and 12. Robert L. Z. Hoye led in writing Sections 1, 2, 3.3.1, 3.3.2, 3.3.3, 3.3.4, 3.3.5, 3.3.6, 3.3.7, 5.1, 5.2, 6.1.2, 6.2.2, 6.3, 6.4.2, 6.5.2, 6.6.2, as well as Figures 2 and 6. Judith L. MacManus-Driscoll led in writing Section 7. All authors contributed to editing the text and figures.

ORCID
Mari Napari https://orcid.org/0000-0003-2690-8343
Tahmida N. Huq https://orcid.org/0000-0002-3581-2151
Robert L. Z. Hoye https://orcid.org/0000-0002-7675-0065
Judith L. MacManus-Driscoll https://orcid.org/0000-0003-4987-6620

REFERENCES
1. Park JW, Kang BH, Kim HJ. A review of low-temperature solution-processed metal oxide thin-film transistors for flexible electronics. *Adv Funct Mater.* 2019;30(20):1904632.
2. Coll M, Fontcuberta J, Althammer M, et al. Towards oxide electronics: a roadmap. *Appl Surf Sci.* 2019;482:1-93.
3. Nomura K, Ohta H, Takagi A, Kamiya T, Hirano M, Hosono H. Room-temperature fabrication of transparent flexible thin-film transistors using amorphous oxide semiconductors. *Nature.* 2004;432(7016):488-492.
4. Petti L, Münzenrieder N, Vogt C, et al. Metal oxide semiconductor thin-film transistors for flexible electronics. *Appl Phys Rev.* 2016;3(2):021303.
5. Hoye RLZ, Musselman KP, MacManus-Driscoll JL. Research update: doping ZnO and TiO_2 for solar cells. *APL Mater.* 2013;1(6):060701.
6. Hoye RLZ, Muñoz-Rojas D, Nelson SF, et al. Research update: atmospheric pressure spatial atomic layer deposition of ZnO thin films: reactors, doping, and devices. *APL Mater.* 2015;3(4):040701.
7. Fortunato E, Barquinha P, Pimentel A, et al. Fully transparent ZnO thin-film transistor produced at room temperature. *Adv Mater.* 2005;17(5):590-594.
8. Garlapati SK, Gebauer JS, Dehm S, et al. Room-temperature processing of printed oxide FETs using ultraviolet photonic curing. *Adv Electron Mater.* 2017;3(9):1600476.
9. Martins R, Nathan A, Barros R, et al. Complementary metal oxide semiconductor technology with and on paper. *Adv Mater.* 2011;23(39):4491-4496.

10. Irwin MD, Servaites JD, Buchholz DB, et al. Structural and electrical functionality of NiO interfacial films in bulk hetero-junction organic solar cells. *Chem Mater.* 2011;23(8):2218-2226.

11. Nomura K, Kamiya T, Hosono H. Ambipolar oxide thin-film transistor. *Adv Mater.* 2011;23(30):34313434.

12. Kim HJ, Lee JH. Highly sensitive and selective gas sensors using p-type oxide semiconductors: overview. *Sensor Actuat B Chem.* 2014;192:607-627.

13. Wang Z, Nayak PK, Caraveo-Frescas JA, Alshareef HN. Recent developments in p-type oxide semiconductor materials and devices. *Adv Mater.* 2016;28(20):3831-3892.

14. Hoye RLZ, Brandt RE, Ievskaya Y, et al. Perspective: maintaining surface-phase purity is key to efficient open air fabricated cuprous oxide solar cells. *APL Mater.* 2015;3(2): 020901.

15. Irwin MD, Buchholz DB, Hains AW, Chang RPH, Marks TJ. P-type semiconducting nickel oxide as an efficiency enhancing anode interfacial layer in polymer bulk-heterojunction solar cells. *Proc Natl Acad Sci USA.* 2008;105(8):2783-2787.

16. Nachman M, Corocaru LN, Ribco LV. Electrical properties of non-stoichiometric nickel oxide. *Phys Status Solid.* 1965;8: 773-783.

17. Zhang JY, Li WW, Hoye RLZ, et al. Electronic and transport properties of Li-doped NiO epitaxial thin films. *J Mater Chem C.* 2018;6:2275-2282.

18. Adjokatse S, Fang HH, Loi MA. Broadly tunable metal halide perovskites for solid-state light-emission applications. *Mater Today.* 2017;20(8):413-424.

19. Lee LC, Huq TN, MacManus-Driscoll JL, Hoye RLZ. Research update: bismuth-based perovskite-inspired photovoltaic materials. *APL Mater.* 2018;6(8):084502.

20. Yang YM, Chen W, Dou L, et al. High-performance multiple-donor bulk heterojunction solar cells. *Nat Photon.* 2015;9: 190-198.

21. Hou J, Inganäs O, Friend RH, Gao F. Organic solar cells based on non-fullerene acceptors. *Nat Mater.* 2018;17:119.

22. Sialvi MZ, Mortimer RJ, Wilcox GD, et al. Electrochromic and colorimetric properties of nickel(II) oxide thin films prepared by aerosol-assisted chemical vapor deposition. *ACS Appl Mater Interfaces.* 2013;5:5675-5682.

23. Xia X, Tu J, Zhang J, Wang X, Zhang W, Huang H. Electrochromic properties of porous NiO thin films prepared by a chemical bath deposition. *Sol Energy Mater Sol Cells.* 2008;92 (6):628-633.

24. Pereira S, Gonçalves A, Correia N, et al. Electrochromic behavior of NiO thin films deposited by e-beam evaporation at room temperature. *Sol Energy Mater Sol Cells.* 2014;120:109-115.

25. Kang C, Cha E, Lee SH, Choi W. In situ fabrication of a graphene-coated three-dimensional nickel oxide anode for high-capacity lithium-ion batteries. *RSC Adv.* 2018;8:7414-7421.

26. Yu L, Wang G, Wan G, et al. Highly effective synthesis of NiO/CNT nanohybrids by atomic layer deposition for high-rate and long-life supercapacitors. *Dalton Trans.* 2016;45:13779-13786.

27. Huang CC, Kao ZK, Liao YC. Flexible miniaturized nickel oxide thermistor arrays via inkjet printing technology. *ACS Appl Mater Interfaces.* 2013;5(24):12954-12959.

28. Koshtyal Y, Nazarov D, Ezhov I, et al. Atomic layer deposition of NiO to produce active material for thin-film lithium-ion batteries. *Coatings.* 2019;9(5):301.

29. Han SW, Kim IH, Kim DH, et al. Temperature regulated-chemical vapor deposition for incorporating NiO nanoparticles into mesoporous media. *Appl Surf Sci.* 2016;385: 597-604.

30. Singh A, Chang SLY, Hocking RK, Bach U, Spiccia L. Highly active nickel oxide water oxidation catalysts deposited from molecular complexes. *Energ Environ Sci.* 2013;6:579-586.

31. Sawatzky G, Allen J. Magnitude and origin of the band gap in NiO. *Phys Rev Lett.* 1984;53(24):2339-2342.

32. Dare-Edwards M, Goodenough J, Hamnett A, Nickolson N. Photoelectrochemistry of nickel(II) oxide. *J Chem Soc Faraday Trans 2* 1981; 77: 643–661

33. Taguchi M, Matsunami M, Ishida Y, et al. Revisiting the valence-band and Core-level photoemission spectra of NiO. *Phys Rev Lett.* 2008;100:206401.

34. Lany S, Osorio-Guillén J, Zunger A. Origins of the doping asymmetry in oxides: hole doping in NiO versus electron doping in ZnO. *Phys Rev B.* 2007;75:241203(R).

35. Alberts L, Lee EW. Magnetostriction in antiferromagnetic nickel oxide. *Proc Phys Soc.* 1961;78(5):728-733.

36. Marmeggi J, Baruchel J. Antiferromagnetic domains in nickel oxide by magnetic neutron laue diffraction. *J Magn Magn Mater.* 1979;10(1):14-24.

37. Choi SC, Koumoto K, Yanagida H. Electrical conduction and effective mass of a hole in single-crystal NiO. *J Mater Sci.* 1986;21(6):1947-1950.

38. Jang WL, Lu YM, Hwang WS, Chen WC. Electrical properties of Li-doped NiO films. *J Eur Ceram Soc.* 2010;30:503-508.

39. Bachmann J, Zolotaryov A, Albrecht O, et al. Stoichiometry of nickel oxide films prepared by ALD. *Chem Vapor Depos.* 2011; 17:177-180.

40. Dubey P, Kaurav N, Devan RS, Okram GS, Kuo YK. The effect of stoichiometry on the structural, thermal and electronic properties of thermally decomposed nickel oxide. *RSC Adv.* 2018;8:5882-5890.

41. Hoye RLZ, Schulz P, Schelhas LT, et al. Perovskite-inspired photovoltaics materials: toward best practices in materials characterization and calculations. *Chem Mater.* 2017;29(5): 1964-1988.

42. Vincent Crist B. A review of XPS data-banks. *XPS Rep.* 2007;1: 1-52.

43. Biesinger MC, Payne BP, Lau LWM, Gerson A, Smart RSC. X-ray photoelectron spectroscopic chemical state quantification of mixed nickel metal, oxide and hydroxide systems. *Surf Interface Anal.* 2009;41(4):324-332.

44. Napari M, Huq TN, Maity T, et al. Antiferromagnetism and p-type conductivity of non-stoichiometric nickel oxide thin films. *Inf Dent.* 2019;2(4):769-774.

45. Gelderman K, Lee L, Donne SW. Flat-band potential of a semiconductor: using the Mott–Schottky equation. *J Chem Educ.* 2007;84(4):685-688.

46. Zhao B, Lee LC, Yang L, et al. In situ atmospheric deposition of ultrasmooth nickel oxide for efficient perovskite solar cells. *ACS Appl Mater Interfaces.* 2018;10:41849-41854.

47. Chen HL, Lu YM, Hwang WS. Characterization of sputtered NiO thin films. *Surf Coat Technol.* 2005;198:138-142.

48. Maruyama T, Arai S. The electrochromic properties of nickel oxide thin films prepared by chemical vapor deposition. *Sol Energy Mater Sol Cells.* 1993;30(3):257-262.

49. Min KC, Kim M, You YH, et al. NiO thin films by MOCVD of Ni(dmamb)$_2$ and their resistance switching phenomena. *Surf Coat Technol.* 2007;201:9252-9255.

50. Navarrete E, Bittencourt C, Umek P, Llobet E. AACVD and gas sensing properties of nickel oxide nanoparticle decorated tungsten oxide nanowires. *J Mater Chem C.* 2018;6:5181-5192.

51. Battiato S, Giangregorio MM, Catalano MR, Lo Nigro R, Losurdo M, Malandrino G. Morphology-controlled synthesis of NiO films: the role of the precursor and the effect of the substrate nature on the films' structural/optical properties. *RSC Adv.* 2016;6:30813-30823.

52. Wang A, Belot JA, Marks TJ. Film microstructure-deposition condition relationships in the growth of epitaxial NiO films by metalorganic chemical vapor deposition on oxide and metal substrates. *J Mater Res.* 1999;14(3):1132-1136.

53. Hagen DJ, Tripathi TS, Terasaki I, Karppinen M. Microstructure and optical properties of ultra-thin NiO films grown by atomic layer deposition. *Semicond Sci Technol.* 2018;33(11):115015.

54. Nigro RL, Battiato S, Greco G, Fiorenza P, Roccaforte F, Malandrino G. Metal organic chemical vapor deposition of nickel oxide thin films for wide band gap device technology. *Thin Solid Films.* 2014;563:50-55.

55. Nigro RL, Fisichella G, Battiato S, et al. An insight into the epitaxial nanostructures of NiO and CeO$_2$ thin film dielectrics for AlGaN/GaN heterostructures. *Mater Chem Phys.* 2015;162:461-468.

56. Ikenoue T, Inoue J, Miyake M, Hirato T. Epitaxial growth of undoped and Li-doped NiO thin films on α-Al$_2$O$_3$ substrates by mist chemical vapor deposition. *J Cryst Growth.* 2019;507:379-383.

57. Wang H, Wu G, Cai X, et al. Effect of growth temperature on structure and optical characters of NiO films fabricated by PA-MOCVD. *Vacuum.* 2012;86:2044-2047.

58. Roffi TM, Nozaki S, Uchida K. Growth mechanism of single-crystalline NiO thin films grown by metal organic chemical vapor deposition. *J Cryst Growth.* 2016;451:57-64.

59. Kang JK, Rhee SW. Chemical vapor deposition of nickel oxide films from Ni(C$_5$H$_5$)$_2$/O$_2$. *Thin Solid Films.* 2001;391(1):57-61.

60. Yeh WC, Matsumura M. Chemical vapor deposition of nickel oxide films from bis-π-cyclopentadienyl-nickel. *Jpn J Appl Phys.* 1997;36(11R):6884-6887.

61. Kondrateva AS, Mishin MV, Alexandrov SE. TOF MS investigation of nickel oxide CVD. *J Am Soc Mass Spectrom.* 2017;28(11):2352-2360.

62. Barr MK, Assaud L, Wu Y, et al. Engineering a three-dimensional, photoelectrochemically active p-NiO/i-Sb$_2$S$_3$ junction by atomic layer deposition. *Electrochim Acta.* 2015;179:504-511.

63. Hufnagel AG, Henß AK, Hoffmann R, et al. Electron-blocking and oxygen evolution catalyst layers by plasma enhanced atomic layer deposition of nickel oxide. *Adv Mater Interfaces.* 2018;5(16):1701531.

64. Raza MH, Movlaee K, Wu Y, et al. Tuning the NiO thin film morphology on carbon nanotubes by atomic layer deposition for enzyme-free glucose sensing. *Chem Electro Chem.* 2019;6(2):383-392.

65. Jeong MG, Kim IH, Han SW, Kim DH, Kim YD. Room temperature CO oxidation catalyzed by NiO particles on mesoporous SiO$_2$ prepared via atomic layer deposition: influence of pre-annealing temperature on catalytic activity. *J Mol Catal A Chem.* 2016;414:87-93.

66. Daub M, Knez M, Goesele U, Nielsch K. Ferromagnetic nanotubes by atomic layer deposition in anodic alumina membranes. *J Appl Phys.* 2007;101(9):09J111.

67. Kim DH, Sim JK, Lee J, et al. Carbon dioxide reforming of methane over mesoporous Ni/SiO$_2$. *Fuel.* 2013;112:111-116.

68. Wang G, Peng X, Yu L, Wan G, Lin S, Qin Y. Enhanced microwave absorption of ZnO coated with Ni nanoparticles produced by atomic layer deposition. *J Mater Chem A.* 2015;3:2734-2740.

69. Zhang R, Wei H, Si W, et al. Enhanced electrocatalytic activity for water splitting on NiO/Ni/carbon fiber paper. *Materials.* 2017;10(1):15.

70. Chae J, Park HS, Kang SW. Atomic layer deposition of nickel by the reduction of preformed nickel oxide. *Electrochem Solid State.* 2002;5:C64.

71. Lu HL, Scarel G, Wiemer C, et al. Atomic layer deposition of NiO films on Si(100) using cyclopentadienyl-type compounds and ozone as precursors. *J Electrochem Soc.* 2008;115(10):H807.

72. Kumagai H, Matsumoto M, Toyoda K, Obara M. Preparation and characteristics of nickel oxide thin film by controlled growth with sequential surface chemical reactions. *J Mater Sci Lett.* 1996;15:1080.

73. Song SJ, Lee SW, Kim GH, et al. Substrate dependent growth behaviors of plasma-enhanced atomic layer deposited nickel oxide films for resistive switching application. *Chem Mater.* 2012;24:4675-4685.

74. Ji SH, Jang WS, Son JW, Kim DH. Characteristics of NiO films prepared by atomic layer deposition using bis(ethylcyclopentadienyl)-Ni and O$_2$ plasma. *Korean J Chem Eng.* 2018;35(12):2474-2479.

75. Premkumar PA, Toeller M, Adelmann C, et al. NiO thin films synthesized by atomic layer deposition using Ni(dmamb)$_2$ and ozone as precursor. *Chem Vapor Depos.* 2012;18:61-69.

76. Ko MH, Shong B, Hwang JH. Low temperature atomic layer deposition of nickel sulfide and nickel oxide thin films using Ni(dmamb)$_2$ as Ni precursor. *Ceram Int.* 2018;44(14):16342-16351.

77. Yang JH, Lee SY, Song WS, et al. Field emission properties of ZnO nanorods coated with NiO film. *J Vac Sci Technol B.* 2008;26(3):1021-1024.

78. Holden KEK, Dezelah CL, Conley JF. Atomic layer deposition of transparent p-type semiconducting nickel oxide using Ni(tBu$_2$DAD)$_2$ and ozone. *ACS Appl Mater Interfaces.* 2019;11(33):30437-30445.

79. Hsu CC, Su HW, Hou CH, Shyue JJ, Tsai FY. Atomic layer deposition of NiO hole-transporting layers for polymer solar cells. *Nanotechnology.* 2015;26(38):385201.

80. Thimsen E, Martinson ABF, Elam JW, Pellin MJ. Energy levels, electronic properties, and rectification in ultrathin p-NiO films synthesized by atomic layer deposition. *J Phys Chem C.* 2012;116:16830-16840.

81. Koushik D, Jošt M, Dučinskas A, et al. Plasma-assisted atomic layer deposition of nickel oxide as hole transport layer for hybrid perovskite solar cells. *J Mater Chem C.* 2019;7:12532-12543.

82. Seo S, Park IJ, Kim M, et al. An ultra-thin un-doped NiO hole transporting layer of highly efficient (16.4%) organic–inorganic hybrid perovskite solar cells. *Nanoscale*. 2016;8:11403-11412.

83. Kot M, Das C, Wang Z, et al. Room-temperature atomic layer deposition of Al_2O_3: impact on efficiency, stability and surface properties in perovskite solar cells. *Chem Sus Chem*. 2016;9 (24):3401-3406.

84. Tang X, Francis LA, Simonis P, et al. Room temperature atomic layer deposition of Al_2O_3 and replication of butterfly wings for photovoltaic application. *J Vac Sci Technol A*. 2012; 30(1):01A146.

85. Napari M, Malm J, Lehto R, et al. Nucleation and growth of ZnO on PMMA by low-temperature atomic layer deposition. *J Vac Sci Technol A*. 2015;33(1):01A128.

86. Napari M, Lahtinen M, Veselov A, Julin J, Østreng E, Sajavaara T. Room-temperature plasma-enhanced atomic layer deposition of ZnO: film growth dependence on the PEALD reactor configuration. *Surf Coat Technol*. 2017;326:281-290.

87. Bishal AK, Sukotjo C, Takoudis CG. Room temperature TiO_2 atomic layer deposition on collagen membrane from a titanium alkylamide precursor. *J Vac Sci Technol A*. 2017;35(1): 01B134.

88. Kikuchi K, Miura M, Kanomata K, Ahmmad B, Kubota S, Hirose F. Room temperature atomic layer deposition of TiO_2 on gold nanoparticles. *J Vac Sci Technol A*. 2017;35(1):01B121.

89. Kemell M, Färm E, Ritala M, Leskelä M. Surface modification of thermoplastics by atomic layer deposition of Al_2O_3 and TiO_2 thin films. *Eur Polym J*. 2008;44(11):3564-3570.

90. Guo HC, Ye E, Li Z, Han MY, Loh XJ. Recent progress of atomic layer deposition on polymeric materials. *Mater Sci Eng C*. 2017;70:1182-1191.

91. Sheng J, Lee JH, Choi WH, Hong T, Kim M, Park JS. Review article: atomic layer deposition for oxide semiconductor thin film transistors: advances in research and development. *J Vac Sci Technol A*. 2018;36:060801.

92. Chen X, Zhang G, Wan J, et al. Transparent and flexible thin-film transistors with high performance prepared at ultralow temperatures by atomic layer deposition. *Adv Electron Mater*. 2019;5(2):1800583.

93. Maydannik PS, Kääriäinen TO, Lahtinen K, et al. Roll-to-roll atomic layer deposition process for flexible electronics encapsulation applications. *J Vac Sci Technol A*. 2014;32(5):051603.

94. Jarvis KL, Evans PJ. Growth of thin barrier films on flexible polymer substrates by atomic layer deposition. *Thin Solid Films*. 2017;624:111-135.

95. Musselman K, Uzoma C, Miller M. Nanomanufacturing: high-throughput, cost-effective deposition of atomic scale thin films via atmospheric pressure spatial atomic layer deposition. *Chem Mater*. 2016;28(23):8443-8452.

96. Musselman K, Muñoz-Rojas D, Hoye RLZ, et al. Rapid open-air deposition of uniform, nanoscale, functional coatings on nanorod arrays. *Nanoscale Horiz*. 2017;2:110-117.

97. Muñoz-Rojas D, Nguyen V, Huerta CM, Jiménez C, Bellet D. Spatial atomic layer deposition. In: Mandracci P, ed. *Chemical Vapor Deposition for Nanotechnology*. Croatia: IntechOpen; 2018. https://doi.org/10.5772/intechopen.82439.

98. You YH, So BS, Hwang JH, et al. Impedance spectroscopy characterization of resistance switching NiO thin films prepared through atomic layer deposition. *Appl Phys Lett*. 2006;89(22):222105.

99. So BS, You YH, Kim KH, et al. Crystallization of amorphous silicon thin films using self-limiting ALD of nickel oxide. *Electrochem Solid St*. 2007;10:J61-J64.

100. Yang TS, Cho W, Kim M, et al. Atomic layer deposition of nickel oxide films using $Ni(dmamp)_2$ and water. *J Vac Sci Technol A*. 2005;23:1238-1243.

101. Liu A, Zhu H, Guo Z, et al. Solution combustion synthesis: low-temperature processing for p-type Cu:NiO thin films for transparent electronics. *Adv Mater*. 2017;29:1701599.

102. Steirer KX, Chesin JP, Widjonarko NE, et al. Solution deposited NiO thin-films as hole transport layers in organic photovoltaics. *Org Electron*. 2010;11:1414-1418.

103. Steirer KX, Richards RE, Sigdel AK, et al. Nickel oxide interlayer films from nickel formate– ethylenediamine precursor: influence of annealing on thin film properties and photovoltaic device performance. *J Mater Chem A*. 2015;3:10949-10958.

104. Jeng JY, Chen KC, Chiang TY, et al. Nickel oxide electrode interlayer in $CH_3NH_3PbI_3$ perovskite/PCBM planar heterojunction hybrid solar cells. *Adv Mater*. 2014;26(24):4107-4113.

105. Shan F, Liu A, Zhu H, et al. High-mobility p-type NiO_x thin-film transistors processed at low temperatures with Al_2O_3 high-k dielectric. *J Mater Chem C*. 2016;4:9438-9444.

106. Liu A, Liu G, Zhu H, et al. Hole mobility modulation of solution-processed nickel oxide thin-film transistor based on high-k dielectric. *Appl Phys Lett*. 2016;108:233506.

107. Manders JR, Tsang SW, Hartel MJ, et al. Solution-processed nickel oxide hole transport layers in high efficiency polymer photovoltaic cells. *Adv Funct Mater*. 2013;23(23):2993-3001.

108. Hoye RLZ, Lee LC, Kurchin RC, et al. Strongly enhanced photovoltaic performance and defect physics of air-stable bismuth oxyiodide (BiOI). *Adv Mater*. 2017;29(36):1702176.

109. Hoye RLZ, Bush KA, Oviedo F, et al. Developing a robust recombination contact to realize monolithic perovskite tandems with industrially common p-type silicon solar cells. *IEEE J Photovolt*. 2018;8(4):1023-1028.

110. Zhang H, Cheng J, Lin F, et al. Pinhole-free and surface-nanostructured NiO_x film by room-temperature solution process for high-performance flexible perovskite solar cells with good stability and reproducibility. *ACS Nano*. 2016;10(1): 1503-1511.

111. Jiang F, Choy WCH, Li X, Zhang D, Cheng J. Post-treatment-free solution-processed non-stoichiometric NiO_x nanoparticles for efficient hole-transport layers of organic optoelectronic devices. *Adv Mater*. 2015;27(18):29302937.

112. Li Y, Liu C, Wang G, Pei Y. Investigation of solution combustion-processed nickel oxide p-channel thin film transistors. *Semicond Sci Technol*. 2017;32(8):085004.

113. Erri P, Pranda P, Varma A. Oxidizer-fuel interactions in aqueous combustion synthesis. 1. Iron(III) nitrate-model fuels. *Ind Eng Chem Res*. 2004;43:3092-3096.

114. Yang J, Wang B, Zhang Y, Ding X, Zhang J. Low-temperature combustion synthesis and UV treatment processed p-type Li: NiO_x active semiconductors for high-performance electronics. *J Mater Chem C*. 2018;6:12584-12591.

115. Kim YH, Heo JS, Kim TH, et al. Flexible metal-oxide devices made by room-temperature photochemical activation of sol–gel films. *Nature*. 2012;489:128-132.

116. Xu X, Cui Q, Jin Y, Guo X. Low-voltage zinc oxide thin-film transistors with solution-processed channel and dielectric layers below 150°C. *Appl Phys Lett*. 2012;101:222114.

117. Raut NC, Al-Shamery K. Inkjet printing metals on flexible materials for plastic and paper electronics. *J Mater Chem C*. 2018;6:1618-1641.

118. Hu H, Zhu J, Chen M, Guo T, Li F. Inkjet-printed p-type nickel oxide thin-film transistor. *Appl Surf Sci*. 2018;441:295-302.

119. Ruscello M, Sarkar T, Levitsky A, et al. Nanocomposite of nickel oxide nanoparticles and polyethylene oxide as printable hole transport layer for organic solar cells. *Sustain Energy Fuels*. 2019;3:1418-1426.

120. Ukoba K, Eloka-Eboka A, Inambao F. Review of nanostructured NiO thin film deposition using the spray pyrolysis technique. *Renew Sustain Energy Rev*. 2018;82:2900-2915.

121. Patil P, Kadam L. Preparation and characterization of spray pyrolyzed nickel oxide (NiO) thin films. *Appl Surf Sci*. 2002;199:211-221.

122. Kamal H, Elmaghraby E, Ali S, Abdel-Hady K. Characterization of nickel oxide films deposited at different substrate temperatures using spray pyrolysis. *J Cryst Growth*. 2004;262(1):424-434.

123. Reguig B, Regragui M, Morsli M, Khelil A, Addou M, Bernede J. Effect of the precursor solution concentration on the NiO thin film properties deposited by spray pyrolysis. *Sol Energy Mater Sol Cells*. 2006;90(10):1381-1392.

124. Yi X, Wenzhong W, Yitai Q, Li Y, Zhiwen C. Deposition and microstructural characterization of NiO thin films by a spray pyrolysis method. *J Cryst Growth*. 1996;167:656-659.

125. Desai J, Min SK, Jung KD, Joo OS. Spray pyrolytic synthesis of large area NiO$_x$ thin films from aqueous nickel acetate solutions. *Appl Surf Sci*. 2006;253(4):1781-1786.

126. Desai JD. Nickel oxide thin films by spray pyrolysis. *J Mater Sci Mater Electron*. 2016;27(12):12329-12334.

127. Han SY, Lee DH, Chang YJ, Ryu SO, Lee TJ, Chang CH. The growth mechanism of nickel oxide thin films by room-temperature chemical bath deposition. *J Electrochem Soc*. 2006;153(6):C382-C386.

128. Varkey A, Fort A. Solution growth technique for deposition of nickel oxide thin films. *Thin Solid Films*. 1993;235(1):47-50.

129. Pejova B, Kocareva T, Najdoski M, Grozdanov I. A solution growth route to nanocrystalline nickel oxide thin films. *Appl Surf Sci*. 2000;165(4):271-278.

130. Martínez-Gil M, Pintor-Monroy MI, Cota-Leal M, et al. Influence of annealing temperature on nickel oxide thin films grown by chemical bath deposition. *Mater Sci Semicond Process*. 2017;72:37-45.

131. Faustini M, Louis B, Albouy PA, Kuemmel M, Grosso D. Preparation of sol-gel films by dip-coating in extreme conditions. *J Phys Chem C*. 2010;114:7637-7645.

132. Wang L, Zhang Z, Cao Y. Preparation of nickel oxide films by sol-gel process. *J Cerm Soc Jpn*. 1993;101(1170):227-229.

133. Nazir Kayani Z, Aslam A, Ishaque R, et al. The effect of the withdrawal speed on properties of nickel oxide thin films. *Z Kristallogr*. 2019;234:647-655.

134. Taşdemirci TÇ. Influence of annealing on properties of SILAR deposited nickel oxide films. *Vacuum*. 2019;167:189-194.

135. Taşköprü T, Bayansal F, Şahinc B, Zora M. Structural and optical properties of co-doped NiO films prepared by SILAR method. *Phil Mag*. 2015;97(1):32-40.

136. Akaltun Y, Çayır T. Fabrication and characterization of NiO thin films prepared by SILAR method. *J Alloys Compd*. 2015;625:144-148.

137. Liu J, Chiam SY, Pan J, Wong LM, Li SFY, Ren Y. Solution layer-by-layer uniform thin film dip coating of nickel hydroxide and metal incorporated nickel hydroxide and its improved electrochromic performances. *Sol Energy Mater Sol Cells*. 2018;185:318-324.

138. Jlassi M, Sta I, Hajji M, Ezzaouia H. Optical and electrical properties of nickel oxide thin films synthesized by sol–gel spin coating. *Mater Sci Semicond Process*. 2014;21:7-13.

139. Ullrich F, Hillebrandt S, Hietzschold S, et al. Correlation between chemical and electronic properties of solution processed nickel oxide. *ACS Appl Energy Mater*. 2018;1(7):3113-3122.

140. Sawaby A, Selim M, Marzouk S, Mostafa M, Hosny A. Structure, optical and electrochromic properties of NiO thin films. *Phys B Condensed Matter*. 2010;405(16):3412-3420.

141. Alburquenque D, Canto MD, Arenas C, Tejo F, Pereira A, Escrig J. Dewetting of Ni thin films obtained by atomic layer deposition due to the thermal reduction process: variation of the thicknesses. *Thin Solid Films*. 2017;638:114-118.

142. Dashjav E, Lipinska-Chwalek M, Grüner D, Mauer G, Luysberg M, Tietz F. Atomic layer deposition and high resolution electron microscopy characterization of nickel nanoparticles for catalyst applications. *Surf Coat Technol*. 2016;307:428-435.

143. Lu HL, Scarel G, Alia M, Fanciulli M, Ding SJ, Zhang DW. Spectroscopic ellipsometry study of thin NiO films grown on Si (100) by atomic layer deposition. *Appl Phys Lett*. 2008;92:222907.

144. Lin T, Li X, Jang J. High performance p-type NiO$_x$ thin-film transistor by Sn doping. *Appl Phys Lett*. 2016;108(23):233503.

145. Nishihara Y, Chikamatsu M, Kazaoui S, Miyadera T, Yoshida Y. Influence of O$_2$ plasma treatment on NiO$_x$ layer in perovskite solar cells. *Jpn J Appl Phys*. 2018;57(4S):04FS07.

146. Kwon U, Kim BG, Nguyen DC, et al. Solution-processible crystalline NiO nanoparticles for high-performance planar perovskite photovoltaic cells. *Sci Rep*. 2016;6:30759.

147. Cosham SD, Richards SP, Manning T, Hill MS, Johnson AL, Molloy KC. Precursors for p-type nickel oxide: atmospheric-pressure metal–organic chemical-vapour deposition (MOCVD) of nickel oxide thin films with high work functions. *Eur J Inorg Chem*. 2017;2017(13):1868-1876.

148. Shim JW, Fuentes-Hernandez C, Dindar A, Zhou Y, Khan TM, Kippelen B. Polymer solar cells with NiO hole collecting interlayers processed by atomic layer deposition. *Org Electron*. 2013;14(11):2802-2808.

149. Islam R, Chen G, Ramesh P, et al. Investigation of the changes in electronic properties of nickel oxide (NiO$_x$) due to UV/ozone treatment. *ACS Appl Mater Interfaces*. 2017;9(20):17201-17207.

150. Liu S, Liu R, Chen Y, Ho S, Kim JH, So F. Nickel oxide hole injection/transport layers for efficient solution processed organic light-emitting diodes. *Chem Mater*. 2014;26:4528-4534.

151. Sun Y, Chen W, Wu Y, He Z, Zhang S, Chen S. A low-temperature-annealed and UV-ozone-enhanced combustion derived nickel oxide hole injection layer for flexible quantum dot light-emitting diodes. *Nanoscale*. 2019;11:10211028.

152. Chu J, Li Y, Fan X, Shao H, Duan W, Pei Y. Multistate data storage in solution-processed NiO-based resistive switching memory. *Semicond Sci Technol.* 2018;33(11):115007.

153. Zrikem K, Song G, Aghzzaf AA, Amjoud M, Mezzane D, Rougier A. UV treatment for enhanced electrochromic properties of spin coated NiO thin films. *Superlattice Microst.* 2019; 127:35-42.

154. Moon C, Kim H. Intense pulsed light annealing process of indium-gallium-zinc-oxide semiconductors via flash white light combined with deep-UV and near-infrared drying for high-performance thin-film transistors. *ACS Appl Mater Interfaces.* 2019;11:13380-13388.

155. Münzenrieder N, Zysset C, Petti L, Kinkeldei T, Salvatore GA, Tröster G. Room temperature fabricated flexible NiO/IGZO pn diode under mechanical strain. *Solid-State Electron.* 2013; 87:17-20.

156. Wang H, Zou C, Zhou L, Tian C, Fu D. Resistive switching characteristics of thin NiO film based flexible nonvolatile memory devices. *Microelectron Eng.* 2012;91:144-146.

157. Bush KA, Palmstrom AF, Yu ZJ, et al. 23.6%-efficient monolithic perovskite/silicon tandem solar cells with improved stability. *Nat Energy.* 2017;2:17009.

158. Li HU, Jackson TN. Flexibility testing strategies and apparatus for flexible electronics. *IEEE Trans Electron Devices.* 2016;63 (5):1934-1939.

159. Duan X, Huang Z, Liu C, Yang J, Tan L, Chen Y. A bendable nickel oxide interfacial layer via polydopamine crosslinking for flexible perovskite solar cells. *Chem Commun.* 2019;55: 3666-3669.

160. Kannan V, Senthilkumar V, Rhee JK. Multi-level conduction in NiO resistive memory device prepared by solution route. *J Phys D Appl Phys.* 2013;46(9):095301.

161. Mali SS, Kim H, Kim HH, Shim SE, Hong CK. Nanoporous p-type NiOx electrode for p-i-n inverted perovskite solar cell toward air stability. *Mater Today.* 2018;21(5):483-500.

162. Chen Y, Hao L, Zhang X, et al. Highly efficient solution-processed phosphorescent organic light-emitting devices with double-stacked hole injection layers. *J Appl Phys.* 2017;122(6): 065304.

163. Yin X, Chen P, Que M, et al. Highly efficient flexible perovskite solar cells using solution-derived NiO$_x$ hole contacts. *ACS Nano.* 2016;10(3):3630-3636.

164. Chen W, Liu FZ, Feng XY, Djurišić AB, Chan WK, He ZB. Cesium doped NiO$_x$ as an efficient hole extraction layer for inverted planar perovskite solar cells. *Adv Energy Mater.* 2017; 7(19):1700722.

165. Liu Z, Zhu A, Cai F, et al. Nickel oxide nanoparticles for efficient hole transport in p-i-n and n-i-p perovskite solar cells. *J Mater Chem A.* 2017;5:6597-6605.

166. Jošt M, Bertram T, Koushik D, et al. 21.6%-efficient monolithic perovskite/Cu(In,Ga)Se$_2$ tandem solar cells with thin conformal hole transport layers for integration on rough bottom cell surfaces. *ACS Energy Lett.* 2019;4(2):583-590.

167. Wang ZY, Lee SH, Kim DH, Kim JH, Park JG. Effect of NiO$_x$ thin layer fabricated by oxygen-plasma treatment on polymer photovoltaic cell. *Sol Energy Mater Sol Cells.* 2010;94(10):1591-1596.

168. Sun N, Fang G, Qin P, et al. Efficient flexible organic solar cells with room temperature sputtered and highly conductive NiO as hole-transporting layer. *J Phys D Appl Phys.* 2010;43 (44):445101.

169. Sun N, Fang G, Qin P, et al. Bulk heterojunction solar cells with NiO hole transporting layer based on AZO anode. *Sol Energy Mater Sol Cells.* 2010;94(12):2328-2331.

170. Park SY, Kim HR, Kang YJ, Kim DH, Kang JW. Organic solar cells employing magnetron sputtered p-type nickel oxide thin film as the anode buffer layer. *Sol Energy Mater Sol Cells.* 2010;94(12):2332-2336.

171. Itoh E, Higuchi Y, Furuhata D, Shirotori T. Enhancement of the open-circuit voltage and hole conduction of tetraphenyl porphyrin/C60 multilayered photovoltaic device by the insertion of oxide hole collection layers. *Jpn J Appl Phys.* 2011;50: 01BC14.

172. Steirer KX, Ndione PF, Widjonarko NE, et al. Enhanced efficiency in plastic solar cells via energy matched solution processed NiO$_x$ interlayers. *Adv Energy Mater.* 2011;1(5): 813-820.

173. Yu W, Shen L, Ruan S, et al. Performance improvement of inverted polymer solar cells thermally evaporating nickel oxide as an anode buffer layer. *Sol Energy Mater Sol Cells.* 2012;98:212-215.

174. Jung J, Kim DL, Oh SH, Kim HJ. Stability enhancement of organic solar cells with solution-processed nickel oxide thin films as hole transport layers. *Sol Energy Mater Sol Cells.* 2012; 102:103-108.

175. Singh A, Gupta SK, Garg A. Inkjet printing of NiO films and integration as hole transporting layers in polymer solar cells. *Sci Rep.* 2017;7:1775.

176. Tirado J, Vásquez-Montoya M, Roldán-Carmona C, et al. Air-stable n–i–p planar perovskite solar cells using nickel oxide nanocrystals as sole hole-transporting material. *ACS Appl Energy Mater.* 2019;2(7):4890-4899.

177. You J, Meng L, Song TB, et al. Improved air stability of perovskite solar cells via solution-processed metal oxide transport layers. *Nat Nanotechnol.* 2016;11:75-81.

178. Mustafa B, Griffin J, Alsulami AS, Lidzey DG, Buckley AR. Solution processed nickel oxide anodes for organic photovoltaic devices. *Appl Phys Lett.* 2014;104(6):063302.

179. Chavhan SD, Hansson R, Ericsson LK, et al. Low temperature processed NiO$_x$ hole transport layers for efficient polymer solar cells. *Org Electron.* 2017;44:59-66.

180. Gibbons J, Beadle W. Switching properties of thin NiO films. *Solid-State Electron.* 1964;7(11):785-790.

181. Sysun V, Bute I, Boriskov P. Modeling of diffusion mechanism of conductive channel oxidation in a Pt/NiO/Pt memory switching structure. *Solid-State Electron.* 2016;123:78-83.

182. MacManus-Driscoll JL, Wells MP, Yun C, Lee JW, Eom CB, Schlom DG. New approaches for achieving more perfect transition metal oxide thin films. *APL Mater.* 2020;8(4): 040904.

183. Lamperti A, Spiga S, Lu H, et al. Study of the interfaces in resistive switching NiO thin films deposited by both ALD and e-beam coupled with different electrodes (Si, Ni, Pt, W, TiN). *Microelectron Eng.* 2008;85(12):2425-2429.

184. Spiga S, Lamperti A, Wiemer C, et al. Resistance switching in amorphous and crystalline binary oxides grown by electron beam evaporation and atomic layer deposition. *Microelectron Eng.* 2008;85(12):2414-2419.

185. Ielmini D, Spiga S, Nardi F, et al. Scaling analysis of sub-micrometer nickel-oxide-based resistive switching memory devices. *J Appl Phys.* 2011;109(3):034506.

186. Wang XL, Liu Z, Wen C, et al. Thickness effect of nickel oxide thin films on associated solution-processed write once-read-many-times memory devices. *Appl Phys A.* 2018;124(6):454.

187. Li Y, Chu J, Duan W, et al. Analog and digital bipolar resistive switching in solution- combustion-processed NiO memristor. *ACS Appl Mater Interfaces.* 2018;10:24598-24606.

188. Liu Z, Tp C, Liu Y, Zhang S. Magnetron sputtered Ni-rich nickel oxide nano-films for resistive switching memory applications. *Int J Appl Ceramic Technol.* 2013;10(1):20-25.

189. Hu SG, Liu Y, Chen TP, et al. Effect of heat diffusion during state transitions in resistive switching memory device based on nickel-rich nickel oxide film. *IEEE Trans Electron Dev.* 2012;59(5):1558-1562.

190. Yu Q, Lim W, Hu SG, Chen T, Deng L, Liu Y. Flexible nano-scale memory device based on resistive switching in nickel oxide thin film. *Nanosci Nanotechnol Lett.* 2012;4:165-168.

191. Cui HP, Li JC, Yuan HL. Bending effect on the resistive switching behavior of a NiO/TiO$_2$ p–n heterojunction. *RSC Adv.* 2018;8:19861-19867.

192. Chen Y, Sun Y, Dai X, et al. Tunable electrical properties of NiO thin films and p-type thin-film transistors. *Thin Solid Films.* 2015;592:195-199.

193. Lee CT, Chen CC, Lee HY. Three dimensional-stacked complementary thin-film transistors using n-type Al:ZnO and p-type NiO thin-film transistors. *Sci Rep.* 2018;8:3968.

194. Sandana VE, Rogers DJ, Teherani FH, Bove P, McClintock R, Razeghi M. P-type thin film field effect transistors based on lithium-doped nickel oxide channels grown by pulsed laser deposition. In: Rogers DJ, Look DC, Teherani FH, eds. *Oxide-Based Materials and Devices X. Proceedins of the SPIE International Society for Optics and Photonics.* Vol 10919. Bellingham, WA: SPIE; 2019:81-85.

195. Sze S, Ng K. *Physics of Semiconductor Devices.* Hoboken, NJ: John Wiley & Sons; 2006:815.

196. Zhang Y, Mei Z, Wang T, et al. Flexible transparent high-voltage diodes for energy management in wearable electronics. *Nano Energy.* 2017;40:289-299.

197. Belgacem CH, El-Amine AA. Theoretical models for anomalously high ideality factor in a Au/SnO$_2$-Si(n)/Al solar cell. *Silicon.* 2018;10:1063-1066.

198. Breitenstein O, Altermatt P, Ramspeck K, Schenk A. The origin of ideality factors n > 2 of shunts and surfaces in the dark I-V curves of Si solar cells. Proceedings of the 21st European Photovoltaic Solar Energy Conference, Dresden, Germany 2006, pp: 625–628.

199. Sun H, Liao MH, Chen SC, Li ZY, Lin PC, Song SM. Synthesis and characterization of n-type NiO:Al thin films for fabrication of p-n NiO homojunctions. *J Phys D Appl Phys.* 2018;51(10):105109.

200. Chen WC, Hsu PC, Chien CW, et al. Room-temperature-processed flexible n-InGaZnO/p-Cu$_2$O heterojunction diodes and high-frequency diode rectifiers. *J Phys D Appl Phys.* 2014;47(36):365101.

201. Müzenrieder N, Zysset C, Kinkeldei T, Tröster G. Design rules for IGZO logic gates on plastic foil enabling operation at bending radii of 3.5 mm. *IEEE Trans Electron Devices.* 2012;59:2153-2159.

202. Kumar Tripathi A, Myny K, Hou B, Wezenberg K, Gelinck GH. Electrical characterization of flexible InGaZnO transistors and 8-b transponder Chip down to a bending radius of 2 mm. *IEEE Trans Electron Devices.* 2015;62:4063-4068.

203. Park JH, Seo J, Park S, et al. Efficient CH$_3$NH$_3$PbI$_3$ perovskite solar cells employing nanostructured p-type NiO electrode formed by a pulsed laser deposition. *Adv Mater.* 2015;27(27):4013-4019.

204. Odobel F, Le Pleux L, Pellegrin Y, Blart E. New photovoltaic devices based on the sensitization of p-type semiconductors: challenges and opportunities. *Acc Chem Res.* 2010;43(8):1063-1071.

205. Lee YM, Lai CH. Preparation and characterization of solid n-TiO$_2$/p-NiO hetrojunction electrodes for all-solid state dye-sensitized solar cells. *Solid-State Electron.* 2009;53(10):1116-1125.

206. Lepleux L, Chavillon B, Pellegrin Y, et al. Simple and reproducible procedure to prepare self-nanostructured NiO films for the fabrication of p-type dye-sensitized solar cells. *Inorg Chem.* 2009;48(17):8245-8250.

207. Qin P, Linder M, Brinck T, Boschloo G, Hagfeldt A, Sun L. High incident photon-to-current conversion efficiency of p-type dye-sensitized solar cells based on NiO and organic chromophores. *Adv Mater.* 2009;21(29):2993-2996.

208. Bakr Z, Wali Q, Fakharuddin A, Schmidt-Mende L, Brown T, Jose R. Advances in hole transport materials engineering for stable and efficient perovskite solar cells. *Nano Energy.* 2017;34:271-305.

209. Yang CH, Lee SC, Chen SC, Lin TC. The effect of annealing treatment on microstructure and properties of indium tin oxides films. *Mater Sci Eng B.* 2006;129(1–3):154-160.

210. Luangchaisri C, Dumrongrattana S, Rakkwamsuk P. Effect of heat treatment on electrical properties of fluorine doped tin dioxide films prepared by ultrasonic spray pyrolysis technique peer-review under responsibility of ISEEC2011. *Proc Eng.* 2012;32:663-669.

211. Park IJ, Kang G, Park MA, et al. Highly efficient and uniform 1 cm^2 perovskite solar cells with an electrochemically deposited NiO$_x$ hole-extraction layer. *Chem Sus Chem.* 2017;10(12):2660-2667.

212. U.S. Department of Energy, The National Renewable Energy Laboratory. Best research-cell efficiency chart. 2019. https://www.nrel.gov/pv/cell-efficiency.html. Accessed December 20, 2019.

213. Yue S, Liu K, Xu R, et al. Efficacious engineering on charge extraction for realizing highly efficient perovskite solar cells. *Energ Environ Sci.* 2017;10:2570-2578.

214. Nam WJ, Gray Z, Stayancho J, et al. ALD NiO thin films as a hole transport-electron blocking layer material for photodetector and solar cell devices. *ECS Trans.* 2015;66:275-279.

215. Xu L, Chen X, Jin J, et al. Inverted perovskite solar cells employing doped NiO hole transport layers: a review. *Nano Energy.* 2019;63:103860.

216. Stranks S, Hoye RLZ, Di D, Friend R, Deschler F. The physics of light emission in halide perovskite devices. *Adv Mater.* 2018;31(47):1803336.

217. Hoye RLZ, Lai ML, Anaya M, et al. Identifying and reducing interfacial losses to enhance color-pure electroluminescence

in blue-emitting perovskite nanoplatelet light-emitting diodes. *ACS Energy Lett*. 2019;4(5):1181-1188.

218. Lee S, Kim D, Hamilton I, et al. Control of interface defects for efficient and stable quasi-2D perovskite light emitting diodes using nickel oxide hole injection layer. *Adv Sci*. 2018;5:1801350.

219. Ji W, Liu S, Zhang H, Wang R, Xie W, Zhang H. Ultrasonic spray processed, highly efficient all-inorganic quantum dot light-emitting diodes. *ACS Photon*. 2017;4(5):1271-1278.

220. Shirasaki Y, Supran GJ, Bawendi MG, Bulovic V. Emergence of colloidal quantum-dot light-emitting technologies. *Nat Photon*. 2013;7:13-23.

221. Mashford BS, Stevenson M, Popovic Z, et al. High-efficiency quantum-dot light-emitting devices with enhanced charge injection. *Nat Photon*. 2013;7:407-412.

222. Caruge JM, Halpert JE, Bulovi´c V, Bawendi MG. NiO as an inorganic hole-transporting layer in quantum-dot light-emitting devices. *Nano Lett*. 2006;6(12):2991-2994.

223. Vasan R, Salman H, Manasreh MO. Solution processed high efficiency quantum dot light emitting diode with inorganic charge transport layers. *IEEE Electron Device Lett*. 2018;39(4):536-539.

224. Cao F, Wang H, Shen P, et al. High-efficiency and stable quantum dot light-emitting diodes enabled by a solution processed metal-doped nickel oxide hole injection interfacial layer. *Adv Funct Mater*. 2017;27(42):1704278.

225. Gangishetty M, Hou S, Quan Q, Congreve D. Reducing architecture limitations for efficient blue perovskite light emitting diodes. *Adv Mater*. 2018;30(20):1706226.

226. Liu Y, Cui J, Du K, et al. Efficient blue light-emitting diodes based on quantum-confined bromide perovskite nanostructures. *Nat Photon*. 2019;13:760-764.

227. Kim J, Park M, Ryu M, Jang J. P-171: foldable organic light-emitting diode display using solution processed p-type nickel oxide. *SID Symp Dig Tech Papers*. 2016;47(1):1760-1763.

228. Mokoena TP, Swart HC, Motaung DE. A review on recent progress of p-type nickel oxide based gas sensors: future perspectives. *J Alloys Compd*. 2019;805:267-294.

229. Dirksen JA, Duval K, Ring TA. NiO thin-film formaldehyde gas sensor. *Sensor Actuat B Chem*. 2001;80(2):106-115.

230. Lahem D, Lontio F, Delcorte A, Bilteryst L, Debliquy M. Formaldehyde gas sensor based on nanostructured nickel oxide and the microstructure effects on its response. *IOP Conf Ser Mater Sci Eng*. 2016;108:012002.

231. Soleimanpour AM, Jayatissa AH, Sumanasekera G. Surface and gas sensing properties of nanocrystalline nickel oxide thin films. *Appl Surf Sci*. 2013;276:291-297.

232. Soleimanpour AM, Hou Y, Jayatissa AH. Evolution of hydrogen gas sensing properties of sol–gel derived nickel oxide thin film. *Sensor Actuat B Chem*. 2013;182:125-133.

233. Khan Y, Garg M, Gui Q, et al. Flexible hybrid electronics: direct interfacing of soft and hard electronics for wearable health monitoring. *Adv Funct Mater*. 2016;26(47):8764-8775.

234. Głab S, Hulanicki A, Edwall G, Ingman F. Metal-metal oxide and metal oxide electrodes as pH sensors. *Crit Rev Anal Chem*. 1989;21(1):29-47.

235. Chou JC, Yan SJ, Liao YH, et al. Characterization of flexible arrayed pH sensor based on nickel oxide films. *IEEE Sensors J*. 2018;18(2):605-612.

236. Jung DUJ, Ahmad R, Hahn YB. Nonenzymatic flexible field-effect transistor based glucose sensor fabricated using NiO quantum dots modified ZnO nanorods. *J Colloid Interface Sci*. 2018;512:21-28.

237. Alam AU, Qin Y, Nambiar S, et al. Polymers and organic materials-based pH sensors for healthcare applications. *Prog Mater Sci*. 2018;96:174-216.

238. Yanagida T, Nagashima K, Oka K, et al. Scaling effect on unipolar and bipolar resistive switching of metal oxides. *Sci Rep*. 2013;3:1657.

239. Ante F, Kälblein D, Zschieschang U, et al. Contact doping and ultrathin gate dielectrics for Nanoscale organic thin-film transistors. *Small*. 2011;7(9):1186-1191.

AUTHOR BIOGRAPHIES

Mari Napari received her PhD in physics from the University of Jyväskylä, Finland, in 2017. From 2017 to 2019, she was a Postdoctoral Research Associate at the Department of Materials Science and Metallurgy, University of Cambridge, United Kingdom, where she worked on the development of p-type oxides for thin-film transistors. Currently, she is a theme lead for Beyond CMOS-electronics research at the Centre for Electronics Frontiers, University of Southampton, UK. Her own research focuses on atomic layer deposition of functional oxide thin films for next-generation logic and memory devices.

Tahmida N. Huq is currently a PhD student at the University of Cambridge, UK. She received her MEng degree in Materials Science and Engineering from Imperial College London. After working at Intel for 2 years, she returned to academia to complete a MRes in Graphene Technology before starting her PhD. Her primary research interests are in exploring defect tolerant solar absorbers, mainly BiOI, and n- and p-type metal oxides for use in thin-film transistors and charge transport layers in optoelectronic devices.

Robert L. Z. Hoye is a Lecturer (Assistant Professor) in the Department of Materials at Imperial College London. There, he also holds the Royal Academy of Engineering Research Fellowship. He completed his PhD at the University of Cambridge (2012-2014), before taking up a postdoctoral

position at the Massachusetts Institute of Technology (2015-2016). Subsequently, he took up two independent Research Fellowships at Cambridge, firstly at Magdalene College (2016-2019) then at Downing College (2019-2020). He moved to set up his group at Imperial in 2020. His research focuses on optoelectronic materials development, including defect-tolerant semiconductors for photovoltaics and lead-halide perovskite LEDs.

Judith Driscoll is Professor in the Materials Science at the University of Cambridge, and she researches oxide thin film electronics, with over 400 publications. She is a Fellow of IOP, APS, MRS, IOM3, Women's Engineering Society, and the Royal Academy of Engineering. She has won the Institute of Physics Joule Medal, the Royal Academy of Engineering Armourers and Brasiers prize, the IEEE James Wong prize and the IOM3 Kroll Medal. She is Founding Editor-in-Chief of the journal APL Materials.

SUPPORTING INFORMATION

Additional supporting information may be found online in the Supporting Information section at the end of this article.

How to cite this article: Napari M, Huq TN, Hoye RLZ, MacManus-Driscoll JL. Nickel oxide thin films grown by chemical deposition techniques: Potential and challenges in next-generation rigid and flexible device applications. *InfoMat*. 2021;3:536–576. https://doi.org/10.1002/inf2.12146